การสังเคราะห์แผ่นทองคำระดับนาโนเมตรและโครงสร้างระดับนาโนเมตรของทองคำคล้าย
ดอกไม้
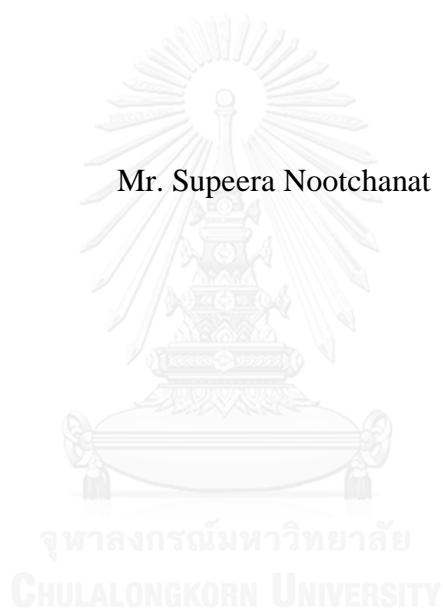
นายสุพีระ นุชนารถ

วิทยานิพนธ์นี้เป็นส่วนหนึ่งของการศึกษาตามหลักสูตรปริญญาวิทยาศาสตรดุษฎีบัณฑิต
สาขาวิชาเคมี ภาควิชาเคมี
คณะวิทยาศาสตร์ จุฬาลงกรณ์มหาวิทยาลัย
ปีการศึกษา 2558

SYNTHESIS OF GOLD NANOSHEETS AND FLOWER-
LIKE GOLD NANOSTRUCTURES

Mr. Supeera Nootchanat

A Dissertation Submitted in Partial Fulfillment of the Requirements
for the Degree of Doctor of Philosophy Program in Chemistry
Department of Chemistry
Faculty of Science
Chulalongkorn University
Academic Year 2015
Copyright of Chulalongkorn University

Thesis Title	SYNTHESIS OF GOLD NANOSHEETS AND FLOWER-LIKE GOLD NANOSTRUCTURES
By	Mr. Supeera Nootchanat
Field of Study	Chemistry
Thesis Advisor	Professor Sanong Ekgasit, Ph.D.
Thesis Co-Advisor	Associate Professor Chuchaat Thammacharoen

Accepted by the Faculty of Science, Chulalongkorn University in Partial Fulfillment of the Requirements for the Doctoral Degree

.... Dean of the Faculty of Science
(Associate Professor Polkit Sangvanich, Ph.D.)

THESIS COMMITTEE

.... Chairman
(Assistant Professor Suchada Chuanuwatanakul, Ph.D.)
.... Thesis Advisor
(Professor Sanong Ekgasit, Ph.D.)
.... Thesis Co-Advisor
(Associate Professor Chuchaat Thammacharoen)
.... Examiner
(Assistant Professor Kanet Wongravee, Ph.D.)
.... Examiner
(Numpon Insin, Ph.D.)
.... Examiner
(Boonrat Lohwongwatana, Ph.D.)
.... External Examiner
(Associate Professor Chinapong Kritayakornupong, Dr.rer.nat.)

สุพีระ นุชนารถ : การสังเคราะห์แผ่นทองคำระดับนาโนเมตรและโครงสร้างระดับนาโน
เมตรของทองคำคล้ายดอกไม้ (SYNTHESIS OF GOLD NANOSHEETS AND
FLOWER-LIKE GOLD NANOSTRUCTURES) อ.ที่ปรึกษาวิทยานิพนธ์หลัก: ศ.
ดร. สนอง เอกสิทธิ์, อ.ที่ปรึกษาวิทยานิพนธ์ร่วม: รศ. ชูชาติ ธรรมเจริญ, 99 หน้า.

ในงานวิจัยนี้นำเสนอกระบวนการสังเคราะห์แผ่นโลหะทองคำระดับนาโนเมตรด้วย
กระบวนการที่ง่ายและมีประสิทธิภาพสูงโดยการใช้ไฮโดรเจนเพอร์ออกไซด์เป็นตัวรีดิวซ์ ใช้แป้ง
เป็นสารช่วยเสถียรและตัวควบคุมโครงสร้างของแผ่นทองคำระดับนาโนเมตร
ไฮโดรเจนเพอร์ออกไซด์เป็นตัวรีดิวซ์ที่ไม่รุนแรงจึงทำให้เกิดการสร้างผลึกของแผ่นทองคำระดับ
นาโนเมตรจากโครงสร้างระดับนาโนเมตรของทองคำคล้ายดอกไม้ในช่วงแรกเริ่มผ่านกลไกทาง
จลนศาสตร์ อนุภาคแผ่นโลหะทองคำขนาดเล็กที่มีโมเลกุลของแป้งเกาะอยู่ที่หน้าตัด {111} จะเกิด
การเชื่อมประสานแบบมีทิศทาง (oriented attachment) กลายเป็นแผ่นทองคำความหนาระดับนา
โนเมตรที่มีขนาดใหญ่ขึ้น โดยมีขนาดใหญ่ถึง 50 ไมโครเมตร และมีความหนาของแผ่นประมาณ
20-50 นาโนเมตร หากไม่ใช้แป้งในการสังเคราะห์ อนุภาคทองคำที่สังเคราะห์ได้จะมีรูปทรงกึ่ง
ทรงกลมที่มีเส้นผ่านศูนย์กลางขนาด 5-10 ไมโครเมตร ผ่านการโตของอนุภาคโดยการเติมอะตอม
ของทองคำบริเวณรอยต่อของโครงสร้างระดับนาโนเมตรของทองคำในช่วงแรกเริ่ม หากความ
เข้มข้นของไฮโดรเจนเพอร์ออกไซด์ที่ใช้ในกระบวนการสังเคราะห์มีความเข้มข้นสูง ลักษณะของ
อนุภาคที่ได้จะเป็นโครงสร้างระดับนาโนเมตรคล้ายดอกไม้ของทองคำ โดยโครงสร้างดังกล่าวเกิด
จากการที่อนุภาคแผ่นโลหะทองคำขนาดเล็กที่เกิดการเชื่อมประสานแบบมีทิศทางเป็นฐานของ
ดอกไม้และเกิดการโตของโครงสร้างของกลีบดอกที่มีโมเลกุลแป้งเกาะอยู่ที่หน้าตัด {111} บน
ฐานของดอกไม้ ผู้วิจัยได้ศึกษาบทประยุกต์ของแผ่นโลหะทองคำระดับนาโนเมตรในการนำไปใช้
ในงานประดับตกแต่งและใช้เป็นเม็ดสี จนไปถึงการประยุกต์ใช้แผ่นทองคำระดับนาโนเมตรและ
โครงสร้างระดับนาโนเมตรของทองคำคล้ายดอกไม้ ในการเป็นวัสดุรองรับในเทคนิคการเพิ่ม
สัญญาณรามานเชิงพื้นผิว

ภาควิชา	เคมี	ลายมือชื่อนิสิต	....
สาขาวิชา	เคมี	ลายมือชื่อ อ.ที่ปรึกษาหลัก	....
ปีการศึกษา	2558	ลายมือชื่อ อ.ที่ปรึกษาร่วม	....

5273906223 : MAJOR CHEMISTRY

KEYWORDS: GOLD NANOSHEETS, FLOWER-LIKE GOLD NANOSTRUCTURES, HYDROGEN PEROXIDE, ORIENTED ATTACHMENT, SURFACE-ENHANCED RAMAN SPECTROSCOPY, STARCH

SUPEERA NOOTCHANAT: SYNTHESIS OF GOLD NANOSHEETS AND FLOWER-LIKE GOLD NANOSTRUCTURES. ADVISOR: PROF. SANONG EKGASIT, Ph.D., CO-ADVISOR: ASSOC. PROF. CHUCHAAT THAMMACHAROEN, 99 pp.

In this work, we report a simple and efficient method for the preparation of large gold nanosheets using H_2O_2 as the green reducing agent and starch as a stabilizer and shape-controlling agent. H_2O_2 provides a weak reducing capability that allows a kinetically controlled growth of nanosheets out of small flower-like nanostructures formed at the initial stage of particle growth. Small nanosheets with starch-bound {111} facet undergo oriented attachment and become large nanosheets with lateral size as large as 50 μm with the thickness of 20–50 nm. Without starch, gold quasi-microspheres with diameters of 5–10 μm are obtained as the dominant product as they grow out of the flower-like nanostructures by filling gold atoms in the gaps between nano-petals. This starch-enable selective formation of large nanosheets is rapidly and efficiently as a 100% conversion can be attained. Interestingly, micrometer-sized flower-like gold nanostructures with nanometer-thick petal assembly are obtained at the extremely high concentration of H_2O_2. The oriented attachment of the small gold nanosheets creates the basal sheets of the flower structures. Then, the growth of the starch-bound {111} facet nano-petals take place on the surface of the basal sheets causing the formation of flower-like gold nanostructures. We explore the applications of gold nanosheets as a pigment for decoration and a solid substrate for surface enhanced Raman spectroscopy. A single particle of the flower-like gold nanostructure can be employed as a substrate for surface enhanced Raman spectroscopy.

Department:	Chemistry	Student's Signature	....
Field of Study:	Chemistry	Advisor's Signature	....
Academic Year:	2015	Co-Advisor's Signature	....

ACKNOWLEDGEMENTS

CONTENTS

LIST OF TABLES

LIST OF FIGURES

Figure   **Page**

Figure   **Page**

Figure   **Page**

Figure   **Page**

Figure   **Page**

Figure   **Page**

LIST OF SCHEMES

LIST OF SYMBOLS

C_r	: Solubility of the particle
C_b	: Concentration of the bulk solution
γ	: Surface energy
v	: Molar volume of the bulk crystal
r	: particle radius
k_B	: Boltzmann's constant
T	: Temperature
$°C$	: Degree Celsius
E_{re}	: Reduction potential
E_{ox}	: Oxidation potential
ΔE_{cell}	: Cell potential
$[HAuCl_4]$	: Concentration of $HAuCl_4$
$[H_2O_2]$	: Concentration of H_2O_2

LIST OF ABBREVIATIONS

SERS   : Surface-enhanced Raman spectroscopy/Surface-enhanced Raman scattering

TERS   : Tip-enhanced Raman spectroscopy/Surface-enhanced Raman scattering

UV-visible   : Ultraviolet-visible

FIB-SEM   : Focused ion beam-scanning electron microscopy

Conc.   : Concentration

NIR   : Near-infrared

TPI-PL   : Two-photon-induced photoluminescence

SEM   : Scanning electron microscopy/Scanning electron microscope

TEM   : Transmission electron microscopy/Transmission electron microscope

HEPES   : 2-[4-(2-hydroxyethly)-1-piperazinyl]ethanesulfonic acid

PVP   : Poly(vinyl pyrrolidone)

SDS   : Sodium dodecyl sulfate

C18N3   : bis-(amidoethylcarbamoylethyl) octadecylamine

DFM   : Dynamic force mode

XRD   : X-ray diffraction

OA   : Oriented attachment

AFM   : Atomic force microscopy

OR   : Ostwald ripening

SAED   : Selected area electron diffraction

fcc   : Face-centered cubic

R6G   : Rhodamine 6G

CHAPTER I

INTRODUCTION

1.1   Gold Nanoparticles

Nanoparticle is a submicroscopic particle with one of its dimension size less than 100 nm. The nanoparticles exhibit novel properties that are different from the bulk counterpart, i.e., the increase of surface area, the decrease of the melting point, the new optical property, as well as the increase of chemical activities. The properties of the nanoparticles strongly depend on their size and shape [1]. Numerous synthesis methods have been developed and metal nanoparticles with various shapes and elemental compositions have been created (Table 1.1). Gold nanoparticles are the famous metal nanoparticles that have been in the interest of scientists for several years. It has been widely employed in numerous applications such as colorimetric sensor [2], surface-enhanced Raman spectroscopy (SERS) [3-8], tip-enhanced Raman spectroscopy (TERS) [9, 10], chemical catalyst [11], as well as biological sensor [12].

Numerous fabrication techniques have been developed to obtain the gold nanoparticles with particular size and shape; e.g., photo irradiation [3, 13-15], thermal synthesis [16-18], chemical reduction [4, 19, 20], laser ablation [21], galvanic reaction [22], and nanolithography [23]. Although there are many synthesis protocols as mentioned above, the chemical reduction method is broadly employed for the preparation of gold nanoparticles. The chemical reduction method does not require complicated instruments and the experimental procedure is straightforward. Moreover, the chemical reduction method is a potential synthesis technique that is suitable for the

pilot-scale manufacturing. Various shape of gold nanoparticles, e.g., rod, sphere, bar, plate or sheet, cube, and wire, can be selectively fabricated by the chemical method. In principle, the chemical reduction approach for the synthesis of gold nanoparticles involves the chemical reduction of gold ions by appropriate reducing agents under the presence of stabilizer or shape-controlling agent, resulting in the directional growth of zero-valance gold nanoparticles. However, in order to accomplish the well shape-controlled synthesis of gold nanoparticles, the reaction still need to be performed at low concentration of the reactant with the presence of an expensive stabilizer.

In this work, we develop the synthesis methods for the fabrication of gold nanosheets and flower-like gold nanostructures based on wet chemical reduction with industrial-scale production capability. The environmentally friendly and inexpensive chemicals are used. The progressive morphological development of the nanoparticles is investigated. Moreover, we further explore the potential application of gold nanosheets and flower-like gold nanostructures as SRES substrates. The gold nanosheets are also exploited as a gold pigment for traditional drawing.

Table 1.1 A variety of shapes obtained from various metal nanocrystals [24].

Structures	Shapes	Schematic drawings	Metals
single-crystal	perfect/truncated cube[a]		Pd, Ag, Au, Pt, Cu, Rh, Bi, Fe
	perfect/truncated octahedron[a]		Pd, Ag, Au, Pt
	perfect/truncated tetrahedron[a]		Ag, Au, Pt, Rh
	rectangular bar		Pd, Ag, Pt
	octagonal rod		Pd, Au, Fe, Co, Ni
	rectangular or octagonal wire		Pb, In, Sn, Sb, Fe, Co
singly twinned	right bipyramid		Pd, Ag
	beam		Ag
multiply twinned	decahedron[a]		Pd, Ag, Au
	icosahedron[a]		Pd, Au
	five-fold twinned pentagonal rod		Pd, Ag, Au, Cu
	five-fold twinned pentagonal wire		Ag, Au, Cu
	triangular/hexagonal plate		Pd, Ag, Au, Cu, Pb, Bi, Co, Ni
	disc		Sn, Co
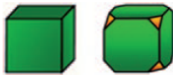
[a] Platonic solid.

1.2 Objectives

1.2.1 To develop a simple and efficient chemical reduction method for the fabrication of gold nanosheets and flower-like gold nanostructures utilizing nontoxic and environmentally friendly chemicals with industrial-scale production capability.

1.2.2 To study the growth mechanism of gold nanosheets and flower-like gold nanostructures in order to control the morphology of the fabricated gold nanostructures.

1.3 Scope of the Dissertation

1.3.1 Study and develop methods for production of gold nanosheets and flower-like gold nanostructures based on simple wet chemical approaches. The concentrations of the reactant, including $HAuCl_4$, starch, H_2O_2, are optimized in order to achieve the synthesis conditions for gold nanosheets and flower-like gold nanostructures. The synthesis methods are optimized to attain the industrial-scale production capability.

1.3.2 Study the growth mechanism of gold nanosheets and flower-like gold nanostructures through the time-dependent morphological evolution using scanning electron microscopy (SEM).

1.3.3 Study the morphology, elemental composition, crystal structures and optical activity of gold nanosheets and flower-like gold nanostructures using optical microscopy, SEM, atomic force microscopy (AFM), energy-

dispersive X-ray spectroscopy, X-ray diffraction (XRD) spectroscopy and ultraviolet-visible (UV-visible) spectroscopy.

1.3.4 Explore the application of gold nanosheets and flower-like gold nanostructures as substrates for SERS and exploit the shiny-glittering effect of gold nanosheets as a pigment for decoration application.

1.4 Expected Outcomes

1.4.1 Achieve the simple and efficient methods for the production of gold nanosheets and flower-like gold nanostructures using nontoxic and environmentally friendly chemicals with industrial-scale production capability.

1.4.2 Gain the insight understanding about the growth mechanism of gold nanosheets and flower-like gold nanostructures.

จุฬาลงกรณ์มหาวิทยาลัย
CHULALONGKORN UNIVERSITY

CHAPTER II

RESEARCH BACKGROUND

2.1   Fabrication of Nanoparticles via Physical and Chemical Method

Since nanostructures exhibit unique shape- and size-dependent properties that are different from their counterparts, the structural-controlled synthesis of nanostructures has gained immense attentions for several years. The nanostructures have been applied to many promising applications as efficient catalysts, optical and electronic materials, medical and chemical sensors [1, 7, 24, 25]. These novel applications could be achieved and selectively tuned by manipulating morphology and composition of the nanostructures.

Preparation of nanoparticles can be accomplished by principal approaches which are consisted of physical method and chemical method (Figure 2.1). Physical method involves the breakage of bulk material into the nanometer-sized particles by mechanical operations such as grinding [26], focused ion beam lithography (Figure 2.2) [27] and laser ablation (Figure 2.3) [21, 28, 29]. Addition of surfactant, capping agents or stabilizers is required in order to stabilize the generated nanoparticles. In contrast, the chemical pathway involves the growth of nanoparticles from metal atoms which are obtained from molecular or ionic precursors [30]. This method is simple and capable of producing small and uniform nanoparticles. Furthermore, advanced experimental apparatuses are not usually required. Therefore, the chemical methods are preferably employed for the nanoparticle preparation than the physical method.
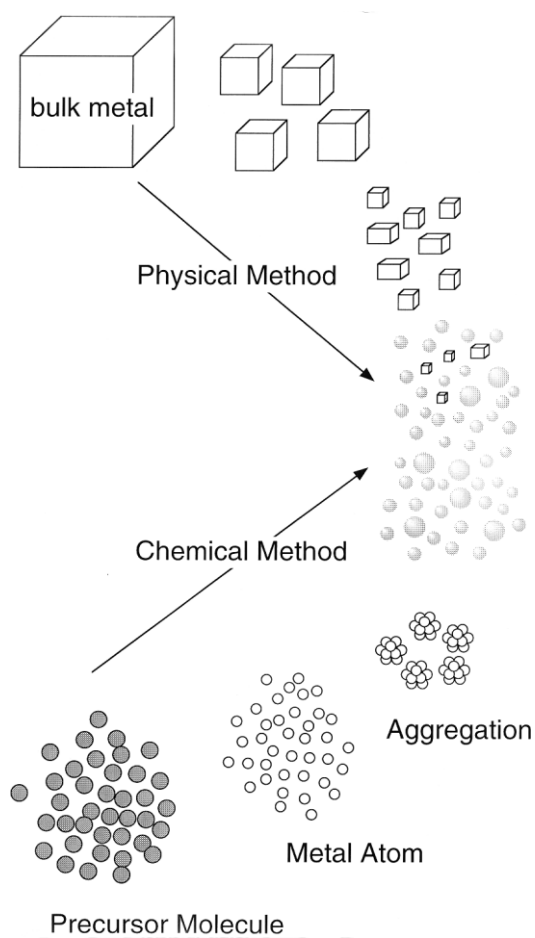
Figure 2.1 Schematic illustration of the preparation of metal nanoparticles by physical

method and chemical method [30].
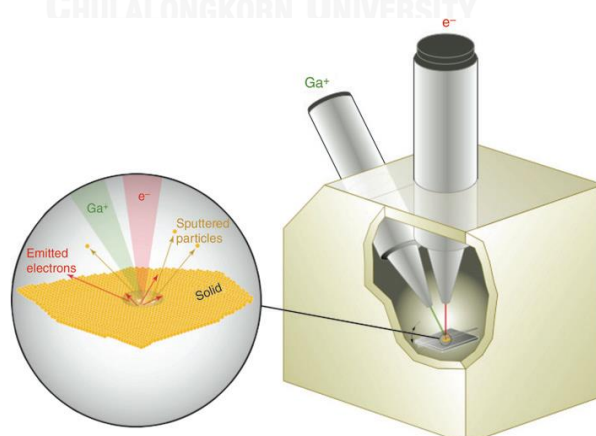
Figure 2.2 Schematic illustration of a dual-beam FIB–SEM instrument. Expanded

image shows the electron and ion beam sample interaction [31].
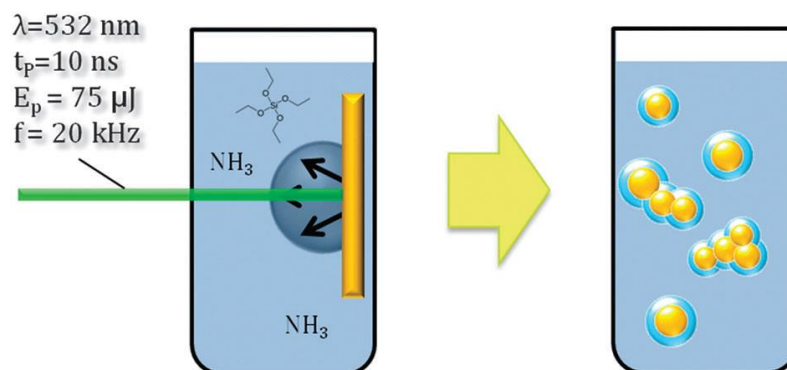
Figure 2.3 Schematic illustration of the fabrication of silica-coated gold nanoparticles by pulsed laser ablation in liquids [28].

The most well-known chemical method for preparation metal nanoparticles is a chemical reduction. The chemical reduction approach involves electron transfer from reducing agents to metal ions, resulting in the formation of zero-valent metal atoms. The generated metal atoms consecutively undergo nucleation and growth into nanoparticles (Figure 2.4). The examples of reducing agent that are usually employed for the preparation of metal nanoparticles are trisodium citrate ($Na_3C_6H_5O_7$), sodium borohydride ($NaBH_4$) and L-ascorbic acid. The chemical method, size and uniformity of the metal nanoparticles can be manipulated by controlling atom aggregation. Utilization of capping agents and stabilizers not only prevent the aggregation of nanoparticles but also regulate the growth direction of the nanocrystals [10, 32, 33].
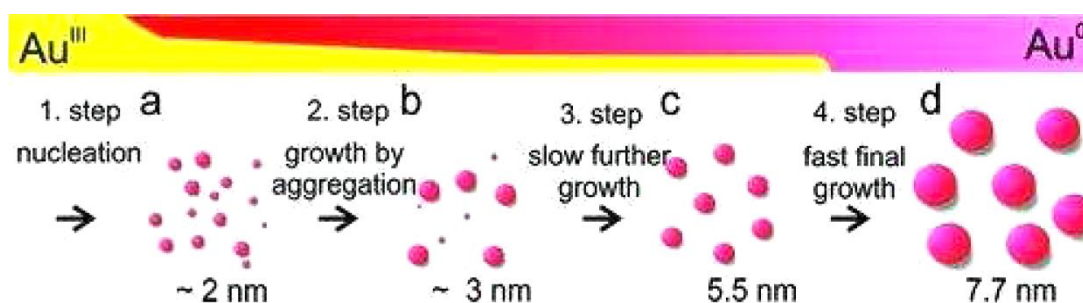
Figure 2.4 Schematic illustration of gold nanoparticle formation [34].

2.2 Theories of Nucleation and Growth

The formation of the nanoparticles can be explained by the nucleation and growth. In this section, three different theories for the nucleation and growth will be described.

2.2.1 LaMer Mechanism

In solution-phase synthesis of metal nanoparticles, metal ions receive electrons from a reducing agent. Zero-valence metal atoms which are the building blocks of a metal nanocrystal are formed. However, the evolution of nuclei and nanocrystals from the precursors is still under unclear [24]. In the early 50's, LaMer and co-workers studied the synthesis of sulfur sols from the decomposition of sodium thiosulfate. They proposed the process of nucleation and growth which could be divided into three steps. First, monomer numbers in the solution rapidly increase. Second, the monomers are subjected to nucleation burst, resulting in the significant decrease of the free monomer numbers in the solution. After this point, the nucleation is almost terminated because of limited concentration of monomers. Third, the growth of the nuclei takes place by the addition of free monomers under the diffusion through the solution [34].

In term of metal nanocrystals, the numbers of metal atoms in the solution immediately increase after the chemical reduction. When the concentration of metal atoms in the solution reaches the supersaturation point, the aggregation of atoms (self-nucleation) occurs to produce nuclei (small clusters of metal atoms). After the formation and growth of nuclei, the concentration of metal atoms in the solution decrease. When the concentration of atoms is lower than the supersaturation point, there is no occurrence of nucleation. The generated nuclei grow to larger nanocrystal with

the supply of metal atoms until reaching the equilibrium state between atoms on the surfaces of nanocrystal and atoms in the solution (Figure 2.5) [24].
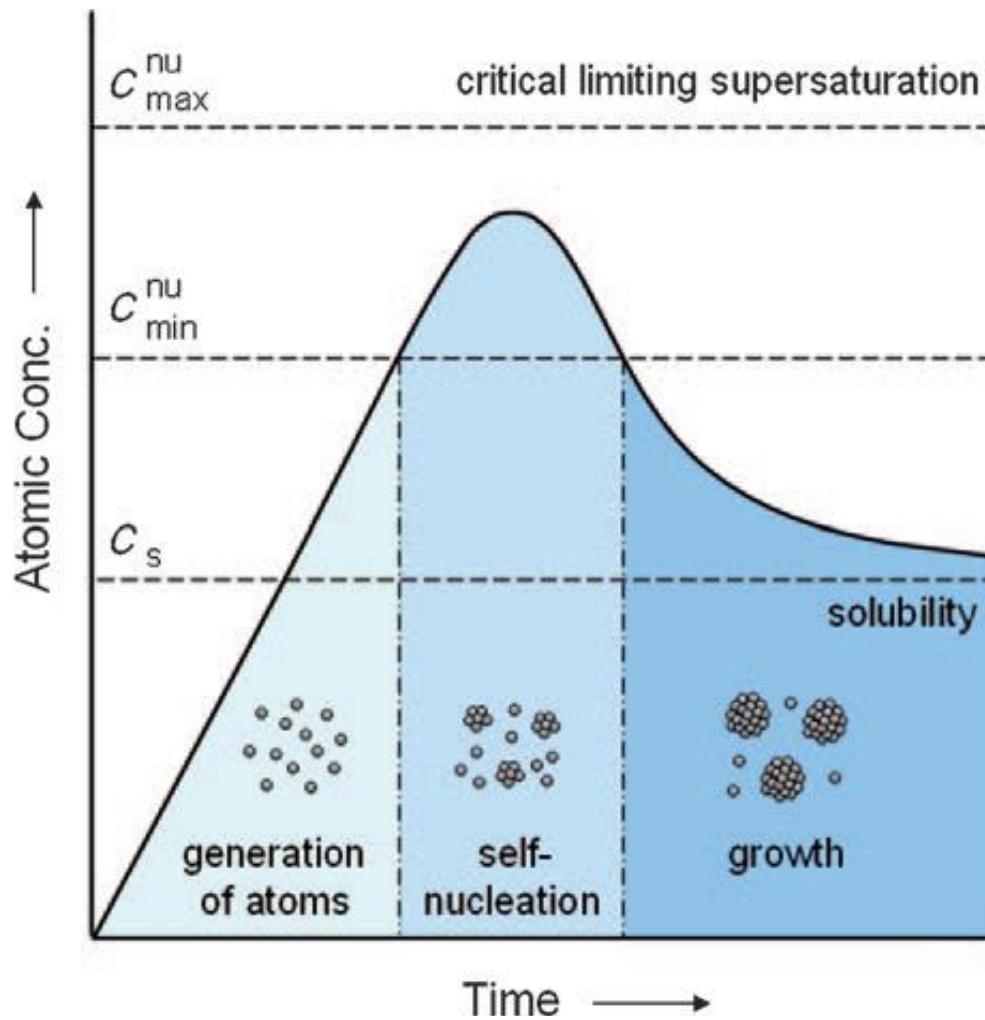
Figure 2.5 Schematic illustration of LaMer mechanism indicating the atomic concentration against time. The generation of atoms, nucleation, and subsequent growth are demonstrated [24].

2.2.2 Ostwald Ripening and Digestive Ripening

In 1900, Ostwald ripening was first introduced as a growth mechanism which caused by the change of nanoparticle solubility. In addition, the solubility of nanoparticles is depended on their size which is described by the Gibbs−Thomson relation (Eq. 2.1).

$$C_r = C_b \exp\left(\frac{2\gamma v}{r\kappa_B T}\right)$$ (Eq. 2.1)

Where C_r is the solubility of the particle, C_b is the concentration of the bulk solution, γ is surface energy, v is the molar volume of the bulk crystal, r is the particle radius, k_B is the Boltzmann's constant and T is the temperature.

The high solubility and the high surface energy of small particles lead to the dissolution into the solution which allows the growth of the larger particles [34]. On the other hand, digestive ripening (inverse of Ostwald ripening) occurs when the smaller particles are produced from the sacrifice of the larger ones [35]. This also explains in term of surface energy of particles in the solution.

2.2.3 Coalescence and Oriented Attachment

The fusion of the nanoparticles during the growth can be described by two mechanisms which are coalescence and oriented attachment (OA). The discriminating factor of the two mechanism is the preferential orientation of the crystal lattice at the grain boundary. In case of coalescence, the attachment occurs without particular preferential orientation. However, the OA occurs with a common crystallographic

alignment, resulting in the continuous crystallographic planes [34, 36, 37]. Figure 2.6 shows the attachment of nanoparticles via (A) coalescence and (B) orientated attachment. Based on the high resolution images, lattice planes between domains obtained from coalescence were randomly orientated, while the perfect alignment of lattice planes was obtained from orientated attachment.
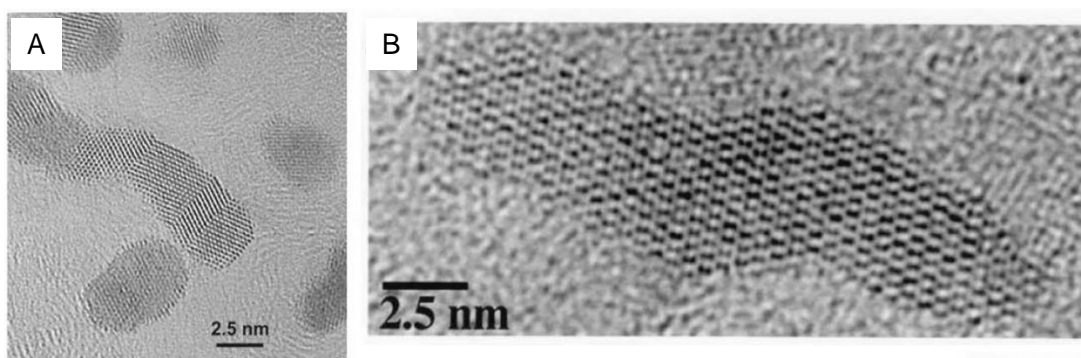
Figure 2.6 (A) formation of the platinum nanowire by coalescence of platinum crystallites (B) The formation of one large crystallite by OA of four titania crystallites [37].

2.3 Gold Nanocrystals

Gold nanocrystals are one of the most remarkable nanomaterials that were employed in various applications as SERS substrates [3, 38, 39], TERS substrates [9, 10], catalyst [40, 41], colorimetric sensor [2, 42], image contrast agents [43] and cancer therapy [44]. The wide range utilization of gold nanocrystals is reinforced by the ability to selectively engineered their nanostructures as rods [45, 46], wires [47], belts [48], plates [10, 18, 49-51], polyhedral [52, 53], cages [54], stars [55, 56], and flowers [4, 57].

2.3.1 Gold Nanosheets and Their Applications

Gold nanoplates and nanosheets are promising functional nanostructures as its morphology with desired degree of anisotropy can be selectively produced by various synthetic methods such as wet chemical, electrochemical, sonochemical, and photochemical techniques. The related optical and physicochemical properties are directly correlated with the morphology. The nanoplates and nanosheets have been employed as organic vapor sensors [58], NIR-absorbing films [59], two-photon-induced photoluminescence (TPI-PL) [60], basic building block for nanocomponents [27], and surface plasmon resonators [61]. Wet chemical techniques are usually utilized for the production of plate-shaped nanostructures, e.g., seed-mediated [50, 51, 62] and one-pot procedures [10, 18, 49, 63], as they are rapid and high-yield methods with the possibility of industrial-scale production (Figure 2.7 and 2.8).

Although, the one-pot synthesis protocol is simpler than the seed-meditated approach, morphological controllability by the latter is better as the nucleation and growth are separated with the minimization of the polydispersity of size and shape [1, 64, 65]. However, most developed synthetic techniques for the fabrication of engineered nanostructures especially those with extreme degree of anisotropy involve the usage of organic solvents, strong reducing agents, polymeric stabilizers, surface capping agents, and surfactants. It is a grand challenge for scientists to develop a simple, green, and efficient synthetic method for selective fabrication of nanostructures with desirable properties which are capable of commercialization and practical for real-life applications.
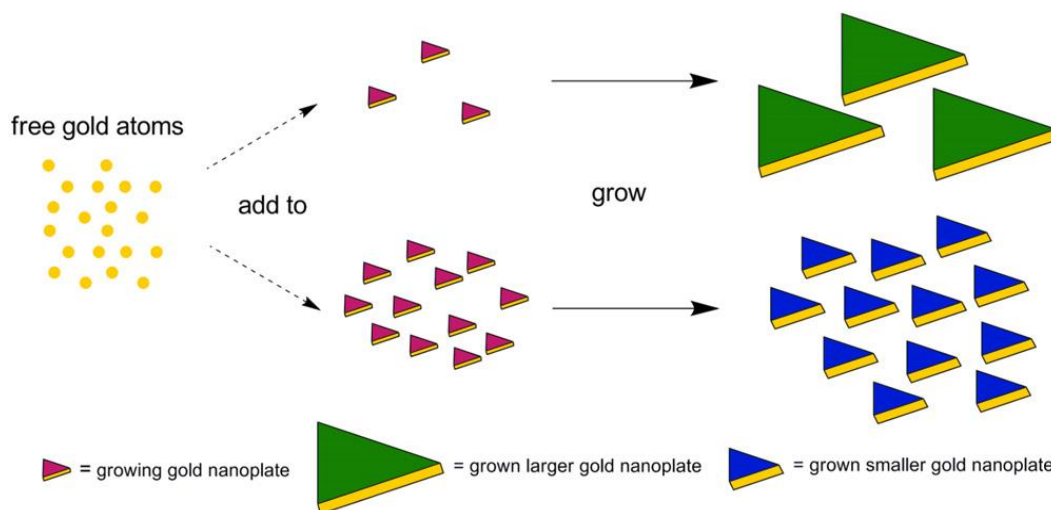
Figure 2.7 Schematic illustration of the gold atom addition to plate-like seeds in a seed-mediated method. If there is a constant number of free gold atoms in the reaction solution, the number of plate-like seeds dictates the size of the gold nanoplates [50].
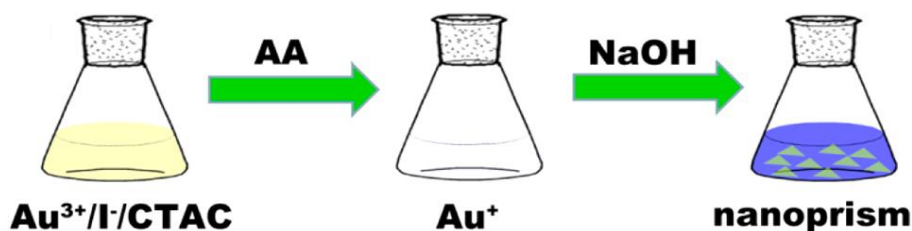
Figure 2.8 Schematic illustration of the synthesis of gold nanoplates using a one-step seedless method [63].

2.3.2 Flower-Like Gold Nanostructures and Their Applications

Among of extensive nanostructures of gold, the flower shape shows the distinctive nanostructures consisting of nanogrooves, sharp edges and tips which not only exhibit a high surface area but also possess many nanojunctions. The flower-like gold nanostructures were employed as SERS substrates [4, 66, 67] and electrochemical

catalysts [68]. Moreover, according to the toxicological investigation, the flower-like gold nanostructures exhibited the acceptable cytotoxicity toward cells [69]. It also employed as nanocarriers of DNA for cellular uptake, drug or gene delivery and contrast agents [70]. Facile chemical techniques have been developed for the fabrication of flower-like gold nanostructures, particularly electrochemical [67, 71] and wet chemical procedures [4, 66, 69, 70, 72]. Although, the electrochemical methods showed the advantage as it provided the well-ordered flower-like gold nanostructures on the substrates (Figure 2.9), it needed specialized expertise and instruments to create the pattern on the substrates [67].
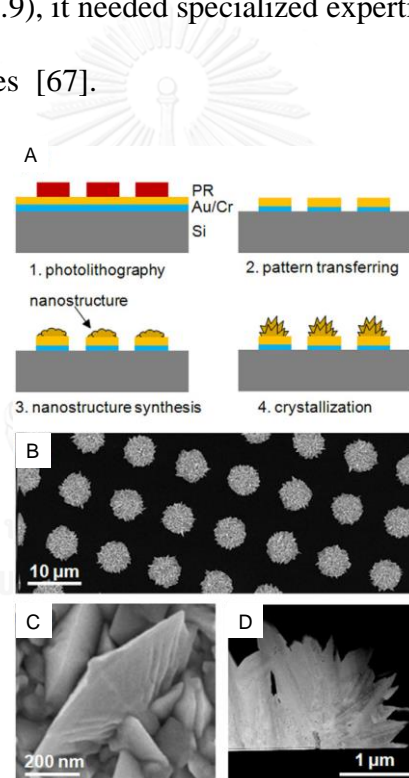
Figure 2.9   (A) Fabrication of the flower-like gold nanostructure array: a conventional lithography and etching technique were combined with an electrodeposition technique. (B) SEM image of the flower-like Au nanostructure array. (C) Close-up SEM image of leaf-like Au nanoflake. (D) Transmission electron microscope (TEM) image of the single Au nanostructure [67].

Unlike the electrochemical methods, the wet chemical procedures offer the effortless way to fabricate the flower-like gold nanostructures with industrial-scale production capability. The size and shape of the nanostructure can be regulated by altering of the synthesis condition (Figure 2.10). In this method, additives play the important role for the formation of the anisotropic nanostructures since they can function as capping agents, shape-directing agents and stabilizers. The specific adsorption on the crystal facets allows the modulation of the surface energy resulting in the modification of growth rate on those facets. This enables the morphological-controlled synthesis of the anisotropic nanostructures. Several additives were used for the fabrication of flower-like gold nanostructures such as 2-[4-(2-hydroxyethly)-1-piperazinyl]ethanesulfonic acid (HEPES) [57], dopamine [66], poly(vinyl pyrrolidone) (PVP), and sodium dodecyl sulfate (SDS) [72], gum Arabic [69] and bis-(amidoethylcarbamoylethyl) octadecylamine (C18N3) [4]. Although, the chemical methods provide the simple way with good morphological controlling, employing of nontoxic chemicals should be considered. Besides, it is a big challenge for scientists to develop a simple, environmentally friendly, inexpensive, and effective method for the fabrication of complex nanostructures.
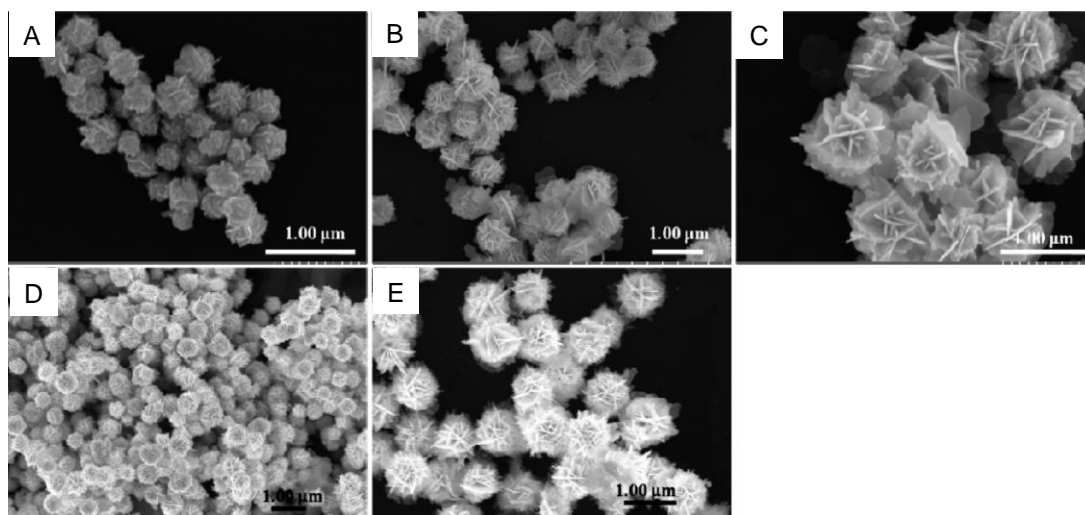
Figure 2.10 SEM images of Au nanostructures indicating the effect of the stabilizer
concentration on the morphology of the flowers. The flower obtained from
different concentrations of C18N3: (A) 0.1, (B) 0.3, (C) 0.4, (D) 0.5, and
(E) 0.6 mM. The concentration of $HAuCl_4$ and ascorbic acid are 1.6 mM
and 20 mM (0.2 mL), respectively [4].

CHAPTER III

EXPERIMENTAL SECTION

3.1 Chemicals

Hydrogen peroxide (H_2O_2, 30% w/w), soluble starch, nitric acid (HNO_3, 65% w/w), hydrochloric acid (HCl, 37% w/w), and sodium borohydride ($NaBH_4$) were purchased from Merck (Thailand). All chemicals were analytical grades and were used as received without additional purification. Gold beads ($\geq$ 99.99% purity, 1–2 mm diameter) were acquired from a local precious metal retailer (Gold Field Refinery Co. Ltd.). Before performing the experiment, all glassware and magnetic bars were cleaned with liquid detergent before submerging in aqua regia for 30 minutes, followed by consecutive rinsing with tap and deionized water. Caution: aqua regia (an extreme corrosive mixture between HCl and HNO_3 with a volume ratio of 3:1) must be handled with great care.

3.2 Preparation of Tetrachloroauric (III) Acid

A stock solution of tetrachloroauric (III) acid ($HAuCl_4$, 1 M) was prepared by dissolving the gold beads in aqua regia (60 mL) under mild stirring and heating (80–100 °C). After the complete dissolution of gold beads, the solution was further evaporated until the residual volume was 10 mL. The gold solution was cooled down to room temperature. The final volume of the solution was adjusted to 100 mL. The prepared gold solution was used as the gold ion source for further experiments.

3.3   Preparation of Gold Nanosheets and Flower-Like Gold Nanostructures

In this work, the preparations of gold nanosheets and flower-like gold nanostructures were accomplished by a simple wet chemical method as depicted in Figure 3.1. To prepare the extra-large gold nanosheets with flat surfaces, we performed the synthesis method as follows [32]. Briefly, in a 50 mL beaker, $HAuCl_4$ (51 µL, 1 M), starch solution (10 mL, 2% w/v) and deionized water (9.936 mL) were mixed under a vigorous stir for 1 h before an addition of H_2O_2 (13 mL, 30% w/w). H_2O_2 was employed as the sole reducing agent. Starch was employed as the stabilizer. The acidic solution with pH 2–pH 3 was further stirred for another 30 minutes before left undisturbed at room temperature overnight. The change of the pale yellow solution to a colorless solution with golden glittering suspension indicated a formation of gold nanosheets. The gold nanosheets were purified by ultracentrifugation and cleaned several time with hot deionized water before storage as an aqueous suspension for further characterizations. In order to evaluate an efficiency of the conversion of gold ions to gold nanosheets, a post reduction of the supernatant by sodium borohydride ($NaBH_4$) was performed. The colorlessness of the supernatant after addition of sodium borohydride indicated that the 100% conversion of gold ions to gold nanosheets was achieved.

To prepare flower-like gold nanostructures, we performed the same wet chemical reduction with a little modification. In general, to a 105 mL beaker, starch solution (25 mL, 2% w/v), $HAuCl_4$ (1.25 mL, 0.5 M) and deionized water (33.3 mL) were mixed together under vigorous stirring for 1 h before an addition of H_2O_2 (16.7 mL, 30% w/w). The solution was further stirred for another 10 minutes before incubation at ambient condition for 2 h. The transformation of pale yellow solution to a clear solution with

dark-brown precipitates together with the formation of air bubbles indicated the formation of flower-like gold nanostructures. The flower-like gold nanostructures were separated from the mixture by ultracentrifugation and were cleaned by hot deionized water. The flower-like gold nanostructures were kept as a suspension in aqueous media for further characterizations.
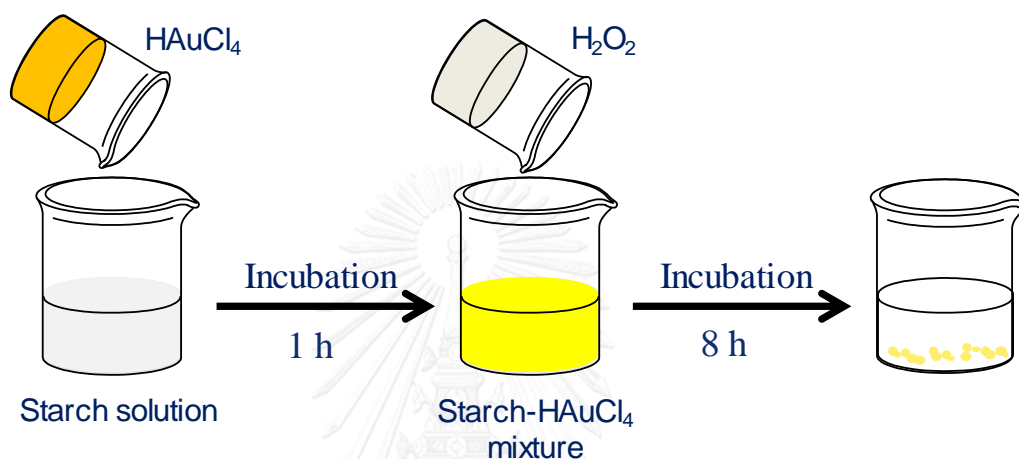
Figure 3.1   A diagram illustrates the synthesis of gold nanosheets and flower-like gold nanostructures.

3.4   Characterization

UV-visible absorption spectroscopy

For UV-visible absorption measurement, a quartz cuvette was used as a sample container. Deionized water was used as a blank sample. UV-visible absorption spectra were measured by a portable fiber optics spectrometer (Ocean Optics USB4000) equipped with a deuterium/halogen lamp light source (DH-2000, Micropack).

Scanning electron microscopy

The morphology of the gold nanosheets and flower-like gold nanostructures were investigated by SEM technique. The nanoparticle samples were dropped on aluminum

stubs and dried in a desiccator for 24 h before the measurement. The morphology of the nanoparticles was analyzed by a scanning electron microscope (JEOL JSM- 6510A, Analytical Scanning Electron Microscope) operated at 20 kV under a high vacuum mode.

Atomic force microscopy

To observe the surface topography of gold nanosheets and flower-like gold nanostructures using AFM technique, the samples were dropped and dried on cover slips for 1 h before performing AFM characterization. The topography measurements were performed on an atomic force microscope (AFM, SPA400). The micro cantilever type SI-DF20 were employed. The AFM measurements were operated in the dynamic force mode (DFM) with scanning frequency of 0.5-1 Hz.

X-ray diffraction

To obtain the crystallographic information of gold nanosheets and flower-like gold nanostructures, we conducted the XRD characterization. A sample was prepared by dropping the nanoparticles suspension onto an XRD sample holder. The holder was dried in the vacuum chamber for 1 h before soaking in hot water in order to remove the starch residue. The holder was dried in the vacuum chamber again for 1 h before performing XRD measurement. XRD characterization was performed on an X-ray diffractometer (Rigaku D/MAX-2200) operated under Cu radiation (40 kV, 30 mA). The diffraction angle covered 20–90 degree with a step size of 0.02 degree.

Raman spectroscopy

The molecular information of samples, e.g., starch and Rhodamine 6G (R6G), were characterized by Raman spectroscopy. The samples were prepared by dropping of the nanoparticles suspension on aluminum foil-covered glass slide. The samples were dried

in the vacuum chamber for 1 h before measurement. Raman characterizations were performed on a Raman spectrometer (DXR Raman Microscope, Thermo Scientific). A 532 nm laser was installed as a light source. The laser power was adjusted in the range of 1-10 mW. The laser aperture was 25 μm pinhole type.

CHAPTER IV

RESULTS AND DISCUSSION

4.1 Formation of Large H_2O_2-Reduced Gold Nanosheets via Starch-Induced Two-Dimensional Oriented Attachment [32]

4.1.1 H_2O_2 as a Green Reducing Agent

When $HAuCl_4$ and H_2O_2 solutions were mixed together under vigorous stirring for 10 minutes, a progress of the reaction could be noticed by an evolution of oxygen gas (due to the redox reaction and the catalytic decomposition of H_2O_2 on the surface of newly generated gold nanoparticles) and a pH drop with an increment of conductivity (due to a liberation of hydrochloric acid) [73, 74]. The bright yellow solution of $HAuCl_4$ was slowly faded and turned colorless within 26 minutes with a development of shiny gold precipitates. In accordance with the visual observation, the time dependent UV-visible spectra revealed the decrease of the absorptions at 313 and 390 nm assigned to ligand-to-metal charge transfer of square-planar halide complexes (Cl→Au) and weak d–d transition, respectively [75]. The spectroscopic change indicates a spontaneous reduction of gold ions to gold metal (Figure 4.1). According to the electrochemical potential under an acidic condition, H_2O_2 could reduce gold ion to gold metal as the net redox potential of the following redox reaction is positive [76].

$$AuCl_4^- + 3e^- \rightarrow Au + 4Cl^- \qquad\qquad E_{re} = +1.002\ V \quad (Eq.\ 4.1)$$

$$H_2O_2 \rightarrow O_2 + 2H^+ + 2e^- \qquad\qquad E_{ox} = -0.695\ V \quad (Eq.\ 4.2)$$

$$2AuCl_4^- + 3H_2O_2 \rightarrow 2Au + 3O_2 + 8Cl^- + 6H^+ \quad \Delta E_{cell} = +0.307\ V \quad (Eq.\ 4.3)$$
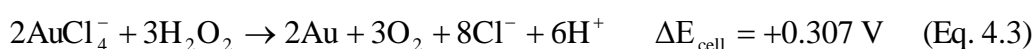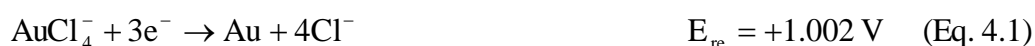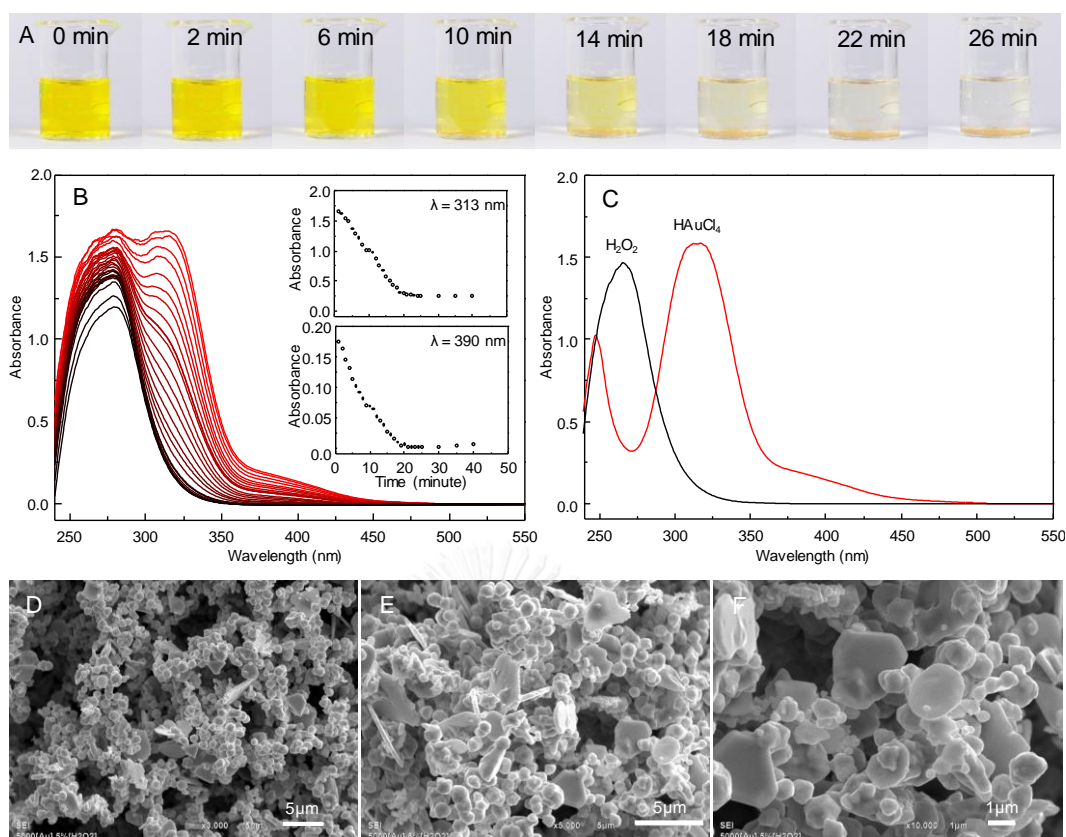
Figure 4.1 (A) Selected digital photographs of the solution containing HAuCl₄ (25.4 mM) and H₂O₂ (1,600 mM). A significant fading of the yellow color of the gold complex as well as a partial precipitation of gold particles were observed within 10 minutes after mixing. At 26 minutes after mixing, gold ions were completely reduced while all gold particles were precipitated. (B, C) UV-visible spectra of the solution corroborate the visual observation as the absorption of gold complex continuously decreases and completely disappears within 20 minutes. H₂O₂ was partially consumed due to the excessive concentration employed. (D-F) The obtained gold particles were hexagonal microplates and quasi-microspheres. Due to an absence of a stabilizer, aggregation among microplates and microspheres induce rapid a precipitation [32].

To realize the potential of H_2O_2 as an efficient reducing agent for anisotropic gold nanosheets synthesis, a concentration-dependent experiment was conducted under a stabilizer-free condition. The reduction of gold ions occurred at every employed concentration of H_2O_2 (Figure 4.2). However, the complete conversion was observed when the concentration of H_2O_2 was greater than 32 mM (Figure 4.2B–4.2F).
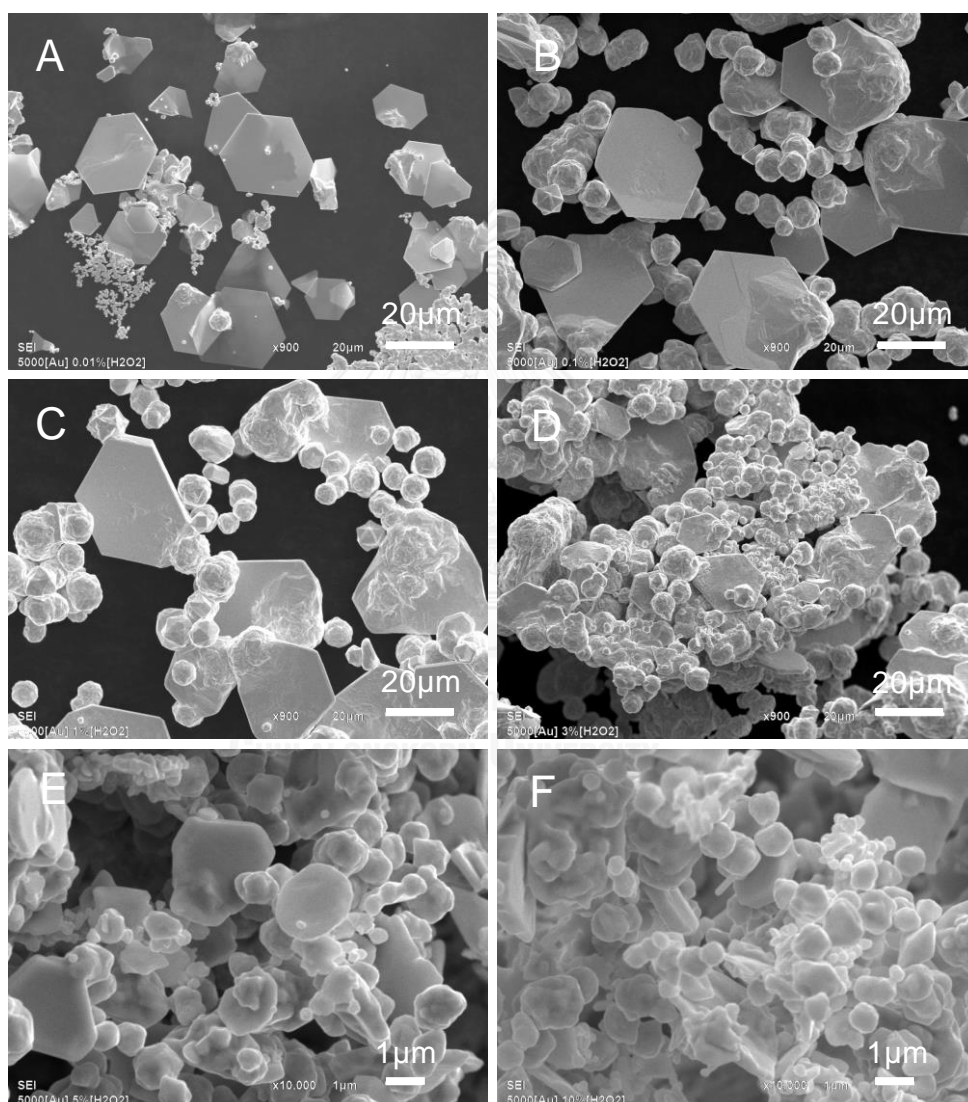
Figure 4.2 SEM micrographs of gold particles obtained by reducing $HAuCl_4$ (25.4 mM) with H_2O_2 of various concentrations: (A) 3.2, (B) 32, (C) 320, (D) 960, (E) 1,600, and (F) 3,200 mM. The reactions were conducted without a stabilizer [32].

Interestingly, under a dilute H_2O_2 of 3.2 mM, Figure 4.2A, almost all of the gold nanostructures were hexagonal microsheets (lateral size of 5–20 μm with thickness of 0.2–0.7 μm). There were some quasi-microspheres with diameter of 0.5–1.5 μm. When the concentration of H_2O_2 was increased to 32 and 320 mM, micrometer thick gold plates and quasi-microspheres with diameter of 5–10 μm were obtained with evidences of microsphere fusion onto the surfaces of gold plates (Figure 4.2B and 4.2C). The structural transition from microplates to quasi-microspheres indicates a rapid nucleation and growth of gold microstructures at high concentration of H_2O_2. Large microsheets with smooth surfaces (Figure 4.2A) disappeared when the concentration of H_2O_2 was further increased to 960, 1,600, and 3,200 mM (Figure 4.2D–4.2F). Most of the obtained gold microstructures were quasi-microspheres (diameter of 1–2 μm) with rough surfaces. Aggregations and fusions of microplates and quasi-microspheres resulted in a complete precipitation within 26 minutes (Figure 4.2D–4.2F and Figure 4.1D–4.1F).

The observed phenomena suggested that H_2O_2 is an efficient reducing agent for gold ions under an acidic condition. Unlike silver, gold is stable under the oxidative environment of H_2O_2. The H_2O_2-reduced gold micro/nanostructures survive the etching and continue growing into larger structures. Predominant thin microsheets produced at a very low concentration of H_2O_2 (Figure 4.2A) indicates a pivotal role of H_2O_2 on selectively preserving and promoting the growth of anisotropic microsheets. In the seed-meditated growth of silver nanoplates, the oxidative etching by H_2O_2 was exploited for selectively dissolving unstable seeds while preserving those with stacking faults. The survival seeds were then subjected to a facet controlled seed meditation growth imposed by surface binding ligands and stabilizers [77-79]. The observed

phenomena suggest that H_2O_2 plays the same role on the formation of anisotropic gold nanosheets as it does for silver nanoplates. However, in this case, H_2O_2 also functions as the reducing agent. A greater degree of supersaturation due to a greater rate of reduction at a higher H_2O_2 concentration results in the formation of quasi-microspheres with noticeable amount of pentagonal rods and decahedrons (Figure 4.2B–4.2D and Figure 4.3).
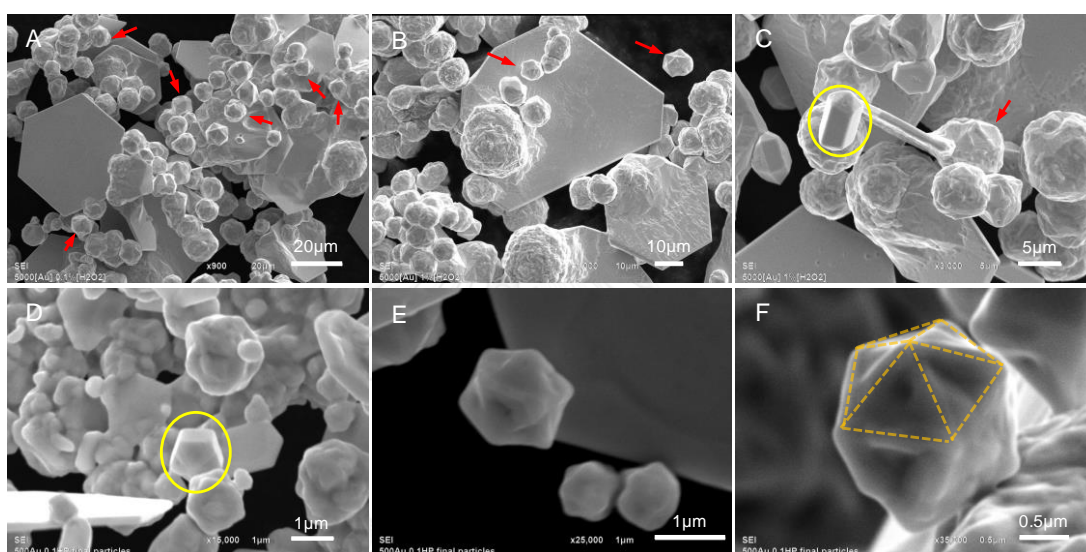
Figure 4.3 SEM micrographs of gold microparticles obtained from the reaction of HAuCl$_4$ (25.4 mM) and H_2O_2 concentration at 32 mM (A, D-F) and 320 mM (B and C) without starch stabilizer. The red arrows in (A), (B) and (C) indicate icosahedron gold quasi-microspheres. The yellow circles in (C) and (D) indicate pentagonal rods. (E and F) icosahedron quasi-microspheres generated during the growth process [32].

4.1.2 Gold Nanosheets with Starch Stabilization

Starch is a polysaccharide with multiple hydroxyl groups enabling a strong binding onto the gold surface [80]. It can also form a complex with gold ions and slow down the rate of reduction [10]. An experimental design imposing a slow reduction and growth of gold nanosheets was accomplished by employing low concentrations of H_2O_2 (6.4 mM) and $HAuCl_4$ (2.54 mM) under starch stabilization. In the system without starch (Figure 4.4A) thick microplates (average lateral size of 14 μm, thickness of 1– 1.5 μm) and quasi-microspheres with rough surfaces (average particle size of 6 μm) were obtained. When starch of any concentration was employed, nanosheets became the major product (Figure 4.4B–4.4F). At a low concentration of starch (0.1% w/v), however, an insufficient stabilization results in thick nanosheets (average lateral size of 8 μm, thickness of 70– 230 nm) with a significant amount of small quasi-microspheres (particles size of 1 μm) (Figure 4.4B). Aggregations of the microspheres and a non-uniform growth on the basal planes of the nanosheets were observed. When starch of greater concentrations (0.5%–2% w/v) were employed, large nanosheets with lateral size up to 20 μm with a thickness of 20 nm were obtained. Most of the nanosheets were hexagonal and truncated triangular with different degree of truncation. The triangular nanosheets were rarely observed. A drastic structural change from microplates and quasi-microspheres to nanosheets suggested that starch influences the formation and growth of the nanosheets and prevents the formation of quasi-microspheres. It can be attributed that starch also preferentially binds onto (111) facet of gold nanosheets, as the thickness of nanosheets was decreased when the concentration of starch was increased (Figure 4.5). Surprisingly, based on a statistical evaluation of 300 nanosheets,

the average size of nanosheets did not significantly change as the concentration of starch was increased. Albeit, the size distribution become broader (Figure 4.4G).
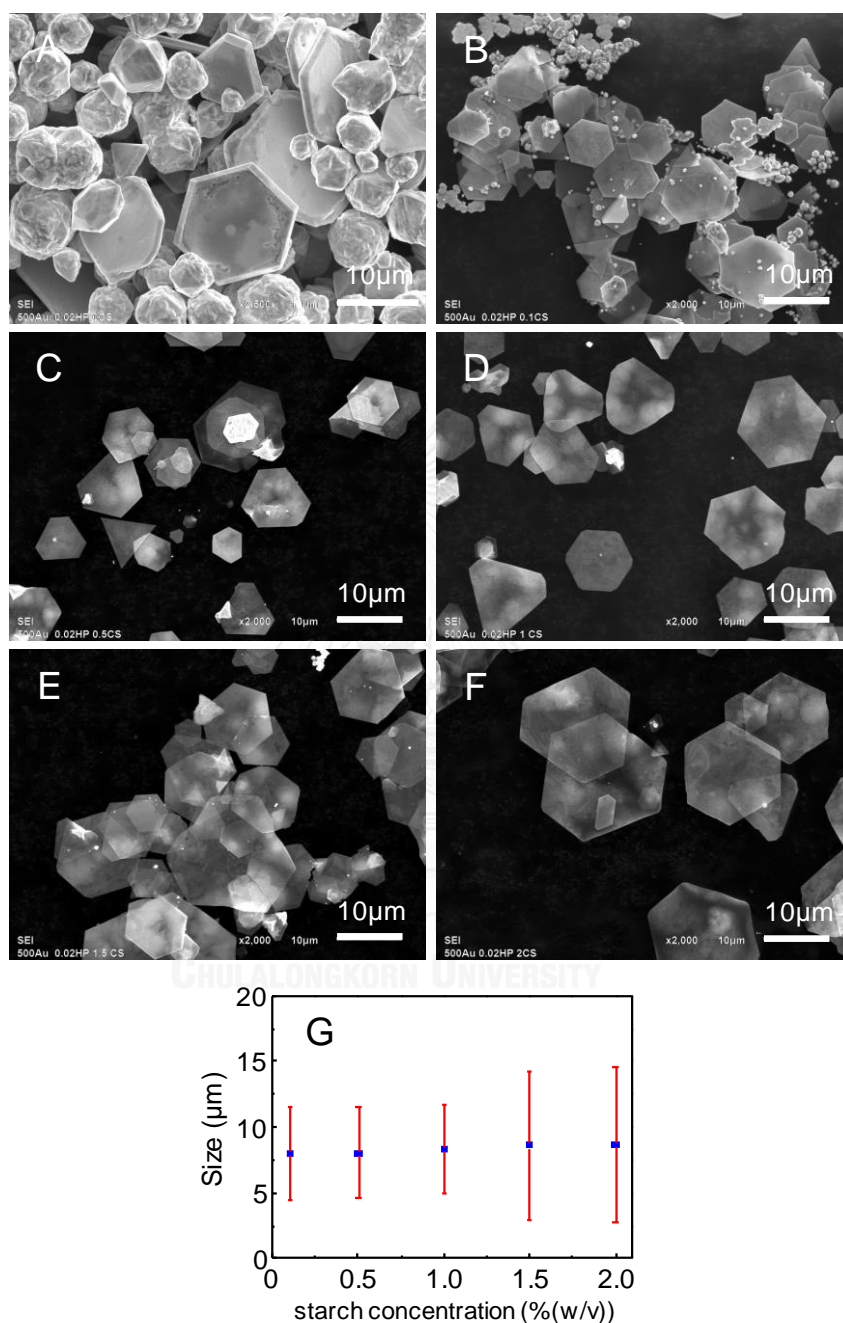
Figure 4.4 SEM micrographs of nanosheets reveal the influence of the starch concentration: (A) 0%, (B) 0.1%, (C) 0.5%, (D) 1%, (E) 1.5%, and (F) 2% w/v. The concentration of $HAuCl_4$ and H_2O_2 are 2.54 mM and 6.4 mM, respectively [32].
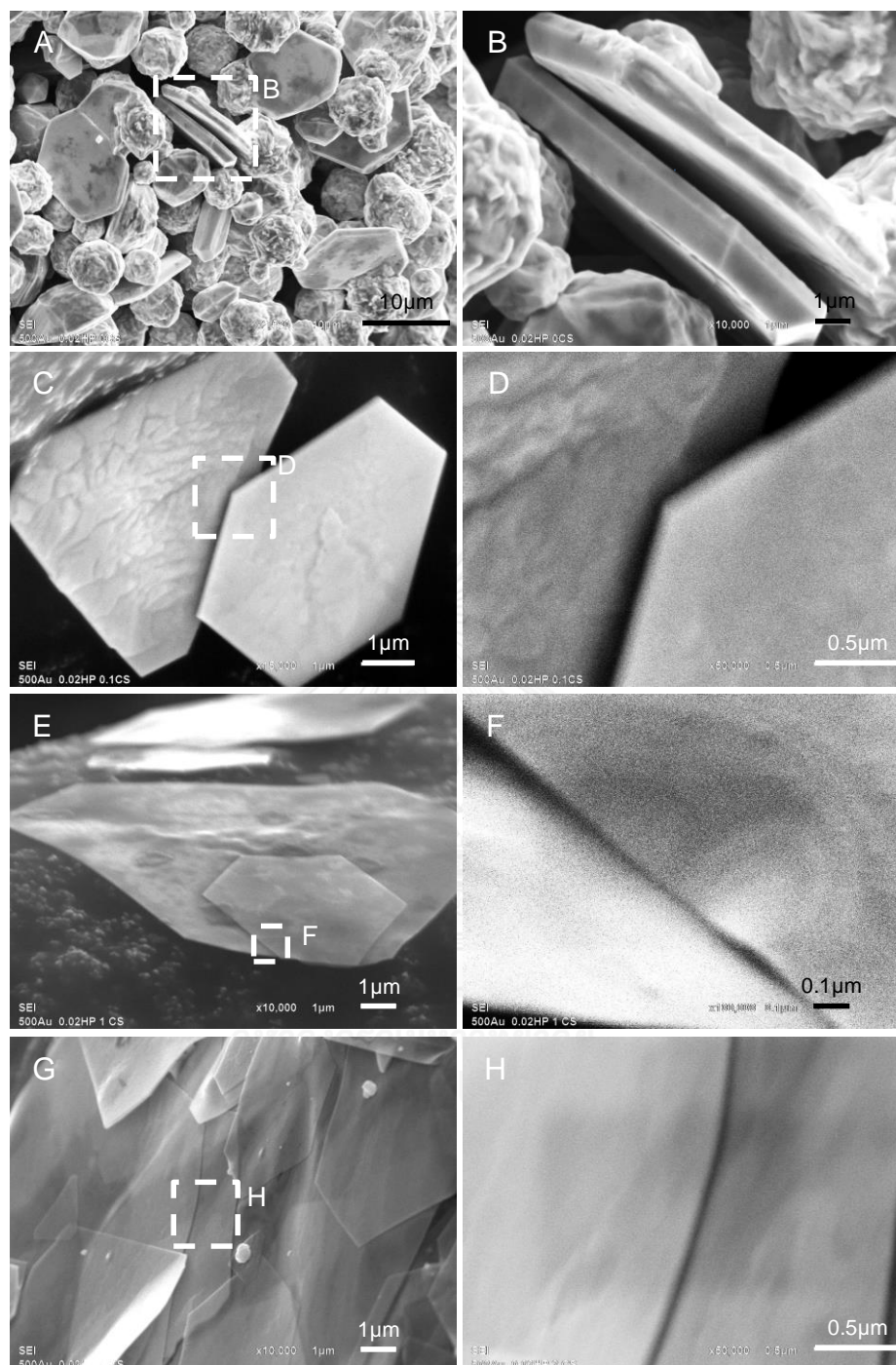
Figure 4.5 SEM micrographs of gold quasi-microspheres, microplates and nanosheets. The thickness of the nanosheets decreases as the concentrations of starch stabilizer was increased. Gold nanosheets were obtained from the reaction of 2.54 mM $HAuCl_4$, 6.4 mM H_2O_2 and starch: (A, B) 0%, (C, D) 0.1%, (E, F) 1% and (G, H) 2% w/v [32].

An OA seems to be the main growth mechanism for the rapid formation of the large nanosheets (Figure 4.4E and 4.2F). The distinct jagged edges together with frequent overlapping edges indicate an assembly of smaller nanosheets. The OA is an important crystal growth mechanism involving spontaneous self-organization of adjacent particles before merging together by the facets of the same crystallographic orientation [81-83]. The report on OA as the mechanism for the formation of micrometer-sized gold nanosheets in this work is one of the exploitations of two-dimensional OA for anisotropic gold nanosheet fabrication [84, 85]. It should be noted that the extra-large nanosheets with an average size of 20 μm could be synthesized within 10 h. For instance, in the system with a concentration of starch greater than 0.5% w/v, a 100% conversion of gold ions into gold nanostructures containing greater than 99% nanosheets was achieved (Figure 4.4E and 4.4F).

To gain an insight understanding on the formation of the large nanosheets via the OA mechanism, a detailed investigation was conducted. In Figure 4.6, the jagged edges generated at the boundary of the attached nanosheets (*i.e.*, due to an imperfect sharp tip and/or size mismatched) are indicated by arrows. An imperfect attachment which results in overlap or curl surfaces are indicated by circles. This imperfect attachment serves as an origin for edges and screw dislocation [86]. Crystals with flat surfaces, smooth edges, and sharp tips were finally obtained after a prolonged reaction (Figure 4.7). The smooth edges of nanosheets were the results of recrystallization, migration of surface atoms, and a filling of adatoms at the notches between imperfect attached edges [81-83, 87].
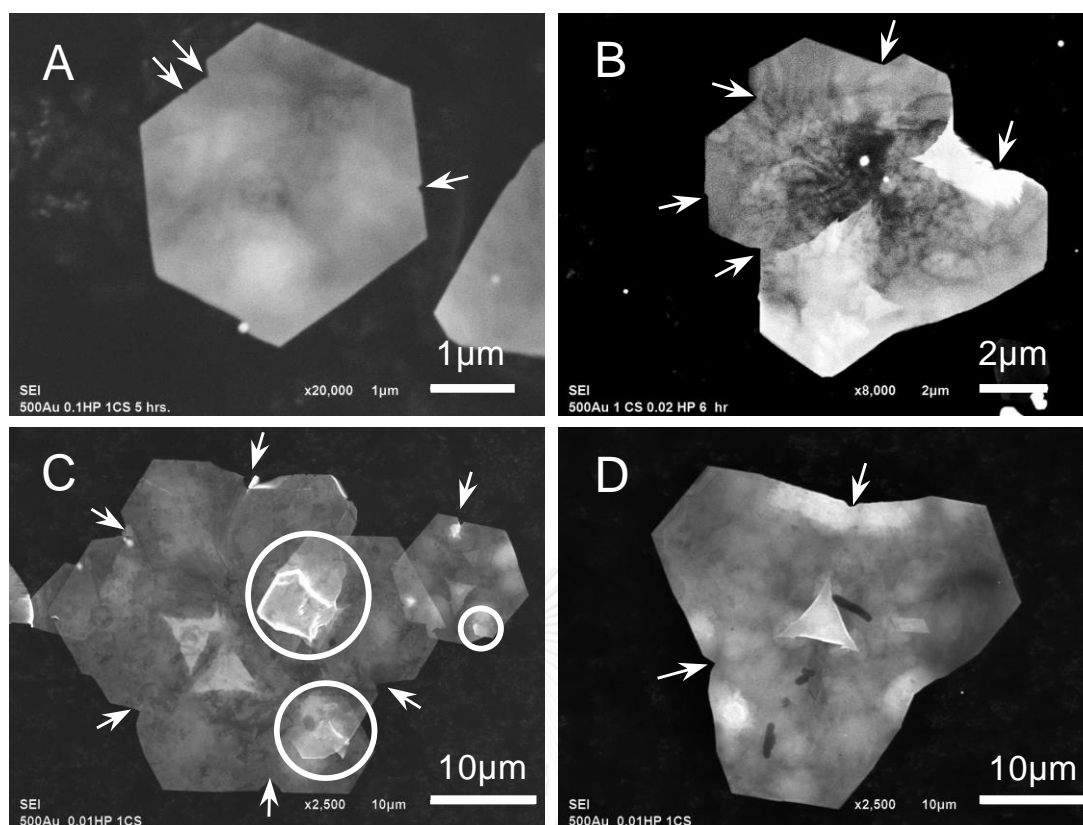
Figure 4.6 SEM micrographs reveal evidences of OA on the formation of small nanosheets (2–5 μm) and large nanosheets (30–40 μm). The small nanosheets are the assemble of smaller nanosheets/nanoplates. The jagged edges are indicated by arrows while overlapping edges are indicated by circles. The nanosheets were synthesized with 1% starch solution and 2.54 mM $HAuCl_4$. The concentrations of H_2O_2 were (A) 32, (B) 6.4, and (C, D) 3.2 mM [32].
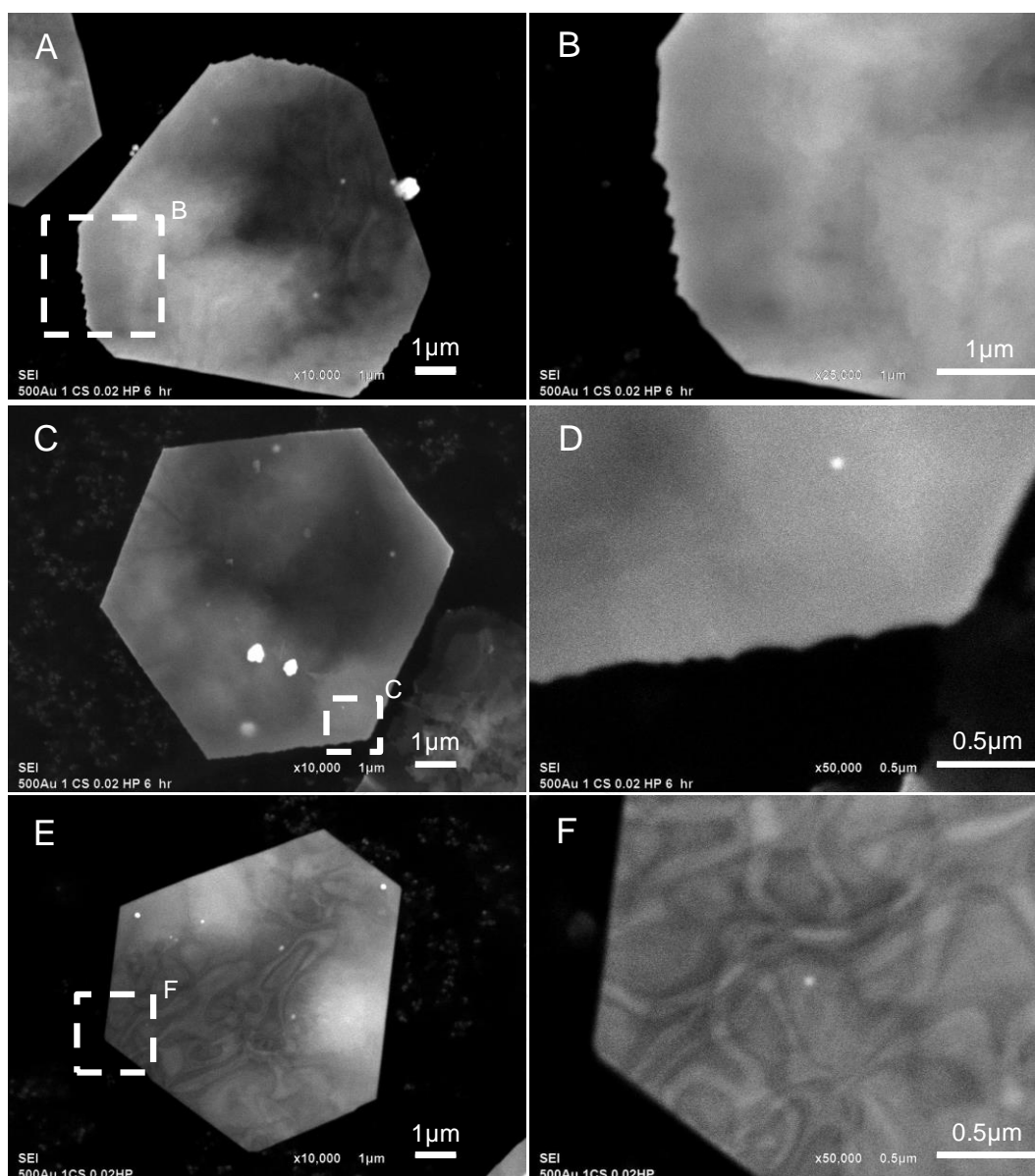
Figure 4.7   SEM micrographs show rough edges of growing gold nanosheets. During the growth process (6 h reaction time, A-D), the edges of the gold nanosheets can be etched by O_2/Cl- [88]. The recrystallization process smooths the rough edges after a prolonged reaction time of 10 h (E, F). Gold nanosheets were obtained from the reaction of 2.54 mM $HAuCl_4$, 6.4 mM H_2O_2 and 1% w/v starch [32].

Figure 4.8A–4.8F are AFM images of nanosheets after cleaning by boiling in hot water several times in order to remove the bound starch molecules on the basal plane. Each treatment took approximately 1 h. There was no starch fragment after the cleaning as the surface roughness of 0.6 nm of glass slide (Figure 4.8D and 4.8J) were in good agreement with those previously reported [89, 90]. The AFM images corroborate the passivation capability of starch as most of the starch molecules adhere onto the flat basal planes. The starch domains are ~100 nm in diameter and ~14 nm in height. When the nanosheets were cleaned with an alkaline peroxide solution (a solution of 30% H_2O_2 at pH 13 adjusted by 3 M NaOH), the residual starch could be noticed as chain-like domains (~100 nm in diameter, ~6 nm in height) (Figure 4.8H–4.8L). The residual starch (<50% of the original) left after a strong oxidative etching indicates a very strong adhesion of starch on the basal planes. AFM line maps in Figure 4.8F and 4.8L reveals the thicknesses of the nanosheets as 25 and 51 nm, respectively. The selective formation of plate structures and OA on the formation of large nanosheets indicates a pivotal role of starch as an effective surface passivating agent capable of selectively controlling the formation of anisotropic nanostructures. This observation is in good agreement with previous reports where a strong surface binding is required to shift the growth mechanism from Ostwald ripening (OR) to OA [81, 82]. Since gold nanostructures are relatively stable in the H_2O_2 environment, etching or dissolution of nanosheets in the reaction medium or H_2O_2 is limited.
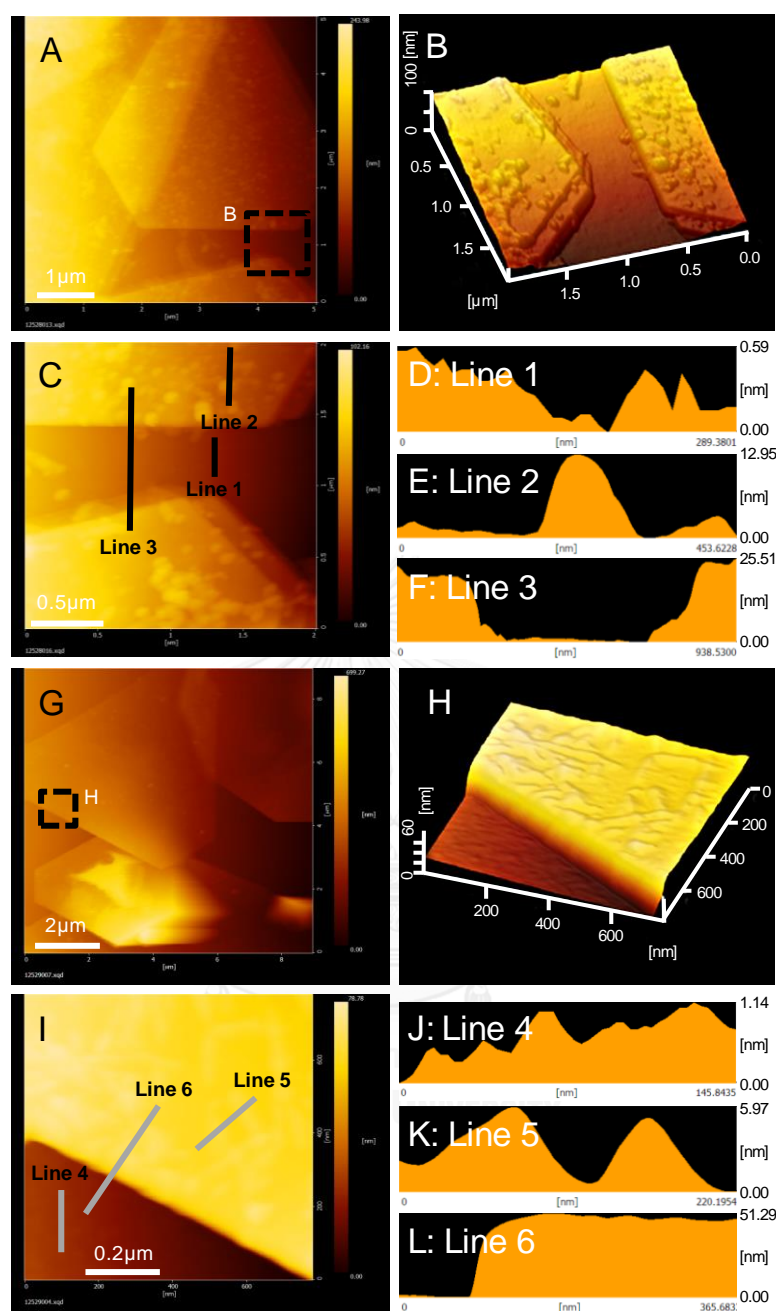
Figure 4.8 AFM images of gold nanosheets (A–F) before and (G–L) after a cleaning with an alkaline peroxide solution. Figure 4.8A, 4.8C, 4.8G, and 4.8H are topographic images. Figure 4.8B and 4.8H are 3D-images of selected areas. Figure 4.8D–4.8F and 4.8J–4.8L are line maps. The nanosheets were prepared by reducing $HAuCl_4$ (2.54 mM) with H_2O_2 (3.2 mM) under 1% starch stabilization [32].

4.1.3   Influence of the Concentration of HAuCl$_4$

An experimental investigation with different concentration of HAuCl$_4$ was conducted in order to verify the extent of nanosheets formation. At low concentration of HAuCl$_4$ (0.51 mM, Figure 4.9A) small nanosheets (1–2 μm) were created. The basal planes of the thin nanosheets are relatively smooth. Jagged edges and overlapping edges indicating an imperfect OA could be observed. As the concentration of HAuCl$_4$ was increased to 2.54 mM, the small nanosheets oriented attach into large nanosheets with an average size of 8 μm (Figure 4.9B). When the concentration of HAuCl$_4$ was further increased to 5.1, 12.7, and 25.4 mM, large nanosheets with average sizes of 23, 39, and 35 μm, were produced, respectively (Figure 4.9C–D). The OA seems to be the sole pathway for the formation of large nanosheets. However, at a high concentration of HAuCl$_4$, large nanosheets with uneven basal planes were obtained (Figure 4.9C–4.9E). The non-uniform thickness of nanosheets was originated from an uneven layer-by-layer epitaxial growth on the basal planes. Interestingly, the expansion of the epitaxial layer stopped at the edges of the basal planes (Figure 4.10). This growth behavior retained the plate structures as the thickness increased. The development of gold nanosheets (micrometer-sized plates with nanometer thickness) to gold microsheets (micrometer-sized plates with micrometer thickness) is realized at the high concentration of HAuCl$_4$. Under the employed conditions, an increment of the lateral size ceased when the concentration of HAuCl$_4$ was greater than 12.7 mM (Figure 4.9F). At a higher concentration, the gold structures grew in thickness rather than the lateral size. This phenomenon indicates an insufficient protection of the basal plane by starch molecules at a high concentration of HAuCl$_4$ as a large number of nanosheets was generated.
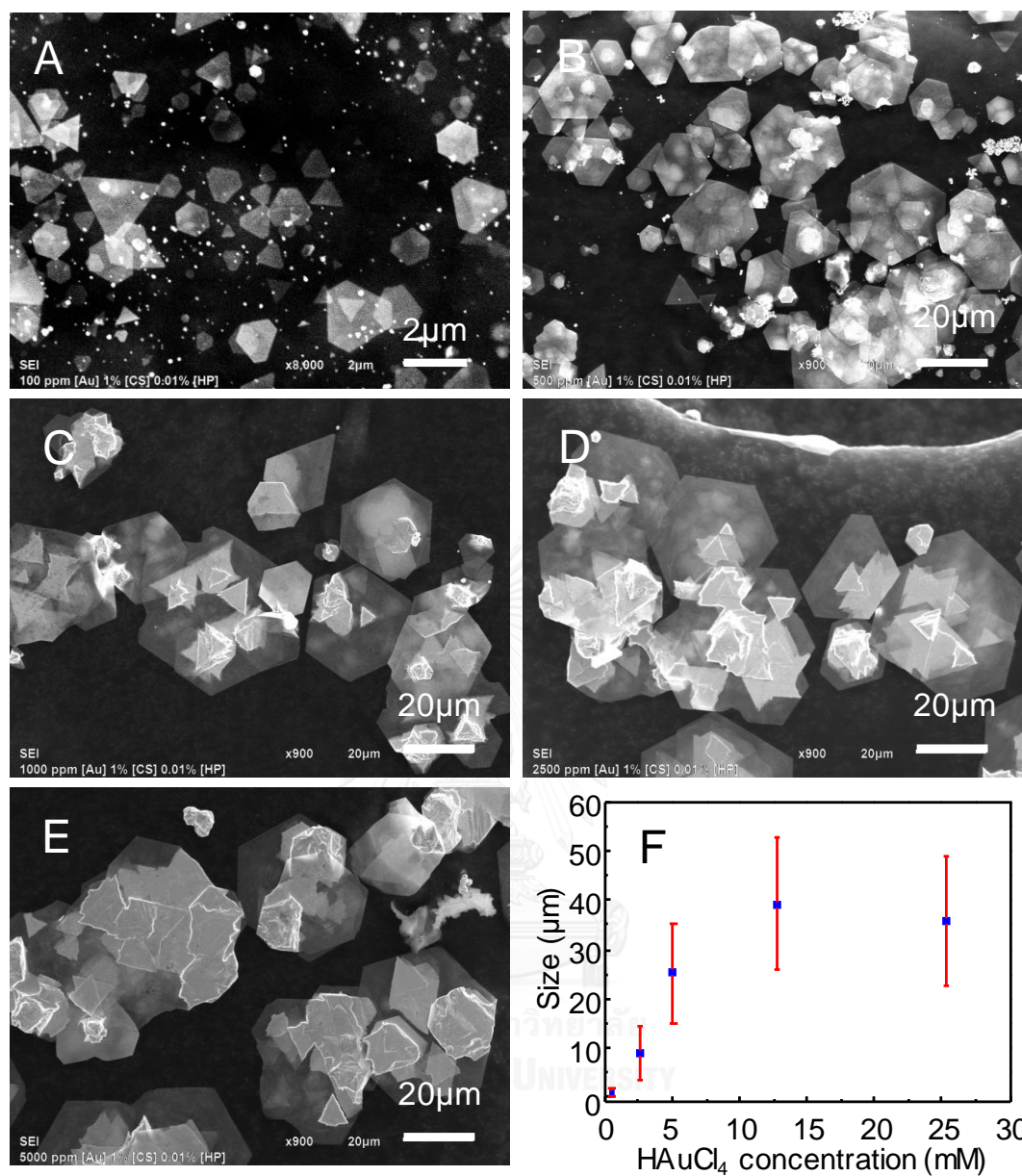
Figure 4.9 SEM micrographs of gold nanosheets obtained with different concentration of $HAuCl_4$: (A) 0.51, (B) 2.54, (C) 5.1, (D) 12.7, and (E) 25.4 mM. The average size was calculated from 300 nanosheets from dissimilar SEM micrographs (F). The concentrations of H_2O_2 and starch were 3.2 mM and 1% w/v, respectively [32].

Starch is a good stabilizer as an aggregation of starch-stabilized gold structures (microparticles, nanoplates, nanosheets, and microsheets) was not observed. However, long chain starch molecules are easily hydrolyzed to short fragments under an acidic condition [91-93]. The hydrolyzed starch may lose their surface passivation capability, which results in an epitaxial growth on the basal planes. The reducing sugars produce by acid hydrolysis of starch also possess weak reducing capability.
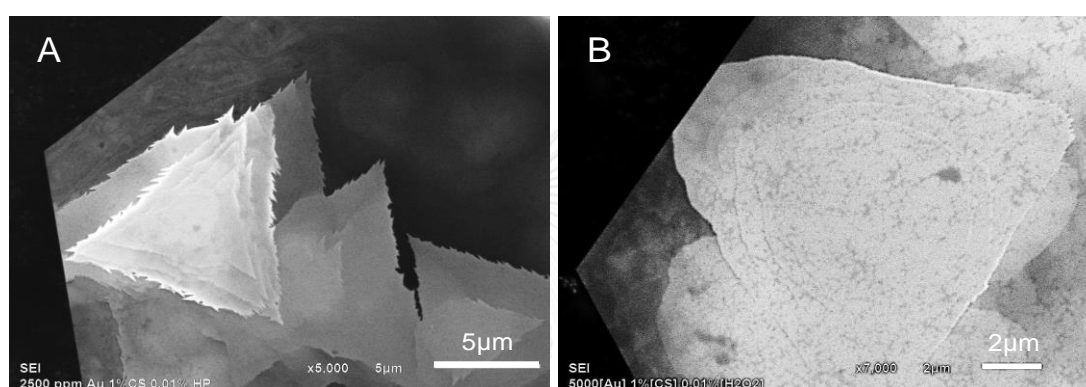
Figure 4.10 SEM micrographs show layer-by-layer epitaxial growth of gold film on the basal planes of gold nanosheets. The growth always ceases at the edge of the basal planes. Gold nanosheets were obtained from the reaction of (A) 12.7 mM and (B) 25.4 mM HAuCl$_4$, 3.2 mM H$_2$O$_2$ and 1% w/v starch [32].

4.1.4   Influence of the Concentration of H_2O_2

As the products with dominated plate structures were generated at low concentration of H_2O_2 (Figure 4.2), a detailed investigation of the H_2O_2 concentration (3.2–32 mM) was performed (Figure 4.11). Large nanosheets with an average size of 9 μm were obtained at a H_2O_2 concentration of 3.2 mM (Figure 4.11A). When the concentration was increased, an average size of nanosheets decreased to 2.5 μm (Figure 4.11G). Although the exact thickness of the nanosheets could not be obtained by SEM measurement due to a difficulty on vertical orientation of nanoplates, the obtained nanosheets were extremely thin as indicated by their relatively transparency. It should be noted that a significant number of spherical microparticles (0.5–1 μm) were also obtained at the high concentration of H_2O_2 (Figure 4.11E and 4.11F). This may be due to a rapid nucleation and growth of a large number of seeds at those concentrations. A large number of seed particles also lead to a small particle size as the limited metal ion supply was rapidly consumed [24, 94].
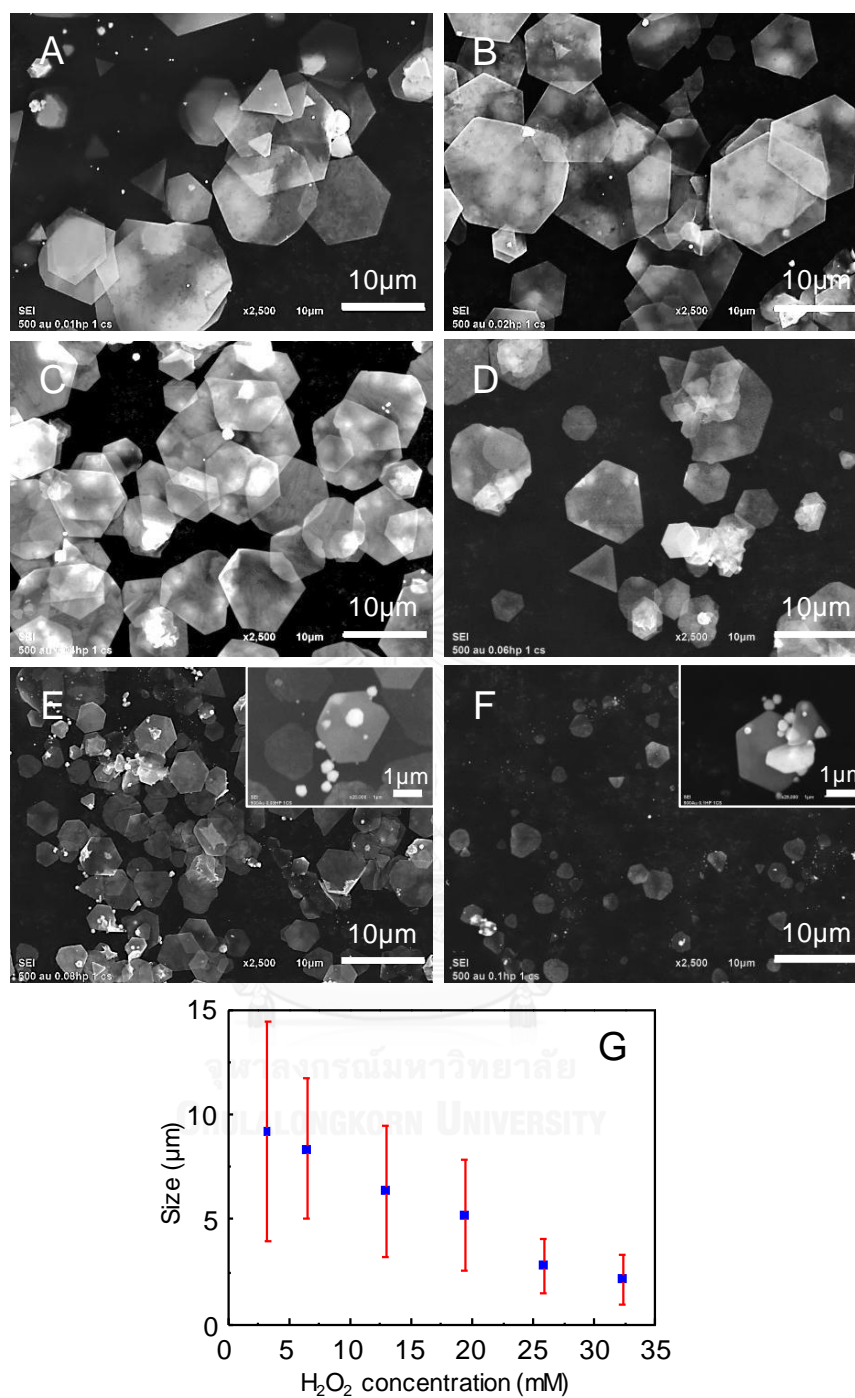
Figure 4.11 SEM micrographs of gold nanosheets synthesized under starch stabilization (1% w/v) with various concentration of H_2O_2 at (A) 3.2, (B) 6.4, (C) 9.6, (D) 19.2, (E) 25.6, and (F) 32 mM. The average size was calculated from 300 nanosheets from dissimilar SEM micrographs (G). The concentration of $HAuCl_4$ was 2.54 mM [32].

4.1.5 Growth Mechanism of Gold Nanosheets

Starch is an efficient stabilizer capable of promoting formation and growth of nanosheets by preferentially binding onto the basal planes. The surface protection assists the oriented attachment among appropriate facet-arranged nanoplates that leads to a rapid formation of extra-large nanosheets with a lateral size as large as 50 μm (Figure 4.9D and 4.9E). However, the passivation of starch is not strong enough as there was an epitaxial growth of gold layer on the basal plane, especially at high concentration of $HAuCl_4$ and/or low concentration of starch. Moreover, the starch chain is fragmented by hydrolysis under acidic conditions which renders lower stabilization capability at high concentration of $HAuCl_4$ (Figure 4.4B, and 4.9C–4.9E).

To gain an insight understanding on the growth mechanism of the nanosheets and quasi-microspheres, time-dependent structural evolutions were performed. Without starch, flower-like gold nanostructures containing several thin nano-petals formed at the early stage as shown in Figure 4.12A. The gap between petals was gradually filled as the particles grew into quasi-microspheres with rough surface (Figure 4.12B and 4.12C). However, for some particular nanostructures, a petal grew faster than the others and a thick gold microplate was generated, (Figure 4.12C and 4.12D). The reaction completed within 120 minutes while microparticles and microplates were obtained. When a greater concentration of H_2O_2 was employed, an even faster reaction occurred and quasi-microspheres were the sole product as shown in Figure 4.13.
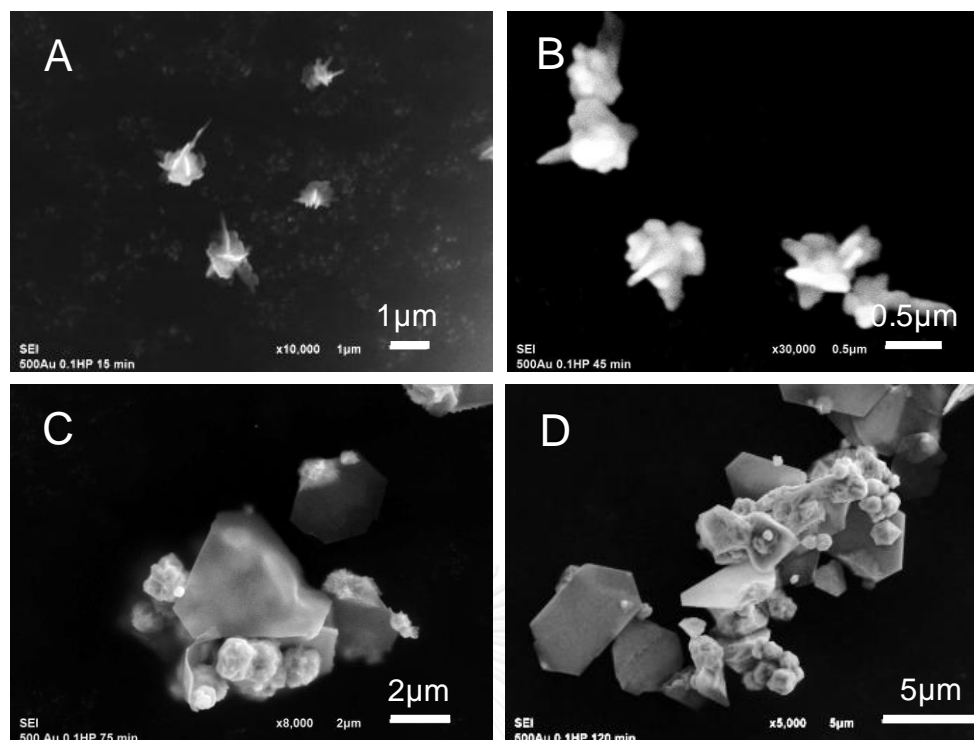
Figure 4.12 Time-dependent SEM micrographs reveal the development of quasi-microspheres from flower-like nanostructures in a system without starch stabilizer: (A) 15, (B) 45, (C) 75, and (C) 120 minutes. The HAuCl$_4$ solution (2.54 mM) was reduced by H$_2$O$_2$ (32 mM) [32].
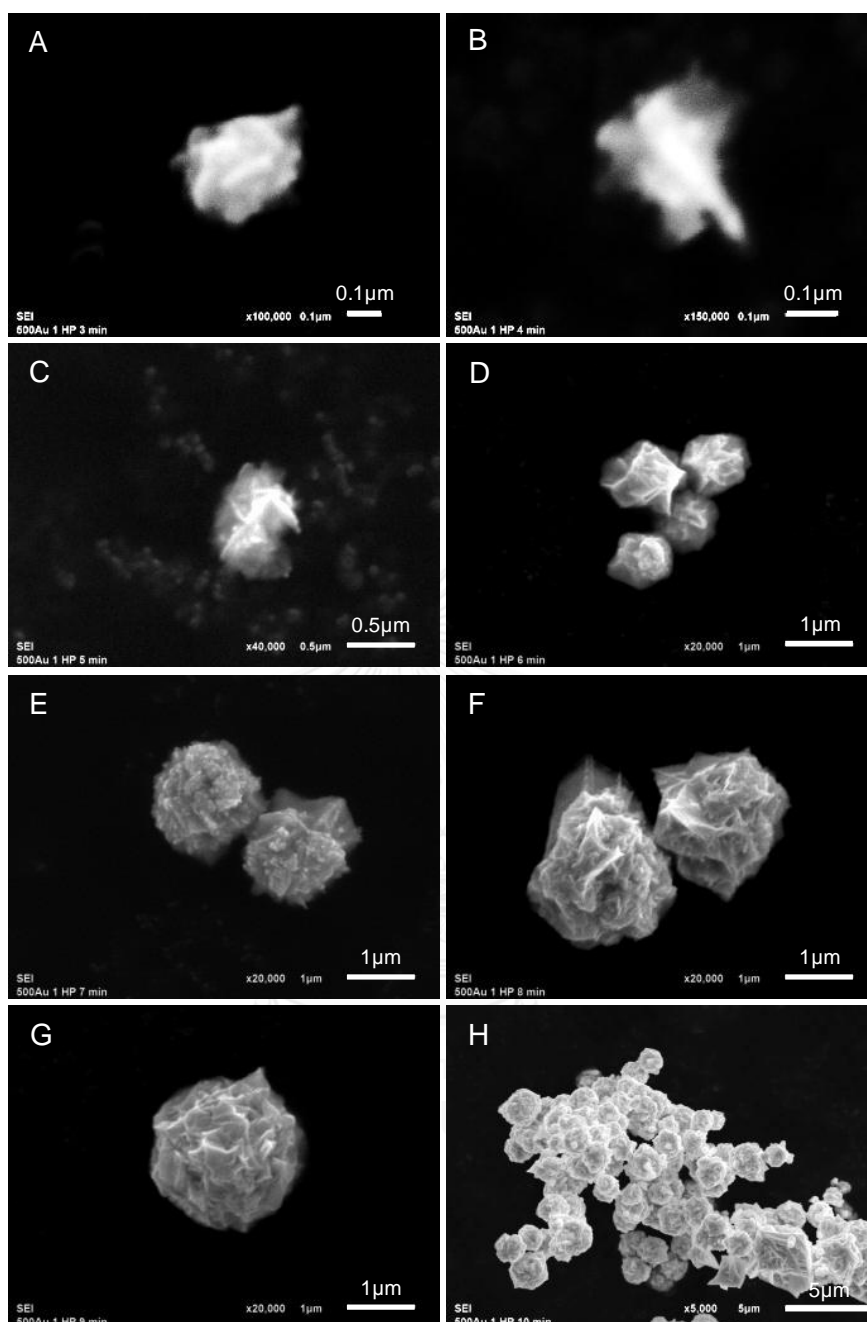
Figure 4.13 Time-dependent SEM micrographs show the development of quasi-spherical gold microparticles. The quasi-spherical gold microparticles were obtained from the reaction of HAuCl$_4$ (2.54 mM) and H$_2$O$_2$ (320 mM) without the starch stabilizer. The SEM micrographs were recorded at (A) 3, (B) 4, (C) 5, (D) 6, (E) 7, (F) 8, (G) 9 and (H) 10 minutes' reaction time [32].

When starch was employed, surprisingly, the same flower-like gold nanostructures also developed at the early stage (Figure 4.14A). However, the rate of reaction was slower than that in the system without starch. The flower-like nanostructures developed into nanoplates as a particular petal outgrew the others (Figure 4.14B). An evidence of the original flower-like structures could be noticed at the edge of some nanosheets (Figure 4.14C). The absence of this signature in some nanosheets is due to the outgrowth at the very early stage of the structural development. The flower-like nanostructures grew into hexagonal and truncated triangular nanosheets (Figure 4.14C and 4.14D). There are some small microspheres (~500 nm in diameter) observed in the system. However, when the rate of reaction was deliberately lowered by decreasing the concentration of H_2O_2 to 6.4 mM, nanosheets are the major product with a trace amount of small microspheres (Figure 4.15).
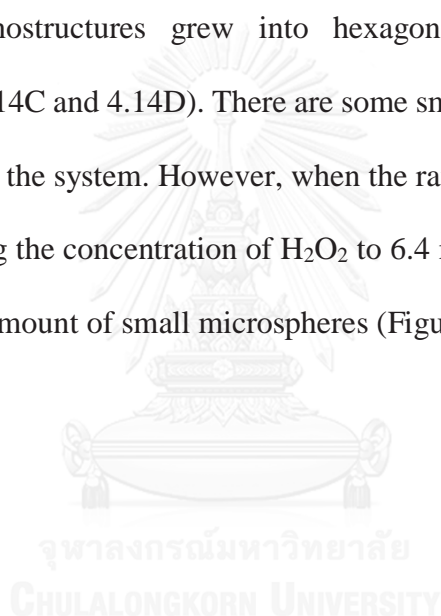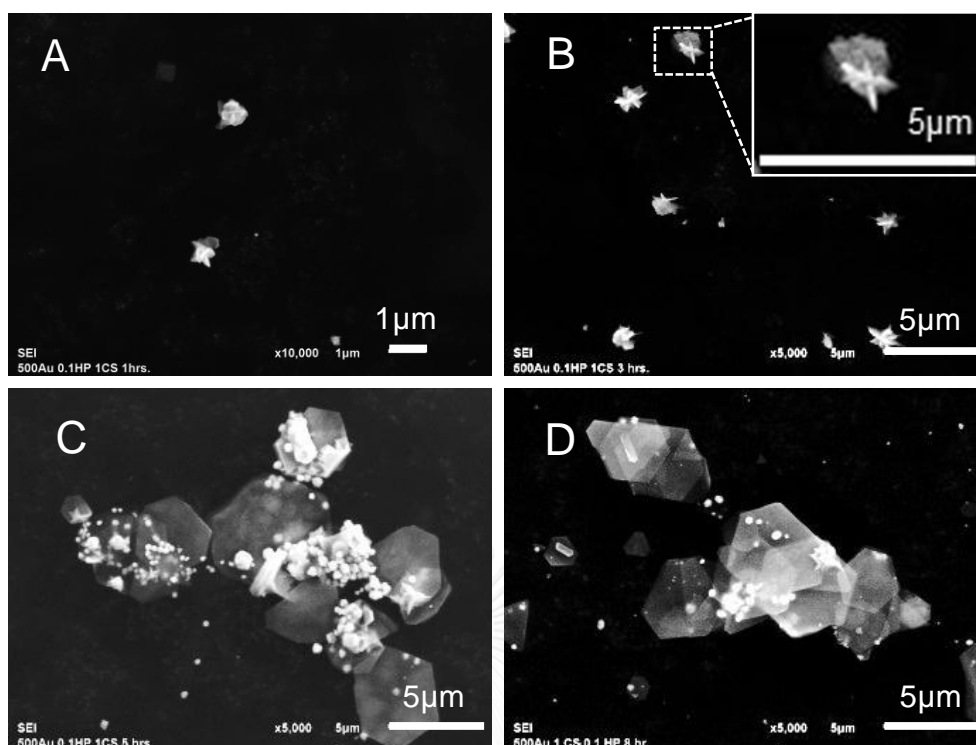
Figure 4.14 Time-dependent SEM micrographs reveal the development of nanosheets
from flower-like nanostructures in a system with starch stabilizer: (A) 1,
(B) 3, (C) 5, and (C) 8 h. The HAuCl$_4$ solution (2.54 mM) was reduced
by H$_2$O$_2$ (32 mM) under starch stabilization (1% w/v) [32].
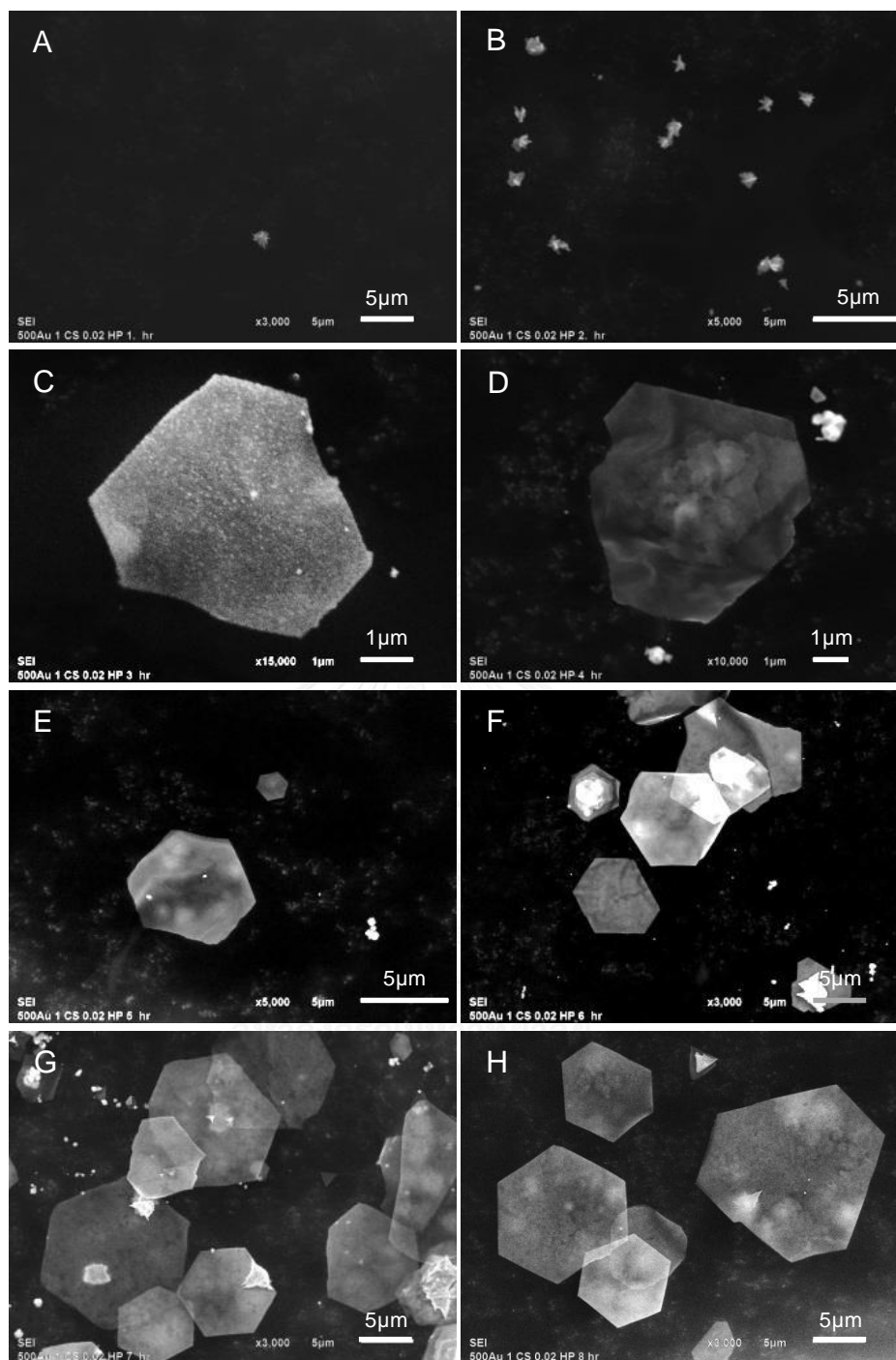
Figure 4.15 Time-dependent SEM micrographs show the development of gold nanosheets. The nanosheets were obtained from the reaction of HAuCl$_4$ (2.54 mM), H$_2$O$_2$ (6.4 mM), and starch (1% w/v). The SEM micrographs were recorded at (A) 1, (B) 2, (C) 3, (D) 4, (E) 5, (F) 6, (G) 7 and (H) 8 h reaction time [32].

Figure 4.16A shows a typical TEM image of large nanosheets. The stripes across the basal plane are originated by the bending of the thin nanosheet as it lies flat on the TEM grid. The selected area electron diffraction (SAED) pattern (Figure 4.16B) was obtained by coupling the electron beam perpendicular to the nanosheet. The hexagonal diffraction spots indicate that the nanosheet is a single crystal and the incident electron beam is perpendicular to {111} facet. In addition to the allowed {220} diffractions, the SAED pattern is dominated by the forbidden (1/3){422} diffractions normally observed in nanoplates and nanosheets with atomically flat surface of gold and silver [19, 95, 96].
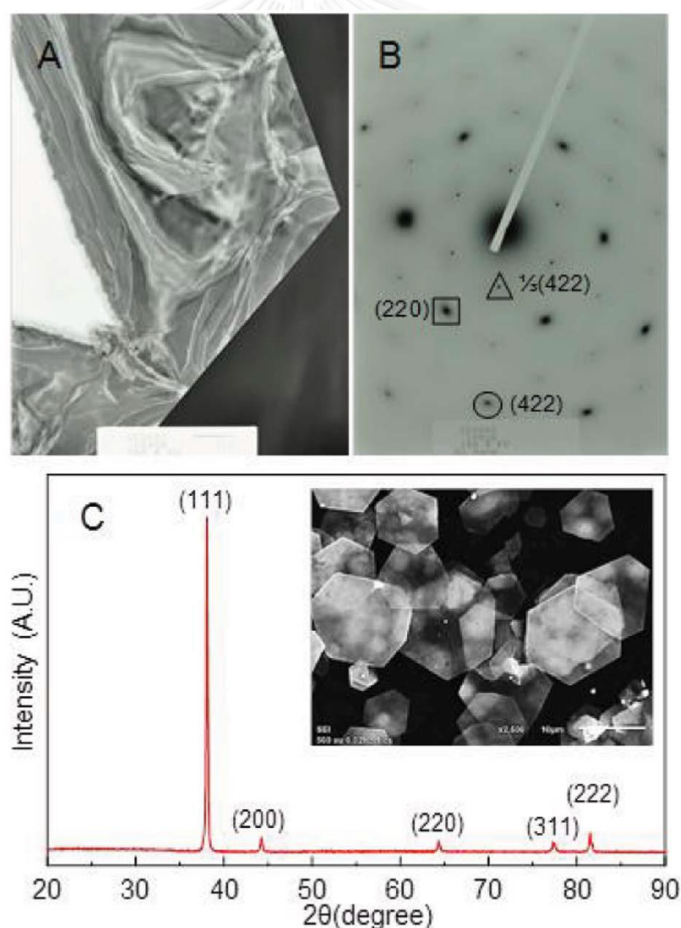
Figure 4.16 (A) A TEM image of a large nanosheet and (B) the corresponding SAED pattern. (C) XRD pattern of the nanosheets [32].

SAED pattern at different part of the large nanosheets were also collected (Figure 4.17). A re-alignment at each measured spot was performed in order to ensure a perpendicular incident of the electron beam. The exact same diffraction patterns confirm that the nanosheets are single crystals bound by {111} facets. The five sharp peaks of the XRD pattern in Figure 4.16C are assigned to {111}, {200}, {220}, {311}, and {222} planes of the face-centered cubic (fcc) crystal of gold. The {111} facets are the dominating facets as the nanosheets show an extremely low value of the relative diffraction intensities of (200)/(111) and (220)/(111) compared to those from the JCPDS 04-0784 standard file, *i.e.*, 0.051 vs. 0.53 and 0.037 vs. 0.33, respectively. Due to the relatively high aspect ratio of the nanosheets, their {111} planes are preferentially oriented parallel to the surface of the supporting substrate [19, 95, 96].

49
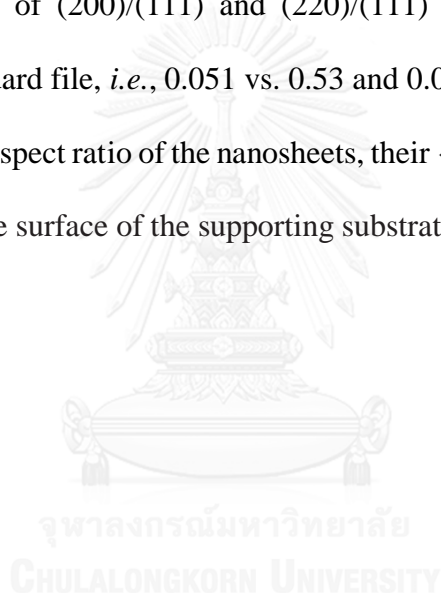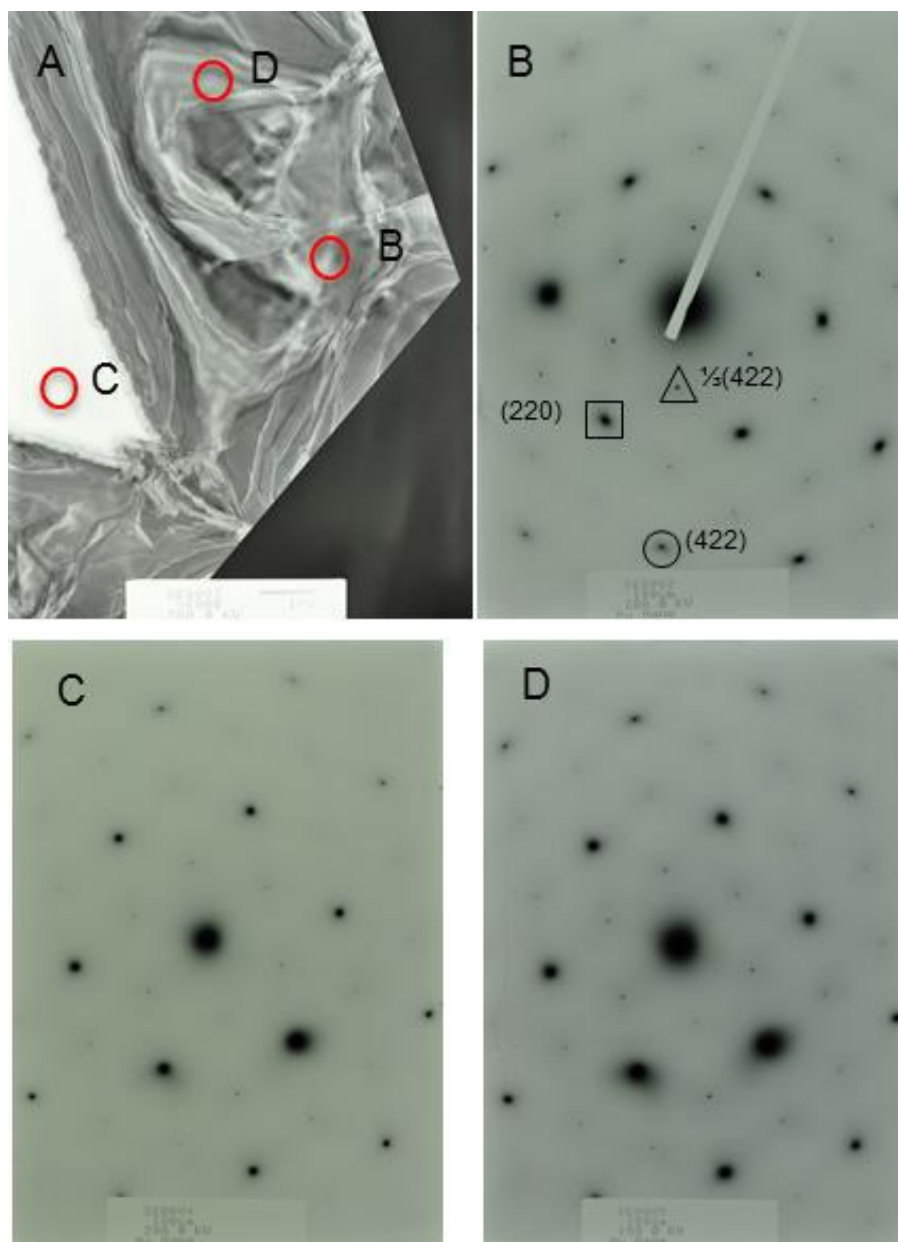
Figure 4.17 (A) TEM image of a nanosheet. The big nanosheets fill up the TEM frame even at a low resolution. (B-D) The corresponding SAED pattern of a nanosheets. The positions for the SAED measurements are indicated in the TEM image. The same SAED patterns with hexagonal diffraction spots confirm that the nanosheet is a single crystal bound by {111} facets [32].

Based on the observed phenomena, we proposed the growth mechanism of the nanosheets and the quasi-microspheres under the H_2O_2 reduction as follows. Gold ions are reduced by H_2O_2 and rapidly grown into flower-like nanostructures with nanometer thin petals (Figure 4.12A and 4.14A). The gaps between petals become active grooves for a deposition of adatoms [97]. Without starch, the flower-like nanoparticles symmetrically grow into quasi-microspheres by filling gold atoms in the gaps (Scheme 4.1). The rough surfaces are later generated by H_2O_2-assisted catalytic growth. However, microspheres with smoother surfaces are obtained under a lower concentration of H_2O_2 (Figure 4.2). When H_2O_2 of low concentration is employed, the rate of reduction is substantially decreased while a particular petal outgrows the others and further develops into a microsheet under a kinetically controlled condition (Figure 4.2 and 4.12). Without starch stabilization, gold microsheets are the dominant structure under a low concentration of H_2O_2 while the quasi-microspheres are dominated at a higher concentration.

In the system with starch stabilization (Scheme 4.2) the surfaces of the flower-like nanostructures are covered while the gap-filling growth mechanism is prevented. The starch stabilization, on the other hand, promotes the lateral growth of petals. The starch-stabilized nanoplates and nanosheets later grow into larger nanosheets via an OA mechanism pathway.
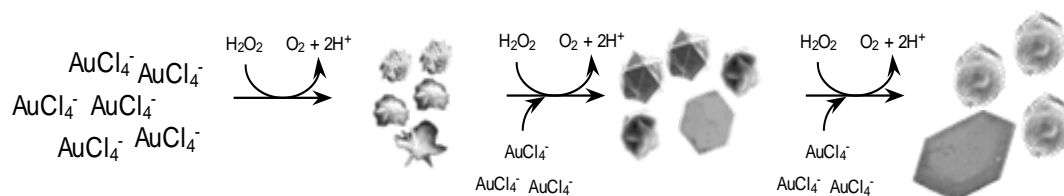
Scheme 4.1 Proposed growth mechanism of the gold quasi-microspheres in the system without starch stabilizer [32].
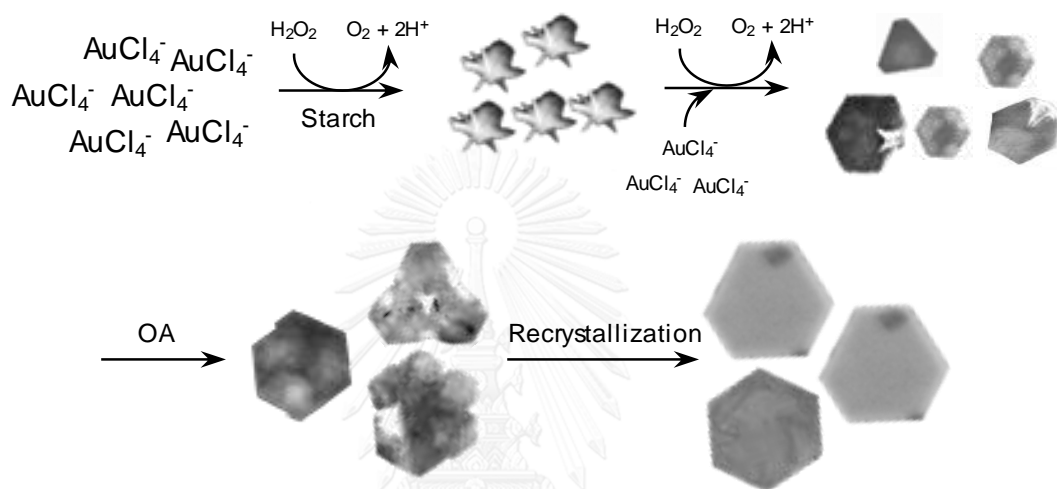
Scheme 4.2 Proposed growth mechanism of the gold nanosheets in the system with starch stabilizer [32].

To explore the potential of our developed green chemical method, a large-scale production of gold nanosheets was performed by a 5 L batch synthesis. The 2.5 g of gold nanosheets with glittering reflection was successfully produced within 10 h. The hexagonal shape nanosheets (lateral size up to 20 μm and thickness of 20–50 nm) are well separated as indicated by the digital photographs, optical micrographs, and SEM micrographs (Figure 4.18). An evidence of OA could be noticed. After the separation of the nanosheets, the post reduction of the supernatant was performed. A development of red gold nanospheres after the sodium borohydride reduction was not observed since

all gold ions were converted to gold nanosheets. Moreover, a 100% selective formation of gold nanosheets was achieved. The acidic supernatant (~pH 2) was neutralized before discharging.

Some potential applications of the gold nanosheets were explored. Although the nanosheets themselves do not have surface-enhanced Raman scattering capability, it can facilitate the SERS phenomenon. The piranha-solution-cleaned nanosheets are free of starch and function as an excellent support for metal nanoparticles. The gold-nanoparticles-decorated nanosheets greatly enhance the scattering intensity as the gaps between nanoparticles and the flat surface of nanosheets become excellent hot spots for SERS measurement (Figure 4.19A). The nanosheets with shiny reflection can be employed as authentication marks in security printing. The gold nanosheets were trailed as a pigment for security printing by mixing with ink. The shiny feature of the gold nanosheet can be easily observed underneath a red ink when viewing under a microscope (Figure 4.19E and 4.19F). A potential application of nanosheet as a pigment for security printing with SERS-assisted molecular tag is being investigated. The gold nanosheets were also exploited as an alternative gold pigment for traditional drawing. Figure 4.19G shows a traditional Thai drawing of a character in the Ramayana Epics made of gold ink (*i.e.*, a mixture of gold nanosheets and a binder) on a silk fabric (100 cm $\times$ 80 cm). The soft and flexible nanosheets adhere very well along the curve surface of silk threads. We plan to use gold-nanosheets ink for traditional art and cultural conservations.
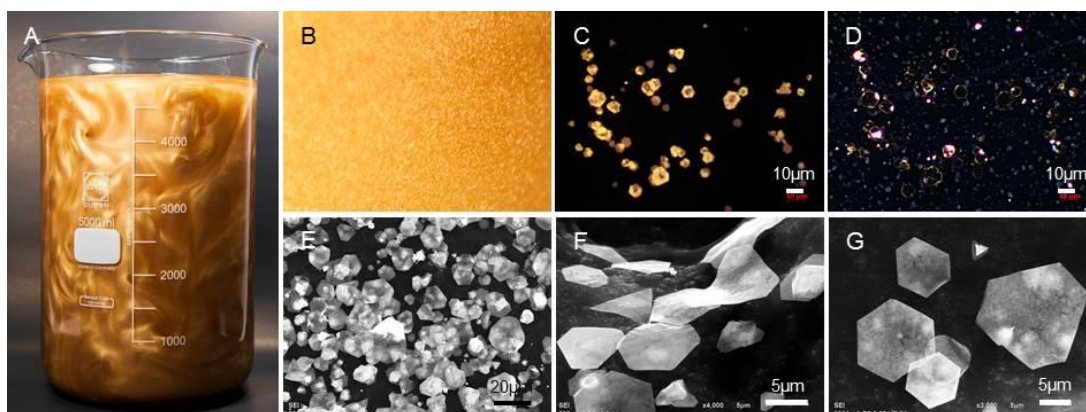
Figure 4.18 A 5 L batch synthesis of gold nanosheets by reducing a 2.54 mM HAuCl$_4$ with 6.4 mM H$_2$O$_2$ under a 1% starch stabilization. A complete conversion of gold ions into nanosheets was achieved within 10 h. (A) A digital photograph depicts the glittering reflection of the gold nanosheets. (B) A close-up digital photograph (100X magnification) reveals the dispersed gold nanosheets. (C, D) Optical micrographs of the gold nanosheets under bright field and dark field illuminations, respectively. (E–G) SEM micrographs of the hexagonal and triangular gold nanosheets mass-scale produced by the developed method [32].
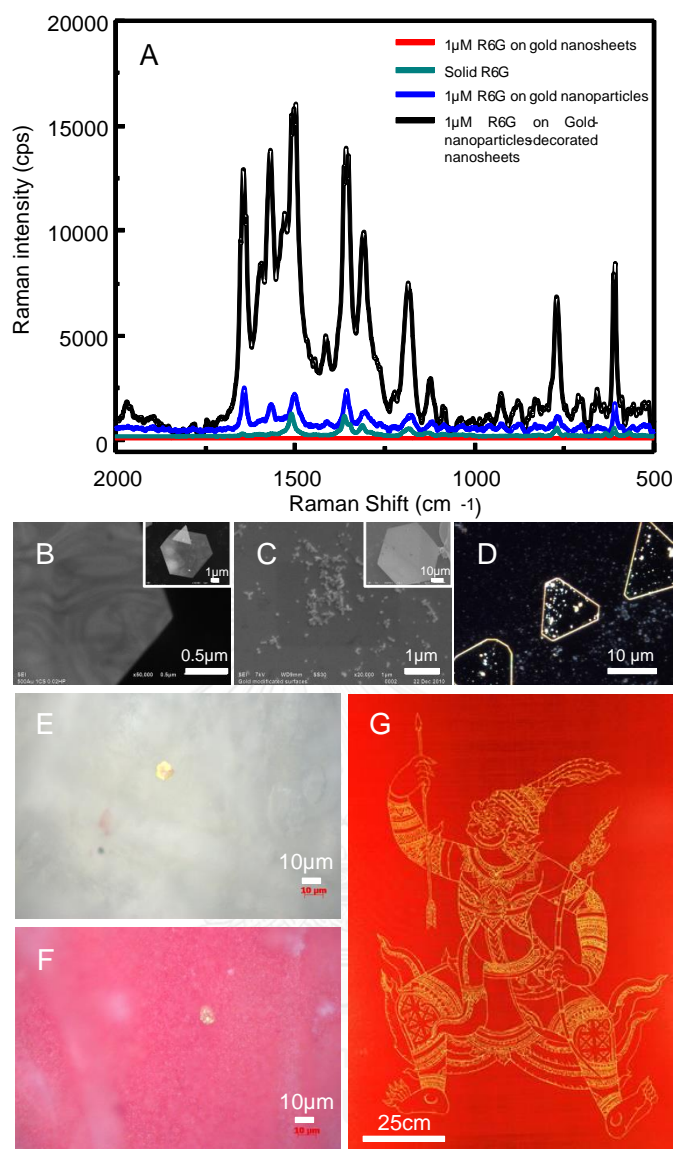
Figure 4.19 Some applications of gold nanosheets as substrate in SERS applications, markers in security printing and gold pigment. (A) SERS spectra of R6G on different gold substrates. (B) Gold nanosheets after cleaning with piranha solution. Gold-nanoparticles-decorated nanosheets: (C) a SEM micrograph and (D) an optical microscope image under a dark-field illumination. (E, F) Gold nanosheet impregnated in colorless and red inks, respectively, used for banknote printing. (G) A traditional Thai drawing made of gold-nanosheets ink on a red silk fabric [32].

4.2 Structural Evolution of Starch-stabilized Gold Nanosheets to Flower-Like Gold Nanostructures Induced by H_2O_2

4.2.1 Formation of Flower-Like Gold Nanostructures

Our previous section demonstrated the synthesis of gold nanosheets using H_2O_2 as a reducing agent and starch as a stabilizer. The combinations between mild reducing capability of H_2O_2 and stabilizing power of starch enable the synthesis of anisotropic nanostructures. Adjustment of H_2O_2 and starch concentration was performed in order to tune the reduction kinetic and degree of stabilization, respectively. The reduction of 2.54 mM $HAuCl_4$ by 6.4 mM H_2O_2 in 1% w/v starch solution was employed for synthesis gold nanosheets (average size of ~8 μm with the thickness of 20–50 nm), (Fig 4.20A). In addition, low concentration of H_2O_2 enables slow reduction rate facilitating the formation of gold nanosheets. When the rate of reduction is relatively slow, the nucleation and growth are subjected to kinetic controls that provide the formation of plate-like seeds that will further grow to the plate-like nanostructures [98, 99]. The growth of plate-like seeds to nanosheets is also promoted by starch due to its preferential binding ability on {111} facet of gold nanosheets [10, 32].

By performing of an experiment at harsh condition (the reduction of 25.4 mM $HAuCl_4$ by 3.2 M H_2O_2 in the system without starch), the quasi-microspheres were obtained as major product with some exciting of polyhedral gold microstructures (Figure 4.20B and Figure 4.21). The size of gold microparticles is 1.2 μm. The partial fusion of stabilized-free gold microparticles could be observed. This can be due to a superior degree of super saturation as a greater number of gold atoms are rapidly generated. Note that, small number gold microsheets were observed (Figure 4.21).

A

[AuCl$_4$]$^-$
[AuCl$_4$]$^-$
    [AuCl$_4$]$^-$
[AuCl$_4$]$^-$
    [AuCl$_4$]$^-$
[AuCl$_4$]$^-$

$\xrightarrow[\text{low [H}_2\text{O}_2\text{]}]{\text{starch}}$

B

[AuCl$_4$]$^-$
[AuCl$_4$]$^-$
    [AuCl$_4$]$^-$
[AuCl$_4$]$^-$
    [AuCl$_4$]$^-$
[AuCl$_4$]$^-$

$\xrightarrow[\text{high [H}_2\text{O}_2\text{]}]{\text{no starch}}$
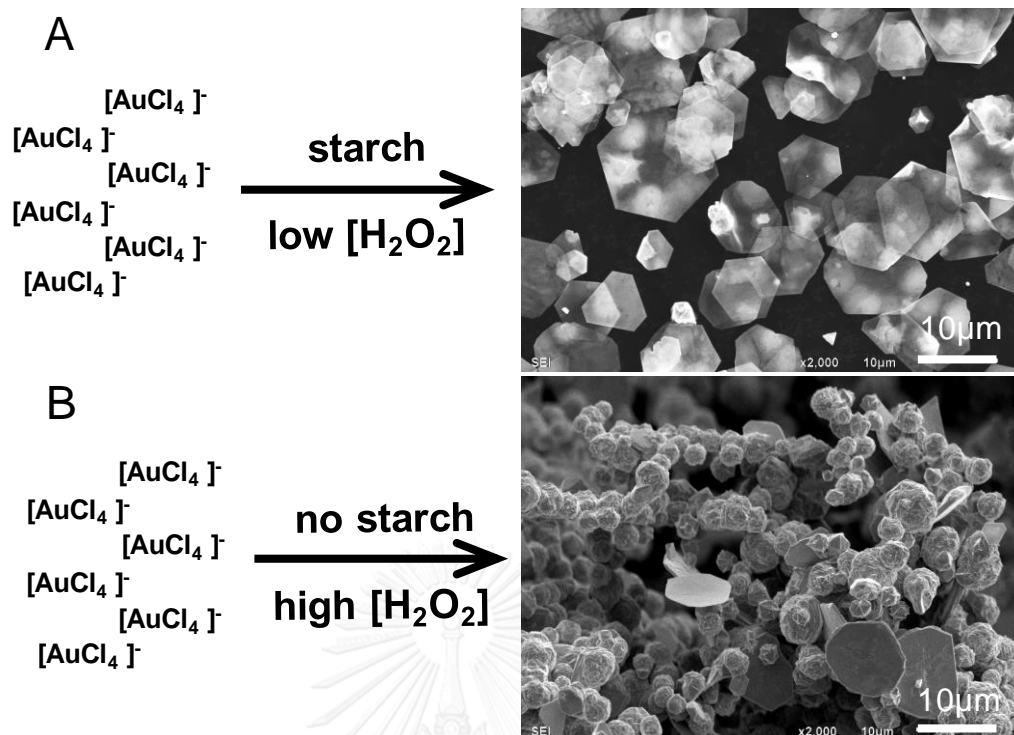
Figure 4.20 Diagram illustrated the preparation of gold nanosheets (A) and gold microparticles (B). Gold nanosheets were obtained from the reaction between 2.54 mM HAuCl$_4$ and 6.4 mM H$_2$O$_2$ in 1% w/v starch solution. Gold microparticles were prepared by a reduction of 25.4 mM HAuCl$_4$ with 3.2 M H$_2$O$_2$.

As we interested in the synthesis of nanostructure by manipulation of reduction kinetic and degree of stabilization, it is interesting to perform the reduction of gold ions with drastically different concentration of H_2O_2 under stabilization condition. The preliminary experiment was performed by the reduction of 2.54 mM $HAuCl_4$ with H_2O_2 in 1% w/v starch solution. The concentration of H_2O_2 was extremely varied. Figure 4.22 shows the SEM images of the gold nanostructures achieved from the reaction. At very low concentration of H_2O_2 (3.2 mM), the gold nanosheets were generated as a major product with the size as large as 15 μm (Figure 4.22A and Figure 4.23). Raising of H_2O_2 concentration from 3.2 to 32 mM caused the decrease of the particle size of gold nanosheets from 9.2 μm to 2.2 μm (Figure 4.23) with a few occurrences of small quasi-spherical shape gold microparticles (Figure 4.22A and 4.22B). The decrease of the size of nanosheets can be attributed to the limitation of metal precursor as it was rapidly consumed at the early state of the growth of nanosheets.
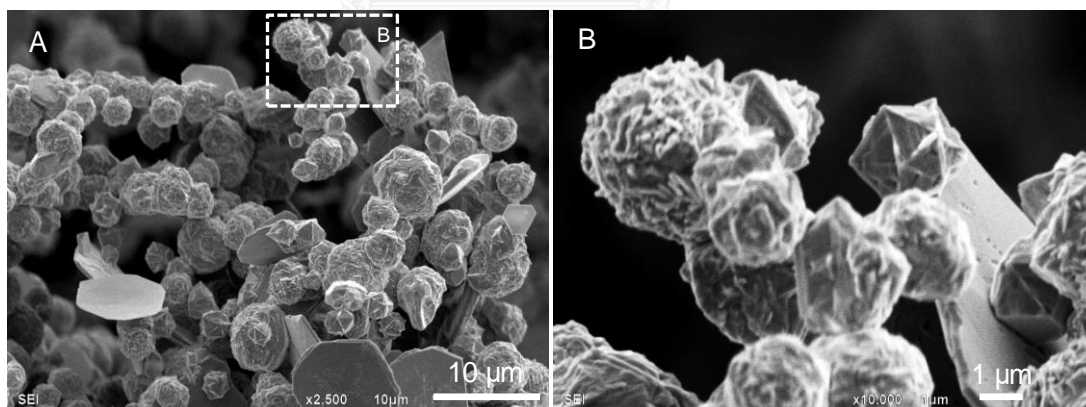
Figure 4.21 Close-up SEM images of H_2O_2-reduced gold microparticles. Gold microparticles were prepared by mixing of 25.4 mM $HAuCl_4$ and 3.2 M H_2O_2.

Interestingly, when the concentration of H_2O_2 was extremely increased to 320, 970 and 1,600 mM, flower-like gold nanostructures with the size as large as 15 μm were obtained (Figure 4.22C–E). The morphology of flower-like gold nanostructures is a stacking arrangement of smooth-surfaced petals which are gold nanosheets with nanometer-scale thickness. The presence of rough surfaced petals was observed when the concentration of H_2O_2 was increased to 3,200 mM. The observed phenomena suggested that using of the reducing capability of H_2O_2 and stabilizing power of starch can be served as a promising synthesis procedure of anisotropic nanostructures. Reduction of gold ions with the extremely high concentration of H_2O_2 under starch stabilization could facilitate the formation of the flower-like gold nanostructures. The detailed investigation for the synthesis parameters on the formation and the growth of the flower-like gold nanostructures were further investigated.
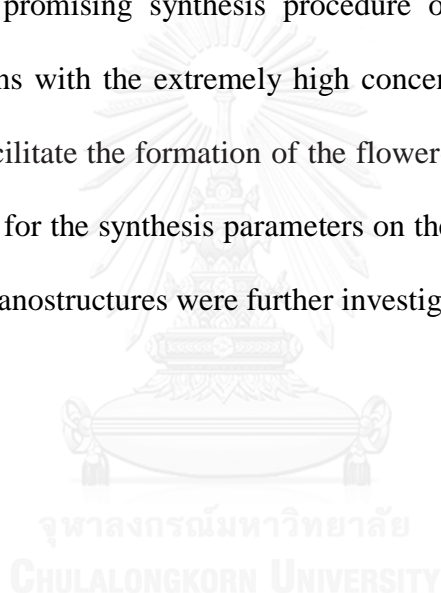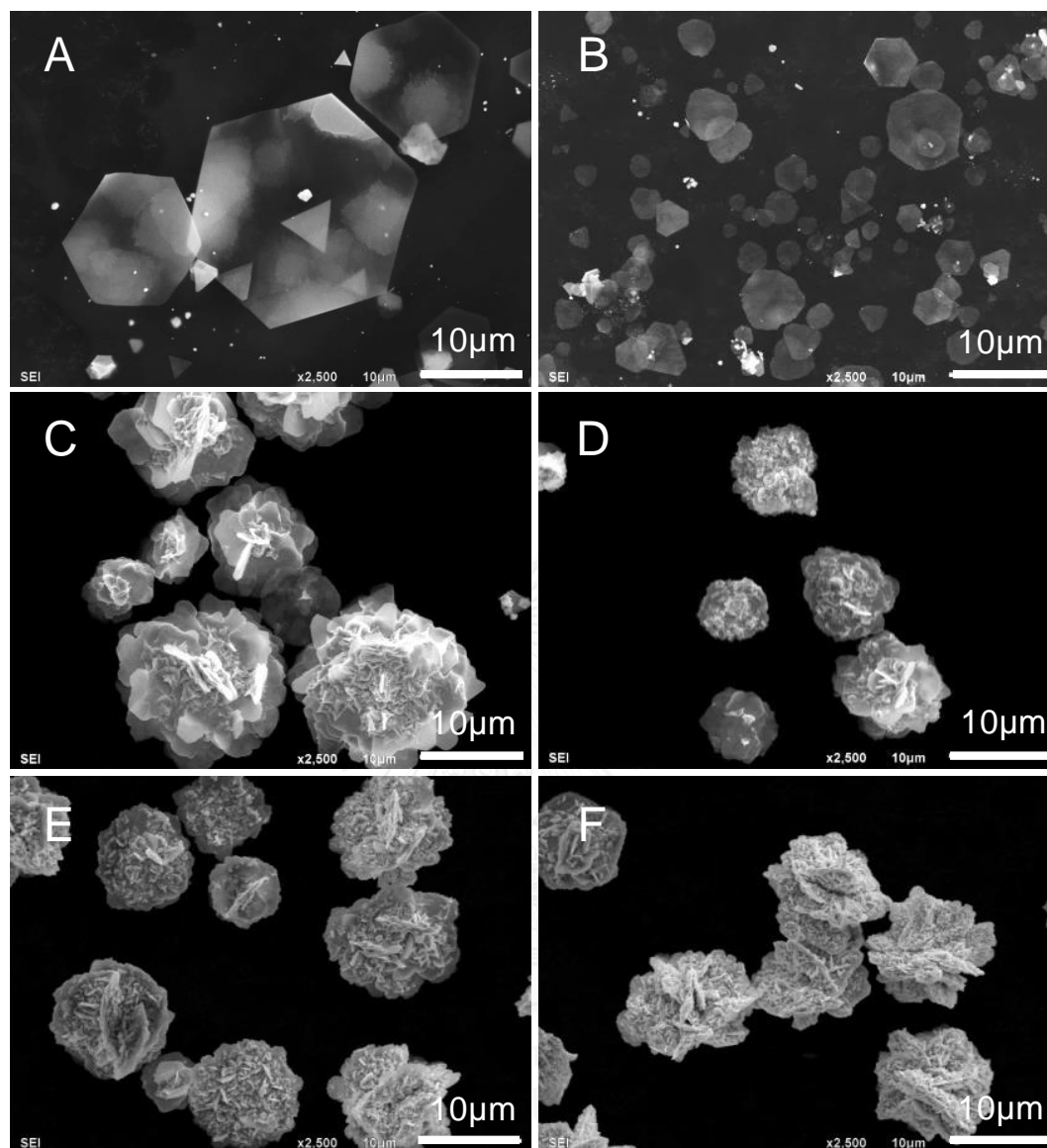
Figure 4.22 SEM images of gold nanosheets and flower-like gold nanostructures obtained from the reduction of gold ions (2.54 mM) with different H_2O_2 concentrations at (A) 3.2 (B) 32 (C) 320 (D) 970 (E) 1,600 (F) 3,200 mM in starch solution (1% w/v).
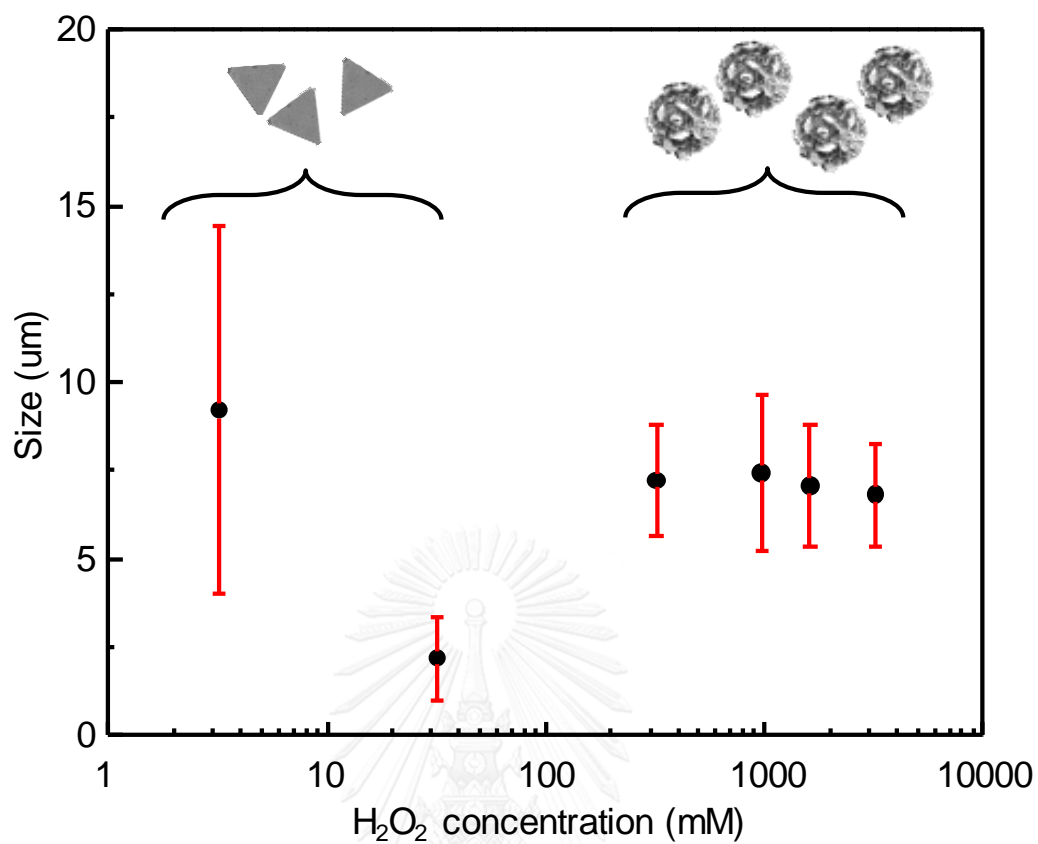
Figure 4.23 The relationship between the average size of gold nanostructures and the concentration of H_2O_2. Gold nanostructures were obtained from the reduction of 2.54 mM $HAuCl_4$ at different H_2O_2 concentrations in 1% w/v starch solution. The average size of the particles was calculated from 100 particles. The insets indicate the morphology of gold particles obtained from each reaction.

4.2.2 The Effect of Gold Ions Concentration

An experimental investigation with different concentration of $HAuCl_4$ was performed with an excessive H_2O_2 concentration of 3.2 M and 1% w/v starch solution. At low concentrations of $HAuCl_4$ (2.54 mM, Figure 4.24A) small flower-like gold nanostructures with the size of ~7 μm were created. The rough surfaces of the basal planes of the petals can be observed and can be the reason of the H_2O_2-assisted catalytic growth due to the low molar ratio of $[HAuCl_4]/[H_2O_2]$. When the concentration of $HAuCl_4$ was increased to 12.7 and 25.4 mM (Figure 4.24B and 4.24C), the flower-like gold nanostructures with smooth petals were obtained with average size of 19.2 and 17.4 μm, respectively. The thicknesses of the petals were in the range of 50–140 nm (Figure 4.25). However, when the concentration of $HAuCl_4$ was further increased to 25.4 mM, large micro/nanosheets with average sizes of 14.4 μm were produced with noticeable amount of flattened flowers. An uneven layer-by-layer epitaxial growth on the basal planes of micro/nanosheets was observed. These phenomena suggest an insufficient protection of the basal plane by starch molecules at a high concentration of $HAuCl_4$ which due to the generation of a large number of micro/nanosheets. Nevertheless, increase of acidity of the system at high concentration of $HAuCl_4$ lead to the acid hydrolysis of long chain starch molecules. This weakens the stabilization power of starch [32, 91-93].
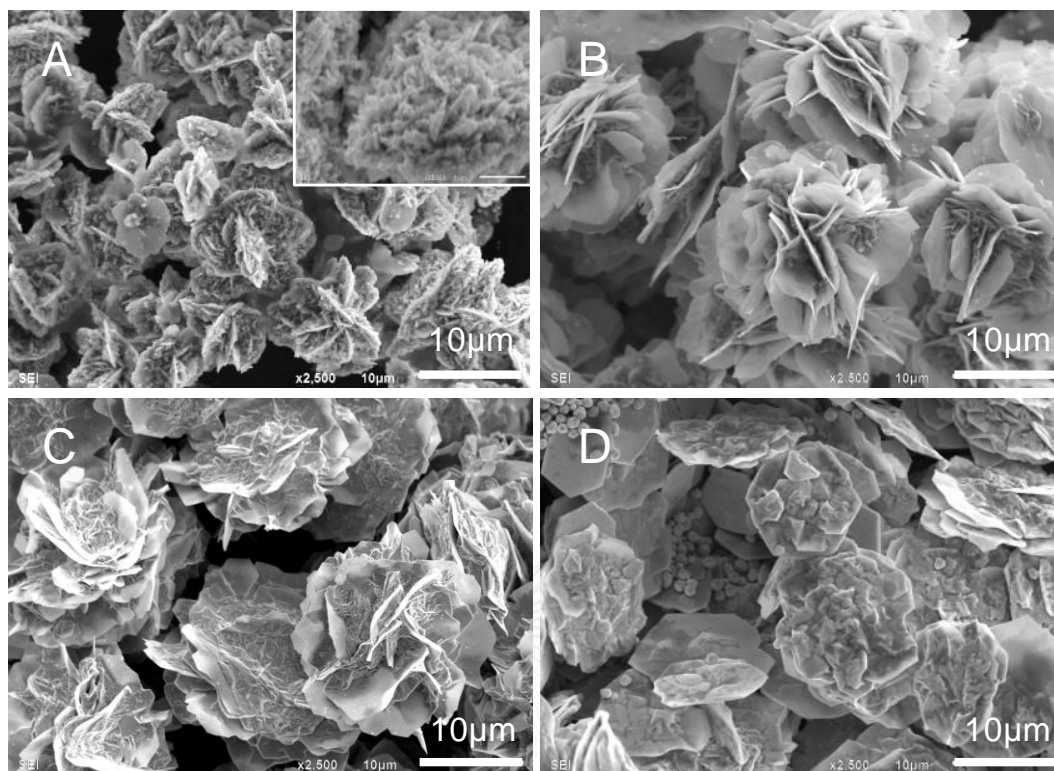
Figure 4.24 SEM images of gold micro/nanostructures indicating the influence of HAuCl$_4$ concentration. The concentrations of HAuCl$_4$ were (A) 2.54 mM, (B) 12.7 mM, (C) 25.4 mM and (D) 50.8 mM while the concentration of starch solution and H$_2$O$_2$ are 1% w/v and 3.2 M, respectively. The insets in (A) shows the surface morphology of the petals.
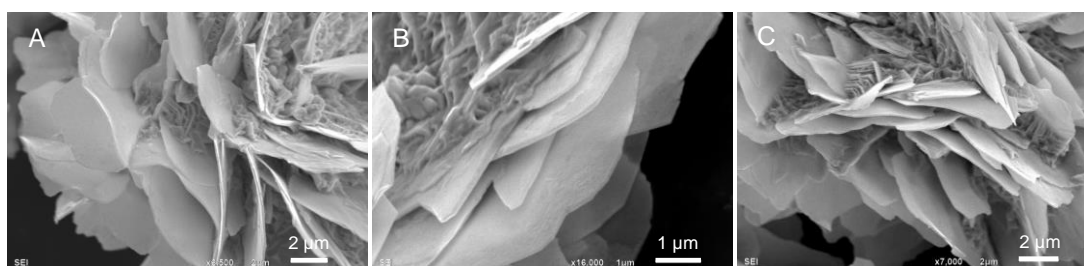
Figure 4.25 Close-up SEM images of flower-like gold nanostructures indicating the stacking of the petal-like structures. The flowers were prepared from the reduction of HAuCl$_4$ (12.7 mM) with H$_2$O$_2$ (3.2 M) in starch solution (1% w/v).

4.2.3 The Effect of Starch Concentration

As showed in the previous section, the observed phenomena suggested that the sufficient surface stabilization is an important for the creation of the flower-like gold nanostructure. To study the effect of surface stabilization, the preparation of the flower-like gold nanostructures at various starch concentrations were performed. The concentration of $HAuCl_4$ and H_2O_2 were 12.7 mM and 3.2 M, respectively. In the system without starch (Figure 4.26A, quasi-microspheres with rough surfaces (average particle size of 5 μm) were obtained. When the concentration of starch increased to 0.1% w/v, an insufficient stabilization caused the formation of thick-irregular-shaped gold micro/nanosheets (average lateral size of 8.9 μm, thickness of 90–220 nm) with a significant amount of small quasi-microspheres (particles size of 1 μm), (Figure 4.26). Aggregations of the microspheres and a non-uniform growth on the basal planes of the nanosheets were observed. The formation of irregular gold nanosheets (average lateral size of 10.8 μm) with noticeable amount of flower-like gold nanostructures (lateral size of ~17μm) was obtained when the stabilization in the system increase (starch concentration of 0.5% w/v), (Figure 4.26C). When greater starch concentrations (1%–2% w/v) were employed, flower-like gold nanostructures with lateral size up to 25 μm were obtained. A structural change from quasi-microspheres and irregular shaped gold micro/nanosheets to flower-like gold nanostructures as the concentration of starch was increased indicates that starch is essential for the formation and growth of the flower-like gold nanostructures. Moreover, starch also prevents the formation of quasi-microspheres in the system.
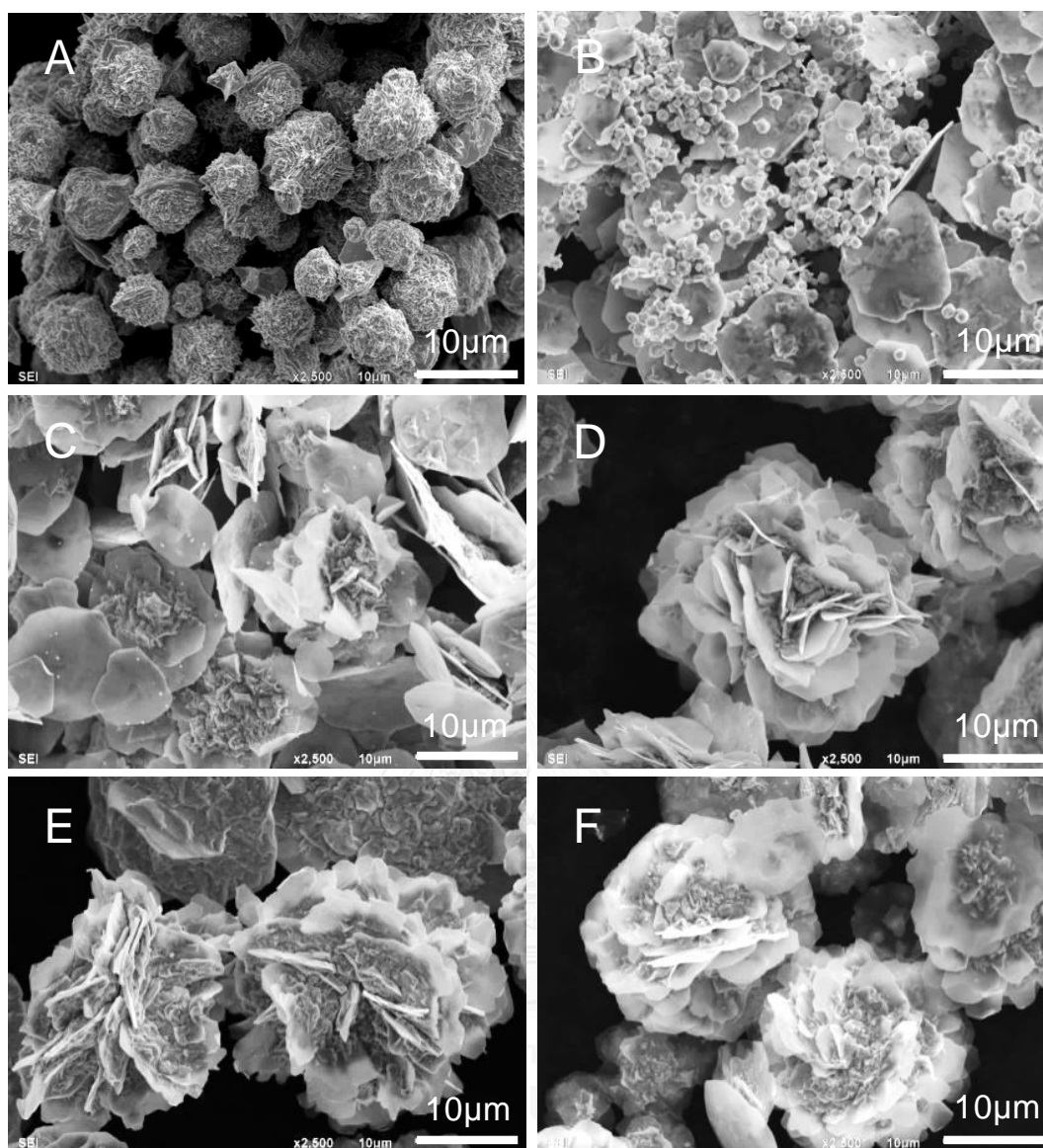
Figure 4.26 SEM images of gold micro/nanostructures obtained from the reaction between HAuCl$_4$ (12.7 mM) and H$_2$O$_2$ (3.2 mM) under starch stabilization. The concentrations of starch were varied at (A) 0, (B) 0.1, (C) 0.5, (D) 1, (E) 1.5, and (F) 2 % w/v.

In case of nanosheets, a non-uniform thickness could be found when the surface passivation ability of starch is insufficient [32]. We observed the same phenomena on the surfaces of the basal planes of petal-like structures of the flowers. Figure 4.27 shows the SEM images of the petal structures indicating an uneven layer-by-layer epitaxial growth on the basal planes of the petals. The epitaxial growth seems to be an origin of the growth of the new petals on the former one. Under the assistance of starch stabilization, the epitaxial growth layers further grow to the larger petal-like structures of the flower (Figure 4.27B and 4.27D).
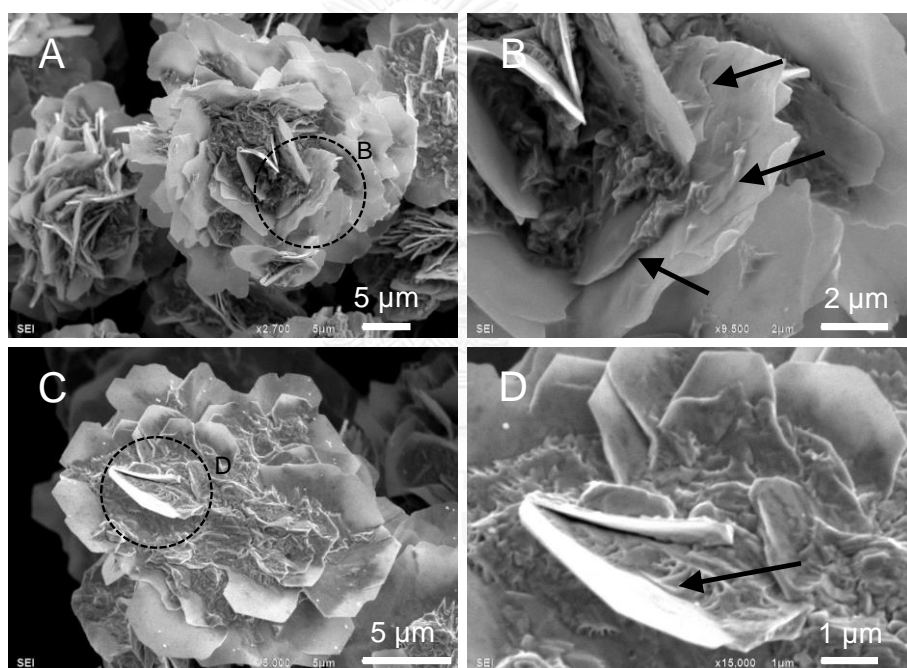
Figure 4.27 SEM images of flower-like gold nanostructures representing the morphology of the surfaces of petals. The arrows in (B) indicated the defects on the surface of petal-like structures which is the growing side of the new petals. The arrow in (D) indicates the new petal outgrowing from the old petal surface. The flower-like gold nanostructures were prepared from the reduction of HAuCl$_4$ (25.4 mM) by H$_2$O$_2$ (3.2 M) in starch solution (1% w/v).

Starch plays an important role in the formation of anisotropic nanostructures. It serves as an efficient surface passivating agent capable of selectively controlling the formation of gold nanosheet or nanoplates [10, 32]. Nevertheless, starch is also an essential ingredient for the formation of the flower-like gold nanostructures (Figure 4.26). Therefore, we expected that starch could also have a strong binding ability on the surface of the flowers. An experiment demonstrating the surface passivation efficiency of starch on surfaces of flower-like gold nanostructures was conducted. The flower particles were separately washed with deionized water, hot deionized water and alkaline-peroxide solution (a solution of 30% H_2O_2 at pH 13 adjusted by 3 M NaOH). Raman spectroscopy was performed to monitor the starch residual on the surfaces of the flower for each cleaning procedures. Figure 4.28 shows the Raman spectra collected from the surface of flower-like nanostructures. The results reveal the Raman spectra of starch molecules on the flowers after cleaning with deionized water and hot deionized water. The disappearance of the starch spectrum could be obtained after the cleaning of the flowers with the alkaline peroxide solution. The complete removal of starch molecules from the surfaces of the flowers after a strong oxidative etching suggests a very good adhesion of starch on the flowers.
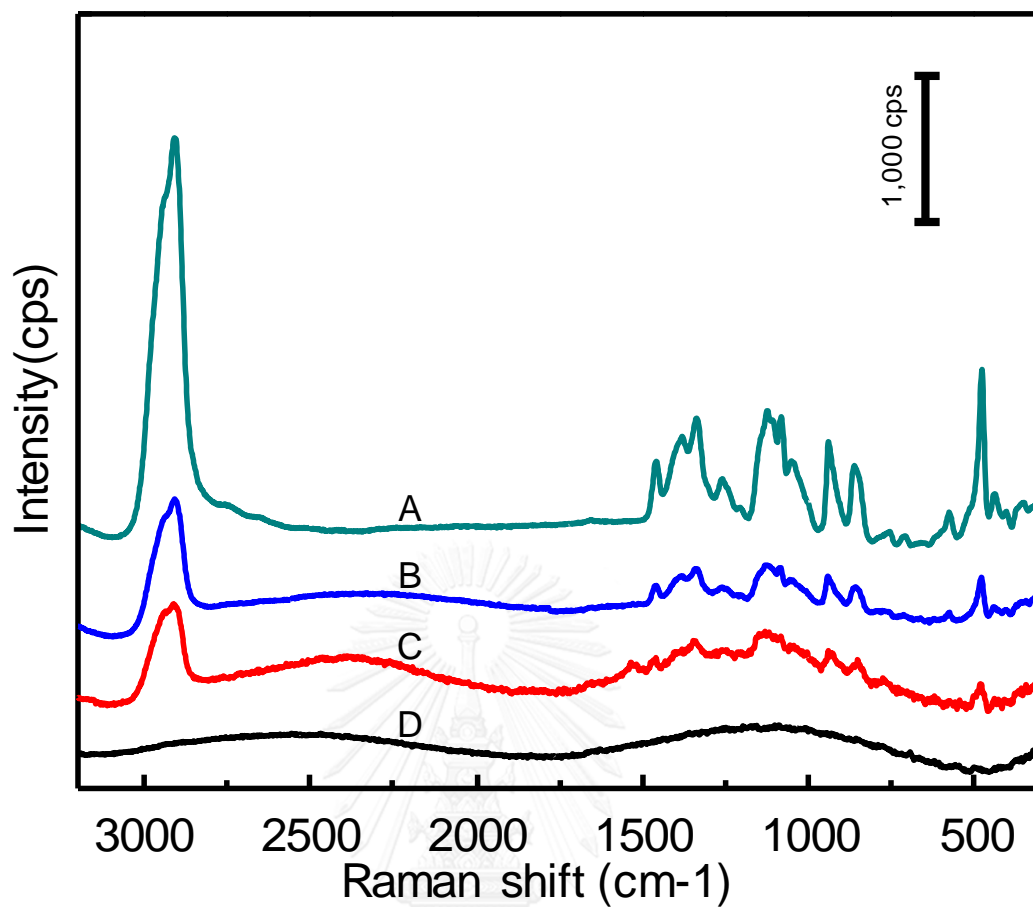
Figure 4.28 Raman spectra of (A) starch film on aluminum foil. The starch molecules
on the surfaces of flower-like gold nanostructures were monitored after
(B) washing with deionized water, (C) washing with hot deionized water,
and (D) washing with alkaline-peroxide solution.

Figure 4.29 shows the XRD patterns of gold microparticles, flower-like gold nanostructures and gold nanosheets. There are five peaks representing the characteristic XRD pattern of the face-centered cubic (fcc) crystal of gold which are assigned to {111}, {200}, {220}, {311}, and {222} planes. In case of nanosheets, very low values of the diffraction ratio of (200)/(111) and (220)/(111) compared to those from the JCPDS 04-0784 standard file (*i.e.*, 0.051 vs. 0.53 and 0.037 vs. 0.33, respectively) could be observed (Figure 4.29C and Figure 4.30). This suggest that the {111} planes are preferentially oriented parallel to the surface of the supporting substrate [19, 32, 95, 96]. The diffraction ratio of (200)/(111) and (220)/(111) were increased for flower-like gold nanostructures (*i.e.*, 0.170 and. 0.181) and quasi-microsphere gold microparticles (*i.e.*, 0.387 and 0.236). Compared to those from nanosheets, the increase of the diffraction ratio observed in the flowers and quasi-microsphere might be attributed to the exposure of other crystallographic facets on the complex nanostructures. The lower diffraction ratio of (200)/(111) and (220)/(111) of flower-like gold nanostructures compared to those from quasi-microsphere could be assigned to the fact that the flower structures are mainly consisted of the nanosheets which is mostly covered with {111} planes.
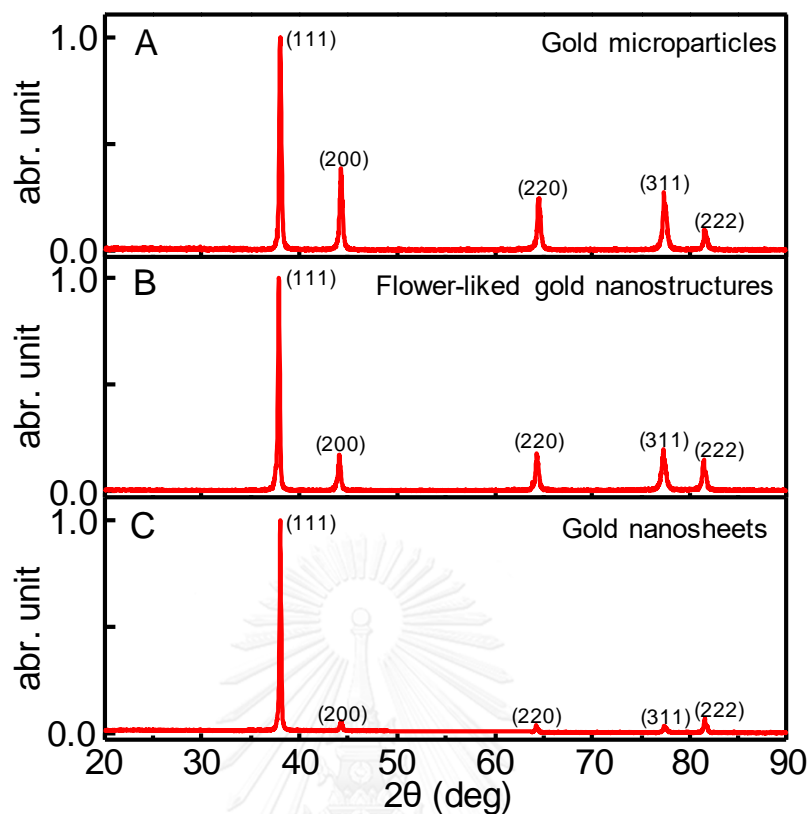
Figure 4.29 The XRD patterns of gold microparticles (A), flower-like gold nanostructures (B), and gold nanosheets (C).
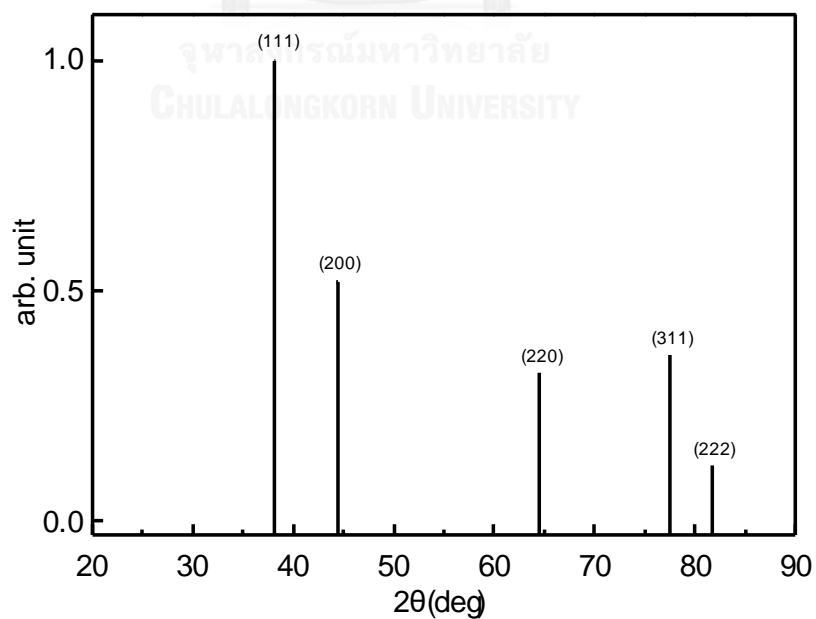
Figure 4.30 The standard XRD pattern of gold (JCPDS 04-0748).

4.2.4 Growth Mechanism of Flower-Like Gold Nanostructures

In order to gain more insight understanding on the growth mechanism of the flower-like gold nanostructures, time-dependent structural evolutions were performed. We collected gold particles every 2 minutes from the reaction medium after mixing of the reactant. Figure 4.31 shows the selected SEM images indicating the structural evolutions of flower-like gold nanostructure. The results reveal that the formation of the basal plate of the flower structures are generated by an attachment of small gold nanosheets via OA growth mechanism as we could clearly observe the jagged edges (Figure 4.31A). The growth the plate edges caused the expansion of the basal plate (Figure 4.31B and 4.31C). The formation of petal-like nanosheets was obtained from an uneven epitaxial growth on the basal planes (Figure 4.31D–4.31H). The gap between petal-like nanosheets was gradually filled as the flower grew into flower-like gold nanostructures with rough fillers between petals (Figure4.31E–4.31H). The reaction completed within 30 minutes while the flower-like gold nanostructures were obtained.
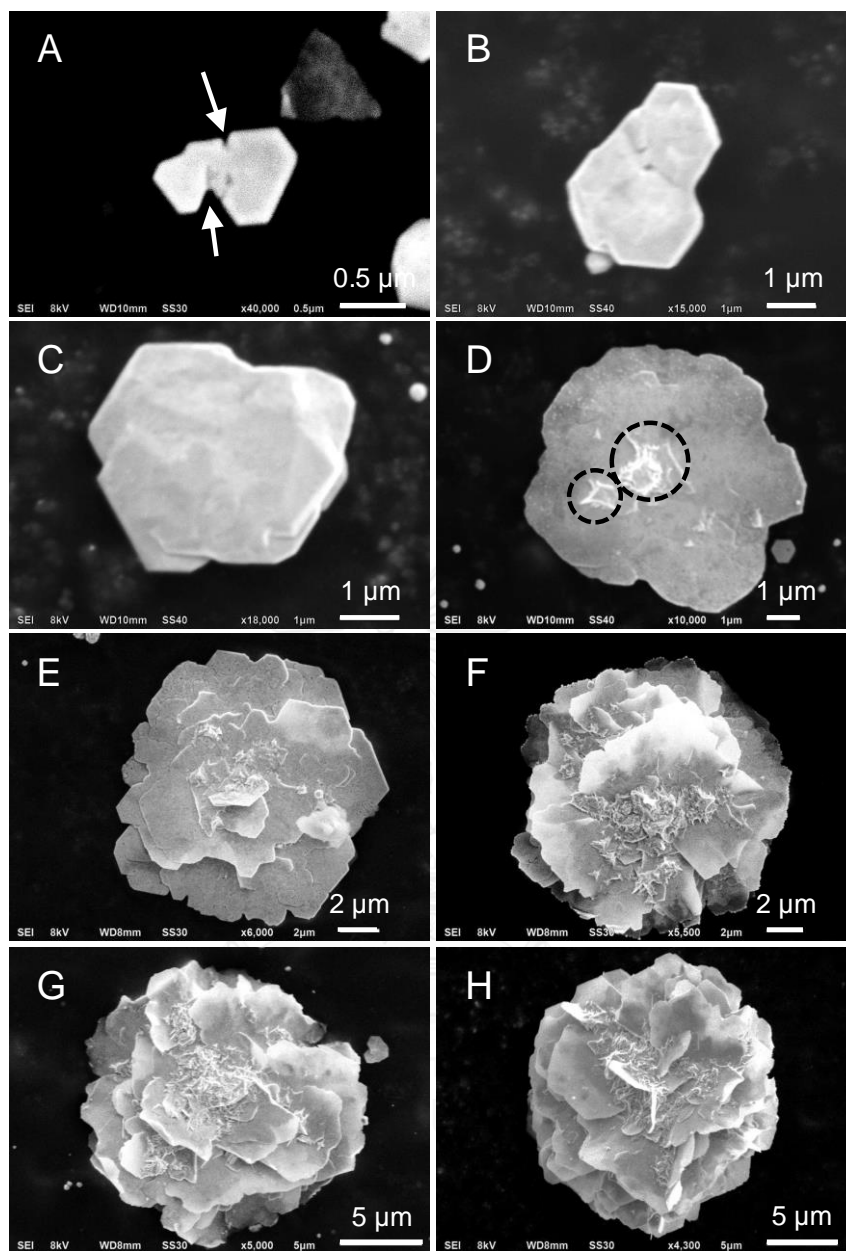
Figure 4.31 Time-dependent SEM images show the development of flower-like gold
nanostructure at (A) 2, (B) 8, (C) 10, (D) 12, (E) 16, (F) 18, (G) 22, and
(H) 24 minutes. The flower-like gold nanostructures were obtained from
the reaction between 25.4 mM $HAuCl_4$ and 3.2 M H_2O_2 in 1% w/v starch
solution. The arrow in (A) indicated jagged edges. The circles in (D) show
the defects on the surfaces of the basal sheets which is the growing sides
of petal-like structures.

Based on the observed evidence, we proposed the growth mechanism of flower-like gold nanostructures as shown in Scheme 4.3. In the system with starch stabilization, gold ions are rapidly reduced by H_2O_2 and grown into small nanosheets. The starch-stabilized nanosheets further grow into larger nanosheets via OA growth mechanism, resulting in the formation of the basal plates of the flowers. The epitaxial growth on the basal planes further grows to the starch-stabilized petal structures together with the creation of rough surfaces between petals due to the H_2O_2-assisted catalytic growth. The starch stabilization promotes lateral growth of petals, resulting in the formation of larger flowers.
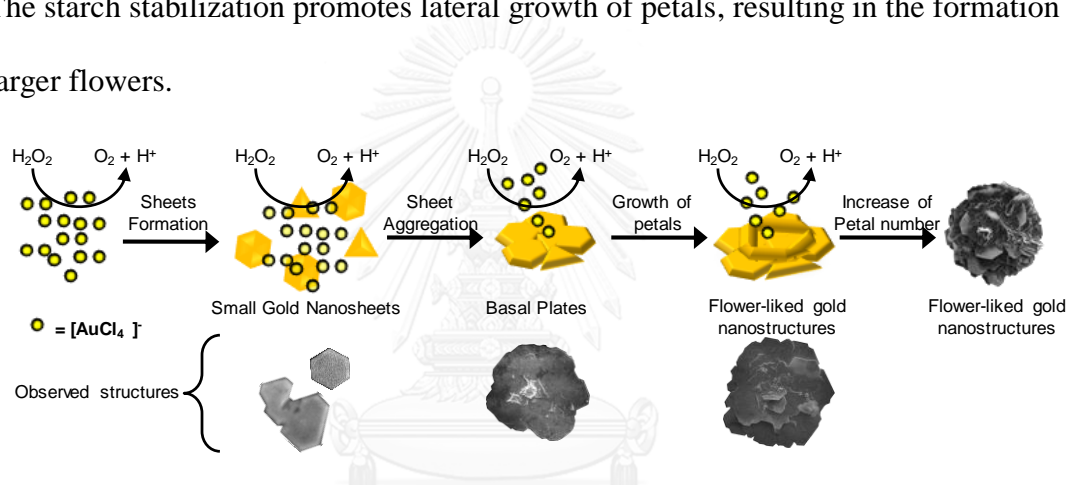
Scheme 4.3 Proposed growth mechanism of flower-like gold nanostructures.

4.2.5   SERS Activity on Flower-Like Gold Nanostructures

There has been reported that dendrite structures are the promising substrates for SERS as it provided SERS hot spot by its sharp corner, edges, or nanoscale junctions [100, 101]. Thus, we explored the SERS activity of the flower-like gold nanostructures because the morphology of the flower-like gold nanostructures is also rough surfaces that might be SERS-active substrates. The flat aluminum foils were used as a controlled substrate to avoid the distress of Raman signal. A 10 µM R6G was used as Raman probe and was drop-coated on cleaned flower-like gold nanostructures for SERS measurement.

Figure 4.32 show the SERS spectra of R6G on flower-like gold nanostructures compared with a Raman spectrum of R6G on a flat aluminum substrate. The results reveal the disappearance of the Raman signal of R6G on the controlled substrates. In contrast, well-defined vibrational fingerprints of R6G comprising of C-C-C in-plane bending (615 cm^{-1}), C-H out-of-plane bending (775 cm^{-1}), C-H in-plane bending (1126 and 1185 cm^{-1}), C-O-C stretching (1314 cm^{-1}), and C-C stretching of aromatic ring (1363, 1512, 1575, and 1651 cm^{-1}) were clearly observed from the SERS spectra of R6G deposited on flow-like gold nanostructures [102].

We further investigate the limit of detection of R6G deposited on the flower-like gold nanostructures. SERS experiments were carefully explored at different concentration of R6G. The SERS signal at 615 cm^{-1} was majorly attended as it delivers a strong-clear-sharp peak. As shown in Figure 4.32, the decrease the R6G concentration leads to the decrease of the Raman intensity. The Raman shift at 615 cm^{-1} was observed even the concentration of R6G is as low as 100 nM. The SERS spectra of R6G disappeared at the concentration lower than 100 nM. The enhancement of the Raman

signal of R6G deposited on the flower-like gold nanostructures might be attributed to the occurrence of the SERS hot spots creating from the overlapping of the petal-like structures between the two flowers or its sharp corner, edges, or nanoscale junctions between the petal-like structures. This suggest that the prepared flower-like gold nanostructure can be used as efficient SERS substrates for trace chemical analysis.
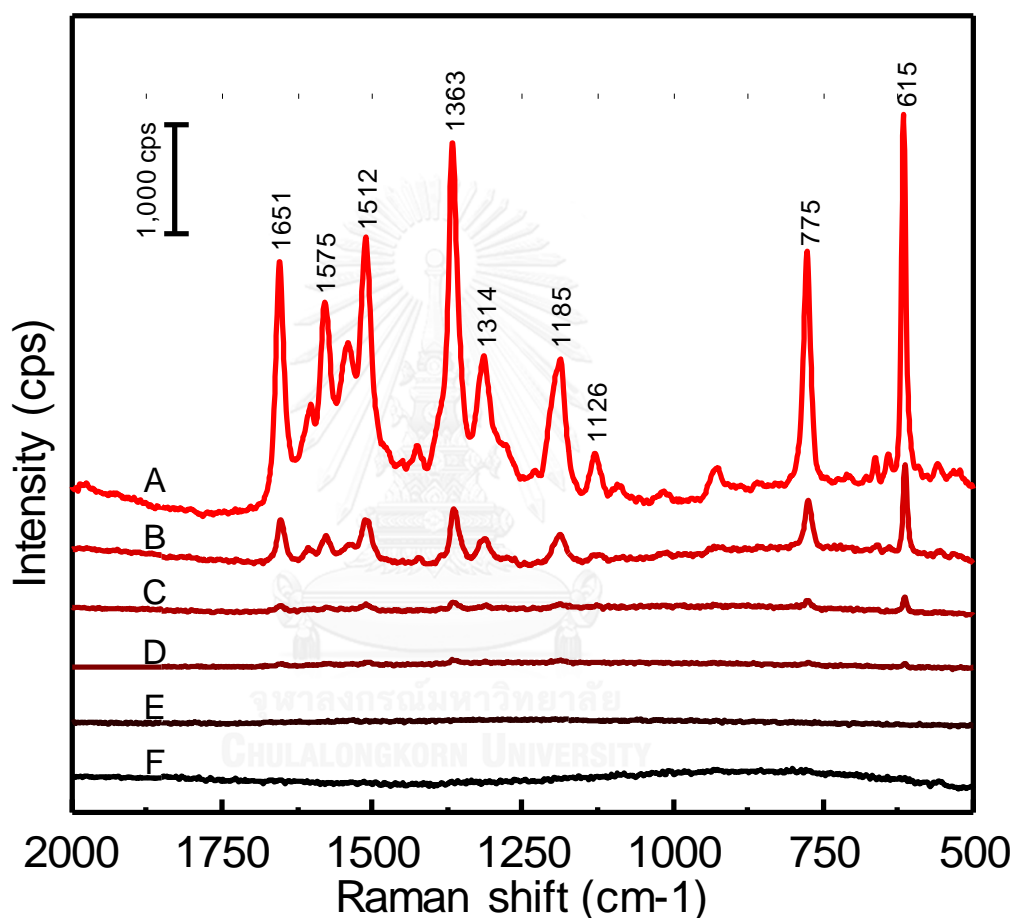
Figure 4.32 SERS spectra R6G deposited on the flower-like gold nanostructures. The concentrations of R6G were varied at (A) 10 μM, (B) 1 μM, (C) 100 nM, (D) 10 nM and (E) 1 nM. (F) The Raman spectrum of 10 μM R6G on flat aluminum foil.

CHAPTER V

CONCLUSION

We have developed simple and efficient synthetic methods for the fabrication of large gold nanosheets and flower-like gold nanostructures using H_2O_2 as the green reducing agent and starch as the stabilizer and shape-controlling agent. The synthesis protocols can be employed for industrial-scale production with competitive price and can be accomplished at room temperature without a need for complicated scientific instruments.

For fabrication of gold nanosheets, starch plays an important role on the formation and growth of the nanosheets. Starch does not only preferentially bind onto the (111) facets of the nanosheets but also prevent the formation of the quasi-microspheres by prohibiting the filling of adatoms at the gaps between petals of the flower-like nanostructures formed at the early stage. Nanoplates and nanosheets developed from the flower-like nanostructures as a particular petal outgrows the others. The starch-bound nanosheets and nanoplates are later assembling into larger nanosheets via OA. The lateral size of the gold nanosheets could be tuned up to 50 μm with the thickness of 20–50 nm by adjusting the concentration of $HAuCl_4$, H_2O_2 and starch stabilizer. Due to the kinetic control of the nucleation step, a particular molar ratio of $[H_2O_2]/[HAuCl_4]$ with difference concentration of H_2O_2 and $HAuCl_4$ is not valid. Without starch, the flower-like nanostructures develop into the quasi-microspheres with rough surfaces. Due to the atomically flat surfaces, gold nanosheets can be employed as a solid substrate for SERS as well as an alternative gold pigment.

Employing the same synthesis protocol with a little modification, flower-like gold nanostructures with the size as large as 25 μm are obtained from the extremely high H_2O_2 concentration. Starch is an essential ingredient for the formation of flower-like gold nanostructures as it functions as a surface passivating agent and promotes the growth of petal-like structures. Insufficient stabilization (i.e., low concentration of starch or high concentration of $HAuCl_4$) lead to the destruction of petal-like structures together with the formation of quasi-microspheres. Flower-like gold nanostructure are developed from the gold nanosheets. At the early growing state, small gold nanosheets assemble into larger basal plates of flower-like gold nanostructures via OA. The epitaxial growth on the basal plates under starch stabilization results the formation of petal-like structures. As flower-like gold nanostructures consist of sharp corners, edges and nanoscale junctions between the petal-like structures, it can be employed as a substrate for SERS application.

REFERENCES

1. Chen, H. M.; Liu, R.-S., Architecture of Metallic Nanostructures: Synthesis Strategy and Specific Applications. *J. Phys. Chem. C* **2011,** *115* (9), 3513-3527.

2. Beqa, L.; Singh, A. K.; Khan, S. A.; Senapati, D.; Arumugam, S. R.; Ray, P. C., Gold Nanoparticle-Based Simple Colorimetric and Ultrasensitive Dynamic Light Scattering Assay for the Selective Detection of Pb(II) from Paints, Plastics, and Water Samples. *ACS Appl. Mater. Interfaces* **2011,** *3* (3), 668-673.

3. Chen, H.; Wang, Y.; Dong, S., Synthesis of Different Gold Nanostructures by Solar Radiation and Their SERS Spectroscopy. *J. Raman Spectrosc.* **2009,** *40* (9), 1188-1193.

4. Jia, W.; Li, J.; Lin, G.; Jiang, L., Two-Step Synthesis of Narrow Size Distribution Nanoflowers Using a Tree-Type Multi-Amine-Head Surfactant as a Template. *Cryst. Growth Des.* **2011,** *11* (9), 3822-3827.

5. Wang, W.-K.; Zheng, M.-L.; Chen, W.-Q.; Jin, F.; Cao, Y.-Y.; Zhao, Z.-S.; Duan, X.-M., Microscale Golden Candock Leaves Self-Aggregated on a Polymer Surface: Raman Scattering Enhancement and Superhydrophobicity. *Langmuir* **2011,** *27* (7), 3249-3253.

6. Heo, J.; Lee, Y. W.; Kim, M.; Yun, W. S.; Han, S. W., Nanoparticle Assembly on Nanoplates. *Chem. Commun.* **2009,** (15), 1981-1983.

7. Bechelany, M.; Brodard, P.; Elias, J.; Brioude, A.; Michler, J.; Philippe, L., Simple Synthetic Route for SERS-Active Gold Nanoparticles Substrate with Controlled Shape and Organization. *Langmuir* **2010,** *26* (17), 14364-14371.

8.   Lee, C. H.; Tian, L.; Singamaneni, S., Paper-Based SERS Swab for Rapid Trace Detection on Real-World Surfaces. *ACS Appl. Mater. Interfaces* **2010,** *2* (12), 3429-3435.

9.   Deckert-Gaudig, T.; Deckert, V., Ultraflat Transparent Gold Nanoplates—Ideal Substrates for Tip-Enhanced Raman Scattering Experiments. *Small* **2009,** *5* (4), 432-436.

10.   Pienpinijtham, P.; Han, X. X.; Suzuki, T.; Thammacharoen, C.; Ekgasit, S.; Ozaki, Y., Micrometer-Sized Gold Nanoplates: Starch-Mediated Photochemical Reduction Synthesis and Possibility of Application to Tip-Enhanced Raman Scattering (TERS). *PCCP* **2012,** *14* (27), 9636-9641.

11.   Han, J.; Liu, Y.; Li, L.; Guo, R., Poly(o-phenylenediamine) Submicrosphere-Supported Gold Nanocatalysts: Synthesis, Characterization, and Application in Selective Oxidation of Benzyl Alcohol. *Langmuir* **2009,** *25* (18), 11054-11060.

12.   Taton, T. A.; Mirkin, C. A.; Letsinger, R. L., Scanometric DNA Array Detection with Nanoparticle Probes. *Science* **2000,** *289* (5485), 1757-1760.

13.   Henglein, A.; Meisel, D., Radiolytic Control of the Size of Colloidal Gold Nanoparticles. *Langmuir* **1998,** *14* (26), 7392-7396.

14.   Mallikarjuna, N. N.; Varma, R. S., Microwave-Assisted Shape-Controlled Bulk Synthesis of Noble Nanocrystals and Their Catalytic Properties. *Cryst. Growth Des.* **2007,** *7* (4), 686-690.

15.   Huang, X.; Qi, X.; Huang, Y.; Li, S.; Xue, C.; Gan, C. L.; Boey, F.; Zhang, H., Photochemically Controlled Synthesis of Anisotropic Au Nanostructures: Platelet-like Au Nanorods and Six-Star Au Nanoparticles. *ACS Nano* **2010,** *4* (10), 6196-6202.

16. Guo, Z.; Zhang, Y.; Mao, Y.; Huang, L.; Gu, N., Synthesis of Microsized Gold Nanoplates by a Self-Seeding Method in Ethanol Solution. *Mater. Lett.* **2006,** *60* (29–30), 3522-3525.

17. Luo, Y., Large-Scale Preparation of Single-Crystalline Gold Nanoplates. *Mater. Lett.* **2007,** *61* (6), 1346-1349.

18. Bouvy, C.; Baker, G. A.; Yin, H.; Dai, S., Growth of Gold Nanosheets and Nanopolyhedra in Pyrrolidinium-Based Ionic Liquids: Investigation of the Cation Effect on the Resulting Morphologies. *Cryst. Growth Des.* **2010,** *10* (3), 1319-1322.

19. Sun, X.; Dong, S.; Wang, E., Large-Scale Synthesis of Micrometer-Scale Single-Crystalline Au Plates of Nanometer Thickness by a Wet-Chemical Route. *Angew. Chem.* **2004,** *116* (46), 6520-6523.

20. Ah, C. S.; Yun, Y. J.; Park, H. J.; Kim, W.-J.; Ha, D. H.; Yun, W. S., Size-Controlled Synthesis of Machinable Single Crystalline Gold Nanoplates. *Chem. Mater.* **2005,** *17* (22), 5558-5561.

21. Amendola, V.; Polizzi, S.; Meneghetti, M., Laser Ablation Synthesis of Gold Nanoparticles in Organic Solvents. *J. Phys. Chem. B* **2006,** *110* (14), 7232-7237.

22. Sajanlal, P. R.; Pradeep, T., Bimetallic Mesoflowers: Region-Specific Overgrowth and Substrate Dependent Surface-Enhanced Raman Scattering at Single Particle Level. *Langmuir* **2010,** *26* (11), 8901-8907.

23. Sun, S.; Leggett, G. J., Generation of Nanostructures by Scanning Near-Field Photolithography of Self-Assembled Monolayers and Wet Chemical Etching. *Nano Lett.* **2002,** *2* (11), 1223-1227.

24. Xia, Y.; Xiong, Y.; Lim, B.; Skrabalak, S. E., Shape-Controlled Synthesis of Metal Nanocrystals: Simple Chemistry Meets Complex Physics? *Angew. Chem. Int. Ed.* **2009,** *48* (1), 60-103.

25. Alexandridis, P., Gold Nanoparticle Synthesis, Morphology Control, and Stabilization Facilitated by Functional Polymers. *Chem. Eng. Technol.* **2011,** *34* (1), 15-28.

26. Cho, K.; Chang, H.; Kil, D. S.; Kim, B.-G.; Jang, H. D., Synthesis of Dispersed $CaCO_3$ Nanoparticles by the Ultrafine Grinding. *J Ind. Eng. Chem.* **2009,** *15* (2), 243-246.

27. Yun, Y. J.; Park, G.; Ah, C. S.; Park, H. J.; Yun, W. S.; Ha, D. H., Fabrication of versatile nanocomponents using single-crystalline Au nanoplates. *Appl. Phys. Lett.* **2005,** *87* (23), 233110-3.

28. Salminen, T.; Honkanen, M.; Niemi, T., Coating of Gold Nanoparticles Made by Pulsed Laser Ablation in Liquids with Silica Shells by Simultaneous Chemical Synthesis. *PCCP* **2013,** *15* (9), 3047-3051.

29. Intartaglia, R.; Das, G.; Bagga, K.; Gopalakrishnan, A.; Genovese, A.; Povia, M.; Di Fabrizio, E.; Cingolani, R.; Diaspro, A.; Brandi, F., Laser Synthesis of Ligand-Free Bimetallic Nanoparticles for Plasmonic Applications. *PCCP* **2013,** *15* (9), 3075-3082.

30. Toshima, N.; Yonezawa, T., Bimetallic Nanoparticles-Novel Materials for Chemical and Physical Applications. *New J. Chem.* **1998,** *22* (11), 1179-1201.

31. Volkert, C. A.; Minor, A. M., Focused Ion Beam Microscopy and Micromachining. *MRS Bull.* **2007,** *32* (05), 389-399.

32. Nootchanat, S.; Thammacharoen, C.; Lohwongwatana, B.; Ekgasit, S., Formation of Large H_2O_2-Reduced Gold Nanosheets via Starch-Induced Two-Dimensional Oriented Attachment. *RSC Adv.* **2013,** *3* (11), 3707-3716.

33. Parnklang, T.; Lertvachirapaiboon, C.; Pienpinijtham, P.; Wongravee, K.; Thammacharoen, C.; Ekgasit, S., H_2O_2-Triggered Shape Transformation of Silver Nanospheres to Nanoprisms with Controllable Longitudinal LSPR Wavelengths. *RSC Adv.* **2013,** *3* (31), 12886-12894.

34. Thanh, N. T. K.; Maclean, N.; Mahiddine, S., Mechanisms of Nucleation and Growth of Nanoparticles in Solution. *Chem. Rev.* **2014,** *114* (15), 7610-7630.

35. Lee, W. r.; Kim, M. G.; Choi, J. r.; Park, J. I.; Ko, S. J.; Oh, S. J.; Cheon, J., Redox−Transmetalation Process as a Generalized Synthetic Strategy for Core−Shell Magnetic Nanoparticles. *J. Am. Chem. Soc.* **2005,** *127*, 16090-16097.

36. Niederberger, M.; Colfen, H., Oriented Attachment and Mesocrystals: Non-Classical Crystallization Mechanisms Based on Nanoparticle Assembly. *PCCP* **2006,** *8*, 3271-3287.

37. Penn, R. L.; Banfield, J. F., Morphology Development and Crystal Growth in Nanocrystalline Aggregates under Hydrothermal Conditions: Insights from Titania. *Geochim. Cosmochim. Acta* **1999,** *63* (10), 1549-1557.

38. Xu, J. Y.; Wang, J.; Kong, L. T.; Zheng, G. C.; Guo, Z.; Liu, J. H., SERS Detection of Explosive Agent by Macrocyclic Compound Functionalized Triangular Gold Nanoprisms. *J. Raman Spectrosc.* **2011,** *42* (9), 1728-1735.

39. Han, X. X.; Zhao, B.; Ozaki, Y., Surface-Enhanced Raman Scattering for Protein Detection. *Anal. Bioanal. Chem.* **2009,** *394* (7), 1719-1727.

40. Zhang, Y.; Cui, X.; Shi, F.; Deng, Y., Nano-Gold Catalysis in Fine Chemical Synthesis. *Chem. Rev.* **2011,** *112* (4), 2467-2505.

41. Zhang, Y.; Cattrall, R. W.; McKelvie, I. D.; Kolev, S. D., Gold, an Alternative to Platinum Group Metals in Automobile Catalytic Converters. *Gold Bull.* **2011,** *44* (3), 145-153.

42. Ai, K.; Liu, Y.; Lu, L., Hydrogen-Bonding Recognition-Induced Color Change of Gold Nanoparticles for Visual Detection of Melamine in Raw Milk and Infant Formula. *J. Am. Chem. Soc.* **2009,** *131* (27), 9496-9497.

43. Lemelle, A.; Veksler, B.; Kozhevnikov, I. S.; Akchurin, G. G.; Piletsky, S. A.; Meglinski, I., Application of Gold Nanoparticles as Contrast Agents in Confocal Laser Scanning Microscopy. *Laser Phys. Lett.* **2009,** *6* (1), 71-75.

44. Su, Y.; Wei, X.; Peng, F.; Zhong, Y.; Lu, Y.; Su, S.; Xu, T.; Lee, S.-T.; He, Y., Gold Nanoparticles-Decorated Silicon Nanowires as Highly Efficient Near-Infrared Hyperthermia Agents for Cancer Cells Destruction. *Nano Lett.* **2012,** *12* (4), 1845-1850.

45. Ye, X.; Jin, L.; Caglayan, H.; Chen, J.; Xing, G.; Zheng, C.; Doan-Nguyen, V.; Kang, Y.; Engheta, N.; Kagan, C. R.; Murray, C. B., Improved Size-Tunable Synthesis of Monodisperse Gold Nanorods through the Use of Aromatic Additives. *ACS Nano* **2012,** *6* (3), 2804-2817.

46. Wu, H.-Y.; Chu, H.-C.; Kuo, T.-J.; Kuo, C.-L.; Huang, M. H., Seed-Mediated Synthesis of High Aspect Ratio Gold Nanorods with Nitric Acid. *Chem. Mater.* **2005,** *17* (25), 6447-6451.

47. Kim, F.; Sohn, K.; Wu, J.; Huang, J., Chemical Synthesis of Gold Nanowires in Acidic Solutions. *J. Am. Chem. Soc.* **2008,** *130* (44), 14442-14443.

48. Zhang, J.; Du, J.; Han, B.; Liu, Z.; Jiang, T.; Zhang, Z., Sonochemical Formation of Single-Crystalline Gold Nanobelts. *Angew. Chem.* **2006,** *118* (7), 1134-1137.

49. Wang, C.; Kan, C.; Zhu, J.; Zeng, X.; Wang, X.; Li, H.; Shi, D., Synthesis of High-Yield Gold Nanoplates: Fast Growth Assistant with Binary Surfactants. *J. Nanomater.* **2010,** *2010.*

50. Fan, X.; Guo, Z. R.; Hong, J. M.; Zhang, Y.; Zhang, J. N.; Gu, N., Size-Controlled Growth of Colloidal Gold Nanoplates and Their High-Purity Acquisition. *Nanotechnology* **2010,** *21* (10), 105602.

51. Umar, A. A.; Oyama, M.; Salleh, M. M.; Majlis, B. Y., Formation of Highly Thin, Electron-Transparent Gold Nanoplates from Nanoseeds in Ternary Mixtures of Cetyltrimethylammonium Bromide, Poly(vinyl pyrrolidone), and Poly(ethylene glycol). *Cryst. Growth Des.* **2010,** *10* (8), 3694-3698.

52. Li, C.; Shuford, K. L.; Park, Q. H.; Cai, W.; Li, Y.; Lee, E. J.; Cho, S. O., High-Yield Synthesis of Single-Crystalline Gold Nano-octahedra. *Angew. Chem.* **2007,** *119* (18), 3328-3332.

53. Huang, C.-C.; Lai, W.-C.; Tsai, C.-Y.; Yang, C.-H.; Yeh, C.-S., Reversible Synthesis of Sub-10 nm Spherical and Icosahedral Gold Nanoparticles from a Covalent Au(CN)$_2$− Precursor and Recycling of Cyanide to form Ferric Ferrocyanide for Cell Staining. *Chem. Eur. J.* **2012,** *18* (13), 4107-4114.

54. Skrabalak, S. E.; Chen, J.; Sun, Y.; Lu, X.; Au, L.; Cobley, C. M.; Xia, Y., Gold Nanocages: Synthesis, Properties, and Applications. *Acc. Chem. Res.* **2008,** *41* (12), 1587-1595.

55. Jiang, Q.; Jiang, Z.; Zhang, L.; Lin, H.; Yang, N.; Li, H.; Liu, D.; Xie, Z.; Tian, Z., Synthesis and High Electrocatalytic Performance of Hexagram Shaped Gold

Particles Having an Open Surface Structure with Kinks. *Nano Res.* **2011,** *4* (6), 612-622.

56. Yamamoto, M.; Kashiwagi, Y.; Sakata, T.; Mori, H.; Nakamoto, M., Synthesis and Morphology of Star-Shaped Gold Nanoplates Protected by Poly(N-vinyl-2-pyrrolidone). *Chem. Mater.* **2005,** *17* (22), 5391-5393.

57. Xie, J.; Zhang, Q.; Lee, J. Y.; Wang, D. I. C., The Synthesis of SERS-Active Gold Nanoflower Tags for In Vivo Applications. *ACS Nano* **2008,** *2* (12), 2473-2480.

58. Ankamwar, B.; Chaudhary, M.; Sastry, M., Gold Nanotriangles Biologically Synthesized using Tamarind Leaf Extract and Potential Application in Vapor Sensing. *Synth. React. Inorg. M.* **2005,** *35* (1), 19-26.

59. Shankar, S. S.; Rai, A.; Ahmad, A.; Sastry, M., Controlling the Optical Properties of Lemongrass Extract Synthesized Gold Nanotriangles and Potential Application in Infrared-Absorbing Optical Coatings. *Chem. Mater.* **2005,** *17* (3), 566-572.

60. Imura, K.; Nagahara, T.; Okamoto, H., Photoluminescence from Gold Nanoplates Induced by Near-Field Two-Photon Absorption. *Appl. Phys. Lett.* **2006,** *88* (2), 023104-1-023104-3

61. Wiley, B. J.; Lipomi, D. J.; Bao, J.; Capasso, F.; Whitesides, G. M., Fabrication of Surface Plasmon Resonators by Nanoskiving Single-Crystalline Gold Microplates. *Nano Lett.* **2008,** *8* (9), 3023-3028.

62. Millstone, J. E.; Métraux, G. S.; Mirkin, C. A., Controlling the Edge Length of Gold Nanoprisms via a Seed-Mediated Approach. *Adv. Funct. Mater.* **2006,** *16* (9), 1209-1214.

63. Chen, L.; Ji, F.; Xu, Y.; He, L.; Mi, Y.; Bao, F.; Sun, B.; Zhang, X.; Zhang, Q., High-Yield Seedless Synthesis of Triangular Gold Nanoplates through Oxidative Etching. *Nano Lett.* **2014,** *14* (12), 7201-7206.

64. Sau, T. K.; Rogach, A. L., Nonspherical Noble Metal Nanoparticles: Colloid-Chemical Synthesis and Morphology Control. *Adv. Mater.* **2010,** *22* (16), 1781-1804.

65. Jana, N. R.; Gearheart, L.; Murphy, C. J., Evidence for Seed-Mediated Nucleation in the Chemical Reduction of Gold Salts to Gold Nanoparticles. *Chem. Mater.* **2001,** *13* (7), 2313-2322.

66. Yi, S.; Sun, L.; Lenaghan, S. C.; Wang, Y.; Chong, X.; Zhang, Z.; Zhang, M., One-Step Synthesis of Dendritic Gold Nanoflowers with High Surface-Enhanced Raman Scattering (SERS) Properties. *RSC Adv.* **2013,** *3* (26), 10139-10144.

67. Ju-Hyun, K.; Taejoon, K.; Seung Min, Y.; Sang Yup, L.; Bongsoo, K.; Yang-Kyu, C., A Well-Ordered Flower-Like Gold Nanostructure for Integrated Sensors via Surface-Enhanced Raman Scattering. *Nanotechnology* **2009,** *20* (23), 235302.

68. Jena, B. K.; Raj, C. R., Synthesis of Flower-like Gold Nanoparticles and Their Electrocatalytic Activity Towards the Oxidation of Methanol and the Reduction of Oxygen. *Langmuir* **2007,** *23* (7), 4064-4070.

69. Wang, L.; Liu, C.-H.; Nemoto, Y.; Fukata, N.; Wu, K. C. W.; Yamauchi, Y., Rapid Synthesis of Biocompatible Gold Nanoflowers with Tailored Surface Textures with the Assistance of Amino Acid Molecules. *RSC Adv.* **2012,** *2* (11), 4608-4611.

70. Wang, Z.; Zhang, J.; Ekman, J. M.; Kenis, P. J. A.; Lu, Y., DNA-Mediated Control of Metal Nanoparticle Shape: One-Pot Synthesis and Cellular Uptake of

Highly Stable and Functional Gold Nanoflowers. *Nano Lett.* **2010,** *10* (5), 1886-1891.

71. Li, M.; Zhao, G.; Geng, R.; Hu, H., Facile Electrocatalytic Redox of Hemoglobin by Flower-Like Gold Nanoparticles on Boron-Doped Diamond Surface. *Bioelectrochemistry* **2008,** *74* (1), 217-221.

72. Ren, Y.; Xu, C.; Wu, M.; Niu, M.; Fang, Y., Controlled Synthesis of Gold Nanoflowers Assisted by Poly(Vinyl Pyrrolidone)–Sodium Dodecyl Sulfate Aggregations. *Colloids Surf. A Physicochem Eng. Asp.* **2011,** *380* (1–3), 222-228.

73. Panda, B. R.; Chattopadhya, A., Synthesis of Au Nanoparticles at "all" pH by H_2O_2 Reduction of $HAuCl_4$. *J. Nanosci. Nanotechnol.* **2007,** *7* (6), 1911–1915.

74. Milligan, W. O.; Morriss, R. H., Morphology of Colloidal Gold--A Comparative Study. *J. Am. Chem. Soc.* **1964,** *86* (17), 3461-3467.

75. Usher, A.; McPhail, D. C.; Brugger, J., A Spectrophotometric Study of Aqueous Au(III) Halide–Hydroxide Complexes at 25–80°C. *Geochim. Cosmochim. Acta* **2009,** *73* (11), 3359-3380.

76. *CRC Handbook of Chemistry and Physics* 90th Edition (CD-ROM Version 2010) ed.; CRC Press/Taylor and Francis: Boca Raton, FL, 2010.

77. Li, N.; Zhang, Q.; Quinlivan, S.; Goebl, J.; Gan, Y.; Yin, Y., H_2O_2-Aided Seed-Mediated Synthesis of Silver Nanoplates with Improved Yield and Efficiency. *ChemPhysChem* **2012,** *13* (10), 2526-2530.

78. Zhang, Q.; Li, N.; Goebl, J.; Lu, Z.; Yin, Y., A Systematic Study of the Synthesis of Silver Nanoplates: Is Citrate a "Magic" Reagent? *J. Am. Chem. Soc.* **2011,** *133* (46), 18931-18939.

79. Tsuji, M.; Gomi, S.; Maeda, Y.; Matsunaga, M.; Hikino, S.; Uto, K.; Tsuji, T.; Kawazumi, H., Rapid Transformation from Spherical Nanoparticles, Nanorods, Cubes, or Bipyramids to Triangular Prisms of Silver with PVP, Citrate, and H_2O_2. *Langmuir* **2012,** *28* (24), 8845-8861.

80. Hussain, S. T.; Iqbal, M.; Mazhar, M., Size Control Synthesis of Starch Capped-Gold Nanoparticles. *J. Nanopart. Res.* **2009,** *11* (6), 1383-1391.

81. Penn, R. L.; Banfield, J. F., Imperfect Oriented Attachment: Dislocation Generation in Defect-Free Nanocrystals. *Science* **1998,** *281* (5379), 969-971.

82. Zhang, J.; Huang, F.; Lin, Z., Progress of Nanocrystalline Growth Kinetics Based on Oriented Attachment. *Nanoscale* **2010,** *2* (1), 18-34.

83. Schliehe, C.; Juarez, B. H.; Pelletier, M.; Jander, S.; Greshnykh, D.; Nagel, M.; Meyer, A.; Foerster, S.; Kornowski, A.; Klinke, C.; Weller, H., Ultrathin PbS Sheets by Two-Dimensional Oriented Attachment. *Science* **2010,** *329* (5991), 550-553.

84. Li, C. C.; Cai, W. P.; Cao, B. Q.; Sun, F. Q.; Li, Y.; Kan, C. X.; Zhang, L. D., Mass Synthesis of Large, Single-Crystal Au Nanosheets Based on a Polyol Process. *Adv. Funct. Mater.* **2006,** *16* (1), 83-90.

85. Kida, T., Synthesis of Gold Nanosheets at a Liquid/Liquid Interface Using an Amphiphilic Polyoxometallate/Surfactant Hybrid Photocatalyst. *Langmuir* **2008,** *24* (15), 7648-7650.

86. Penn, R. L., Kinetics of Oriented Aggregation. *J. Phys. Chem. B* **2004,** *108* (34), 12707-12712.

87. Lim, B.; Yu, T.; Park, J.; Zheng, Y.; Xia, Y., Mixing an Aqueous Suspension of Pd or Au Nanocrystals with a Less Polar Solvent Can Cause Changes to Size, Morphology, or Both. *Angew. Chem. Int. Ed.* **2011,** *50* (27), 6052-6055.

88. Guo, Z.; Zhang, Y.; Xu, A.; Wang, M.; Huang, L.; Xu, K.; Gu, N., Layered Assemblies of Single Crystal Gold Nanoplates: Direct Room Temperature Synthesis and Mechanistic Study. *J. Phys. Chem. C* **2008,** *112* (33), 12638-12645.

89. Zhang, S.; Berguiga, L.; Elezgaray, J.; Roland, T.; Faivre-Moskalenko, C.; Argoul, F., Surface Plasmon Resonance Characterization of Thermally Evaporated Thin Gold Films. *Surf. Sci.* **2007,** *601* (23), 5445-5458.

90. Riedel, T.; Brynda, E.; Dyr, J. E.; Houska, M., Controlled Preparation of Thin Fibrin Films Immobilized at Solid Surfaces. *J. Biomed. Mater. Res. A* **2009,** *88A* (2), 437-447.

91. Kunlan, L.; Lixin, X.; Jun, L.; Jun, P.; Guoying, C.; Zuwei, X., Salt-Assisted Acid Hydrolysis of Starch to D-Glucose under Microwave Irradiation. *Carbohydr. Res.* **2001,** *331* (1), 9-12.

92. Chung, H.-J.; Jeong, H.-Y.; Lim, S.-T., Effects of Acid Hydrolysis and Defatting on Crystallinity and Pasting Properties of Freeze-Thawed High Amylose Corn Starch. *Carbohydr. Polym.* **2003,** *54* (4), 449-455.

93. Shujun, W.; Jinglin, Y.; Jiugao, Y.; Jiping, P.; Hongyan, L., Structure Characterization of C-Type Starch Granule by Acid Hydrolysis. *Food Hydrocolloid.* **2008,** *22* (7), 1283-1290.

94. Barlow, D. A.; Baird, J. K.; Su, C.-H., Theory of the Von Weimarn Rules Governing the Average Size of Crystals Precipitated from a Supersaturated Solution. *J. Cryst. Growth* **2004,** *264* (1–3), 417-423.

95. Guo, Z.; Zhang, Y.; Huang, L.; Wang, M.; Wang, J.; Sun, J.; Xu, L.; Gu, N., One-Step Controlled Synthesis of Anisotropic Gold Nanostructures with Aniline as the Reductant in Aqueous Solution. *J. Colloid Interface Sci.* **2007,** *309* (2), 518-523.

96. Sun, X.; Dong, S.; Wang, E., High-Yield Synthesis of Large Single-Crystalline Gold Nanoplates through a Polyamine Process. *Langmuir* **2005,** *21* (10), 4710-4712.

97. Lofton, C.; Sigmund, W., Mechanisms Controlling Crystal Habits of Gold and Silver Colloids. *Adv. Funct. Mater.* **2005,** *15* (7), 1197-1208.

98. Lim, B.; Camargo, P. H. C.; Xia, Y., Mechanistic Study of the Synthesis of Au Nanotadpoles, Nanokites, and Microplates by Reducing Aqueous HAuCl$_4$ with Poly(vinyl pyrrolidone). *Langmuir* **2008,** *24* (18), 10437-10442.

99. Xiong, Y.; Xia, Y., Shape-Controlled Synthesis of Metal Nanostructures: The Case of Palladium. *Adv. Mater.* **2007,** *19* (20), 3385-3391.

100. Huang, D.; Bai, X.; Zheng, L., Ultrafast Preparation of Three-Dimensional Dendritic Gold Nanostructures in Aqueous Solution and Their Applications in Catalysis and SERS. *J. Phys. Chem. C* **2011,** *115* (30), 14641-14647.

101. Joseph, D.; Geckeler, K. E., Surfactant-Directed Multiple Anisotropic Gold Nanostructures: Synthesis and Surface-Enhanced Raman Scattering. *Langmuir* **2009,** *25* (22), 13224-13231.

102. Vosgröne, T.; Meixner, A. J., Surface- and Resonance-Enhanced Micro-Raman Spectroscopy of Xanthene Dyes: From the Ensemble to Single Molecules. *ChemPhysChem* **2005,** *6* (1), 154-163.

APPENDIX

RESEARCH ACHIEVEMENTS

We have successfully developed the simple and efficient methods for the fabrication of gold nanosheets and flower-liked gold nanostructures under consideration of using non-harmful and environmentally friendly chemicals with industrial-scale production capability. Our works were achieved many awards from the nation, scientific societies and international organizations. Moreover, our works also were accepted in peer-review journals. The list of research achievements is showed below.

1. In 2010, we received the consolation prize for oral presentation in The Science Forum 2010, title: Nanostructure assembly of golden apple snail's egg shell.

คณะวิทยาศาสตร์
จุฬาลงกรณ์มหาวิทยาลัย

รางวัลชมเชย

ในการประชุมวิชาการ (The Science Forum 2010) ครั้งที่ ๑๘ ประจำปี ๒๕๕๓
ประเภทบรรยาย Session: Applied Science and Technology

นายสุพีระ นุชนารถ

ระหว่างวันที่ ๑๑ - ๑๒ มีนาคม ๒๕๕๓ ณ อาคารมหามกุฎ คณะวิทยาศาสตร์
ให้ไว้ ณ วันที่ ๑๒ เดือน มีนาคม พุทธศักราช ๒๕๕๓

(ศาสตราจารย์ ดร.สุพจน์ หารหนองบัว)
คณบดีคณะวิทยาศาสตร์

(ศาสตราจารย์ ดร.สมศักดิ์ ปัญหา)
รองคณบดีฝ่ายวิจัย

2.   In 2010, we received the outstanding poster award in Pure and Applied Chemistry International Conference 2010, title: Nanostructure assembly of golden apple snail's egg shell.

3. In 2011, we obtained the third prize of poster presentation in The 28th Annual Conference of the Microscopy Society of Thailand, title: Investigation of the surface modification of 2-D gold nanoplates by the simple wet chemical method.

4. In 2011, we received the consolation prize for poster presentation award in The Science Forum 2011, title: Structural evolution of gold nanoplates to gold nanoflowers initiated by hydrogen peroxide induced degradation of starch.

คณะวิทยาศาสตร์
จุฬาลงกรณ์มหาวิทยาลัย

รางวัลชมเชย

ในการประชุมวิชาการ (The Science Forum 2011) ครั้งที่ ๑๙ ประจำปี ๒๕๕๔
ประเภทโปสเตอร์ Session: Applied Sciences and Technology

นายสุพีระ นุชนารถ

ระหว่างวันที่ ๑๐ - ๑๑ มีนาคม ๒๕๕๔ ณ อาคารมหามกุฏ คณะวิทยาศาสตร์
ให้ไว้ ณ วันที่ ๑๑ เดือน มีนาคม พุทธศักราช ๒๕๕๔

(ศาสตราจารย์ ดร.สุพจน์ หารหนองบัว)
คณบดีคณะวิทยาศาสตร์

(ศาสตราจารย์ ดร.สมศักดิ์ ปัญหา)
รองคณบดีฝ่ายวิจัย

จุฬาลงกรณ์มหาวิทยาลัย
CHULALONGKORN UNIVERSITY

5. In 2012, we obtained the third award in oral presentation in The 29th Annual Conference of the Microscopy Society of Thailand, title: Structural evolution from gold nanoplates to flower-liked gold nanostructures.

6.   In 2012, we obtained the gold medal from 40th International Exhibition of Inventions of Geneva 2012, title: Reflective gold nanocrystals.

7. In 2012, we obtained the outstanding award from 4th Sci & Tech Initiative and
   Sustainability Awards (4th STISA), title: Enhancement of the values and images
   of Thai cosmetics and Thai spa using 99.99% gold nanocrystals from sustainable
   green nanotechnology.

8. In 2013, we published our work in an international journal, title: Formation of
   large H_2O_2-reduced gold nanosheets via starch-induced two-dimensional oriented
   attachment, S. Noochanat, C. Thammacharoen, B. Lohwongwatana, S. Ekgasit,
   RSC Adv., 2013, 3, 3707-3716.

9.   In 2013, we achieved the honor award from the senate of Thailand as we have

developed a scientific knowledge benefiting Thai society.

VITA

Name: Mr. Supeera Nootchanat

Address: Sensor Research Unit (SRU), Department of Chemistry, Faculty of Science Chulalongkorn University, Bangkok

Thailand.

Tel/fax: (+66)2-218-7585

E-mail: magiga_@hotmail.com

Education

2008 B.Sc. (1st Class Honours) in Chemistry, Silpakorn University, Thailand

2015 Ph.D. in physical chemistry at Chulalongkorn University, Thailand

2015 Ph.D. in electronic and electrical engineering, Niigata University, Japan

Advisors

Prof. Dr. Sanong Ekgasit (Thailand)

Assoc. Prof. Dr. Akira Baba (Japan)

Research field

1. Synthesis and characterization of metals (gold) nanoparticles

2. Fabrication of metal nanoparticles for novel properties

3. Photovoltaic